The investigation of mechanisms underlying iron overload induced adiponectin resistance

Michelle Prioriello

A Thesis submitted to the Faculty of Graduate Studies in Partial Fulfillment of the Requirements for the Degree of Master of Science.

Graduate Program in Biology

York University

Toronto, Ontario

August 2017

ABSTRACT

Recent research is aiming to elucidate the molecular mechanisms of metabolic syndrome-associated diseases. This study investigates iron overload-induced adiponectin resistance in cardiovascular disease and diabetes. Iron overloaded primary neonatal cardiomyocytes, L6 skeletal muscle myoblasts, and an *in vivo* mouse model was used to examine adiponectin resistance. Data indicates the induction of adiponectin resistance after iron treatment, and that this may occur by changes in adiponectin signalling proteins via the regulation of FOXO1 transcription factor. A decrease in adiponectin sensitivity was not observed in the iron overload mouse model used here, although this may be dependent on amount and duration of iron overload. Overall, this study sheds light on the complex balance of adiponectin signalling under iron overload conditions in heart and skeletal muscle. The data indicates that iron can induce adiponectin resistance, and thus helps to elucidate the cellular mechanisms via which metabolic syndrome disease complications can occur.

ACKNOWLEDGEMENTS

I would like to take the time to thank my incredible supervisor, Dr. Gary Sweeney, for the unforgettable opportunity to complete my graduate studies in his lab. Without his excellent guidance, knowledge and patience, I would not have become the graduate student that I am today.

I would also like to thank my examining committee, Dr. Michael Scheid, Dr. Christopher Perry and Dr. Tara Haas for their valuable time spent to evaluate and discuss my thesis. Your academic input is greatly appreciated.

Special thanks to current and previous lab members for your constant teamwork, advice and positive energy, for which this graduate experience would have not been possible. Special acknowledgements to Karam Dahyaleh, Nancy Dang, James Jang and Palanivel Rengasamy for your contributions to the project, and especially to Amos Song, for all of your generous help throughout my graduate studies.

Most importantly, I would like to express my gratitude to my family and friends. I would like to thank Alannah Zambri, Tiziana Mancini and Eva DeRango. For without your laughs, and countless memories of fun, the completion of this thesis would not have been possible. I would also like to thank my dear Stefano Marrella for your love and constant encouragement throughout our journey as graduate students together. Lastly, I would like to thank my parents. Your countless love and support throughout my academic career will be cherished everyday for a lifetime.

TABLE OF CONTENTS

LIST OF FIGURES

Chapter 1 Figures

Chapter 2 Figures

Chapter 3 Figures

Appendix A Figures

LIST OF ABBREVIATIONS

ACC	Acetyl-CoA (Coenzyme A) carboxylate
AdipoR1	Adiponectin receptor 1
AdipoR2	Adiponectin receptor 2
AdRon	AdipoRon
Akt	Protein kinase B
AMP	Adenosine monophosphate
AMPK	Adenosine monophosphate-activated protein kinase
APPL1	Leucine zipper motif
AS	AS1842856
ATP	Adenosine triphosphate
AUC	Area under curve
BMI	Body Mass Index
BSA	Bovine serum albumin
CaMKK	Ca2+/calmodulin-dependent protein kinase kinase
CBP/p300	CREB Binding Protein
CDK1	Cyclin-dependent kinase 1
CoA	Coenzyme A
db/db	Diabetic phenotype (Homozygous mouse model)
Dcytb	Reductase duodenal cytochrome b
DMSO	Dymethyl sulfoxide
DMT1	Divalent metal-ion transporter 1
ER	Endoplasmic reticulum

fAd	Full length adiponectin
FBS	Fetal bovine serum
FOXO1	Forkhead box protein O1
gAd	Globular adiponectin
GLUT4	Glucose transporter type 4
GTT	Glucose tolerance test
HAMP	Hepcidin antimicrobial peptide
HBS	Hepes buffer saline
HCP1	Haem carrier protein 1
HF	High fat
HFE2/HJV	Hemojuvelin
HMW	High molecular weight
HO1	Haem oxygenase 1
HRP	Secondary horseradish peroxidase
IL-6	Interleukin 6
IO	Iron overload
IP	Intraperitoneal
IRE-CFP	Iron response element - cyan fluorescent protein
ITT	Insulin tolerance test
IV	Intravenous
JNK	c-Jun N-terminal kinases
kDA	Kilodalton

KO	Knockout
LMW	Low molecular weight
LPL	Lipoprotein lipase
LV	Left ventricular
MAPK	P38 mitogen-activated protein kinases
MI	Myocardial infarction
MMW	Middle molecular weight
MTT	Methylthiazolyldiphenyl-tetrazolium bromide
NADPH	Nicotinamide adenine dinucleotide phosphate
NeoCM	Neonatal cardiomyocytes
ob/ob	Obese phenotype (Homozygous mouse model)
PCC	Pearson's overlap correlation coefficient
PFA	Paraformaldehyde
PGSK	Phen Green™ SK
PK	Peak
PPAR	Peroxisome proliferator-activated receptors
PVDF	Polyvinylidene fluoride
Rab5	Ras-related protein
ROS	Reactive oxygen species
SDS-PAGE	Sodium dodecyl sulfate polyacrylamide gel electrophoresis
SGK	Serum and glucocorticoid inducible kinase
SIRT1/2	Silent Information Regulator 2
T-cad	T-cadherin

TFR2	Transferrin receptor protein 2
Thr	Threonine
TNFα	Tumor necrosis factor α

Chapter 1: Introduction and Research Aims

1.1 Metabolic syndrome and associated complications

According to Metabolic Syndrome Canada, metabolic syndrome affects 1 in 5 Canadians[1], and accounts for 43% of deaths annually[1]. Metabolic syndrome is a combination of reversible physiological and molecular abnormalities that are positively correlated with the development of serious health conditions such as cardiovascular disease and type 2 diabetes[2]. Symptoms such as abdominal weight gain, hypertension, as well as elevated triglyceride, glucose and cholesterol levels are all metabolic syndrome contributors. If diagnosed with 2 of 5 of these conditions, a patient may be at high risk, while having 3 of 5 risks diagnoses a patient with metabolic syndrome[3]. Metabolic syndrome is treatable by making lifestyle changes such as maintaining a healthy weight, by exercising daily and by consuming a healthy diet[2]. However, lifestyle changes may not be the answer to all individuals. Thus, further investigations are required to better understand the molecular regulation of metabolic syndrome.

1.1.1. Heart Failure

The metabolic syndrome characteristics mentioned previously are known to be associated with increased risk of heart failure[4], whereby, cardiovascular disease is the number one cause of death worldwide[5]. A positive correlation between obesity and heart failure was first evident in the Framingham Heart study. This study investigated the relationship between Body Mass Index (BMI) and the prevalence of heart failure. An increased risk of heart failure in a given population was demonstrated via analysis of cardiovascular disease risk factors such as hypertension and blood suagr[6].

The development of heart failure comprises both structural and functional abnormalities that impairs the heart from pumping sufficient blood supply to the body[7]. Heart failure is caused by a loss in functional myocardial cells after cardiac injury, which can result from etiologies such

as hypertension, ischemic heart disease and diabetes[7]. Moreover, heart failure results from a compensation for inadequate cardiac output. For instance, heart palpitations or an increased heart rate can result in insufficient blood flow in heart failure patients[7]. On the contrary, it has been reported that some cardiovascular disease risk factors are also known to play a cardioprotective role under certain circumstances - this is known as "reverse epidemiology". Specifically, high blood pressure and obesity have been shown to play beneficial roles in heart failure patients[8,9]. Overall, the relationship between these two risk factors is one that should be more thoroughly investigated.

1.1.2. Diabetes

In 1922, Banting and Best discovered insulin; a hormone now known to regulate blood glucose levels[10]. When the body is unable to produce or respond to insulin, this results in a diseased state known as diabetes, whereby an abnormal metabolism of carbohydrates results in elevated blood sugar levels. Three types of diabetes include Type 1, type 2 and type 3 diabetes. Type 1 diabetes, or juvenile onset diabetes, results from an autoimmune response against insulin producing islet cells in the pancreas. This results in elevated glucose levels in the blood stream, in turn leading to weight loss and increased risk of heart disease, stroke and kidney failure[11]. Type 2 diabetes, previously called adult onset diabetes, is caused by insulin resistance. Insulin resistance is the inability of cells to utilize normal insulin levels, which results in elevated plasma glucose[11]. This arises from reduced glucose uptake in muscle and other tissues, as well as beta cell failure. Furthermore, type 2 diabetes is also positively correlated with cardiovascular disease risk[11]. Lastly, recent research has now proposed a new category of diabetes, known as type 3 diabetes, or "brain diabetes". This type of diabetes is associated with elevated glucose levels in the brain, which may explain the shared molecular mechanisms with diabetes and elderly cognitive decline, more commonly known as Alzheimer's disease.

Moreover, several studies have investigated the positive relationship between metabolic syndrome and type 2 diabetes risk[12,13]. For example, a study investigating the correlation between BMI and diabetes showed a strong relationship between a BMI over 40kg/m^2 and self-reported diabetes, as well as hypertension and elevated cholesterol[14]. Additionally, previous literature has also demonstrated a correlation between metabolic syndrome and type 2 diabetes via insulin resistance mechanisms[15]. However, further investigation is required to help understand the molecular regulation of metabolic syndrome associated diabetes.

1.2 Obesity and adipokines

Recently, factors such as high fat diets and sedentary lifestyle have resulted in a global epidemic known as obesity[16]. Recently, obesity has become a rising topic in the fields of molecular biology and physiology because of its capability to increase the likelihood of various diseases that result in decreased life expectancy and morbidity[17]. Obesity is characterized by an accumulation of visceral fat tissue, and is marked by a BMI of 30kg/m^2 in Western society[17]. Visceral fat accumulation in obesity grows by two mechanisms. The first being hyperplasia, defined as elevated adipocyte number, which occurs at early stages of adipose tissue growth[18]. This is then followed by hypertrophy, defined by an increase in cell size, which occurs due to lipid storage overload, resulting in lipid redistribution into other metabolic tissues[19]. Hypertrophic adipose tissues also have an altered adipokine secretion profiles. Adipokines are adipose tissue-specific cytokines (cell signalling proteins). For example, leptin was the first discovered adipokine in 1994. Leptin is a 16 kilodalton (kDa) protein, also known as the satiety hormone, is involved in decreasing food intake and increasing energy consumption in healthy individuals. It is found to be inversely correlated with increasing amounts of adipose tissue[20]. Conversely, lipocalin-2 is an adipokine found to be positively correlated with body fat percentage, and is involved in apoptosis (cell death) regulation and iron metabolism. Lastly, adiponectin is an

adipokine known to play multiple beneficial roles in cellular homeostasis, and will be the focus of this introduction.

1.2.1. Adiponectin structure

Adiponectin, also known as AdipoQ, Acrp30 and apM1, is a 30kDa protein that is found in abundantly high levels in circulation and is found at concentrations of ~1-30µg/ml[21,22]. Adiponectin is comprised of a 247 amino acid sequence and consists of three domains: an amino-terminal signal sequence, a collagenous domain, and a carboxyl-terminal globular domain at the C-terminal end[22,23]. The adiponectin monomer is found in two forms in circulation: full length adiponectin (fAd) and globular adiponectin (gAd). Full length adiponectin (fAd) is found in three oligomeric forms: high molecular weight (HMW), middle molecular weight (MMW) and low molecular weight (LMW)[24], found in oligomer, hexamer and trimer chains, respectively. Specifically, three monomers attach through interactions via their globular domains (LMW), two trimers use the collegoneous domain to form a hexamer (MMW), and 4-6 trimers will form an oligomer in the same manner (HMW)[25]. The oligomerization states of adiponectin have been previously shown to be important for biological functioning[26]. Moreover, fAd can become cleaved by leukocyte elastase to release the C-terminal fragment and create what is known as globular adiponectin (gAd)[27].

1.2.2. Adiponectin in metabolic syndrome

Adiponectin plays many beneficial roles against metabolic syndrome associated diseases through its anti-inflammatory, anti-apoptotic, anti-diabetic and cardioprotective properties[17]. Moreover, adiponectin has been shown to be inversely proportional to body fat percentage in adults[28,29]. For instance, a study in 1996 showed reduced adiponectin levels in obese (ob/ob) mice[30], and a 1999 study showed decreased plasma adiponectin levels in obese patients[31]. Moreover, studies have revealed that this decrease in adiponectin is explained by

both environmental and genetic factors. For instance, a reduction in adiponectin can be caused by any point mutation in the adiponectin gene[32]. Furthermore, a decrease in adiponectin can also occur as a result of unhealthy lifestyle choices such as a high-fat diet and lack of exercise. This is supported by previous studies which have shown that a healthy diet and combined with exercise significantly increased adiponectin levels via insulin signalling regultion[33,34]. Overall, this decrease in adiponectin in obese individuals has the potential to lead to metabolic diseases. The following information will focus on adiponectin in cardiovascular and diabetes.

1.2.2.1. Adiponectin and cardiovascular disease

Previous research has demonstrated a cardioprotective role of adiponectin against cardiovascular disease, as well as its potential as a therapeutic target[35]. For instance, studies in adiponectin knockout (KO) mice showed increased cardiac hypertrophy and mortality, suggesting a cardioprotective role by adiponectin[36,37]. Another study showed that adiponectin is protective against severe cardiac fibrosis[38]. Additionally, clinical investigations have confirmed a rapid decline in adiponectin levels following acute myocardial infarction (MI)[39]. Moreover, significant reduction in adiponectin levels were observed under oxidative stress conditions in cultured cardiomyocytes. Reactive oxygen species (ROS) and oxidative cell death were significantly decreased with adiponectin treatment[40]. Despite these findings, the relationship between adiponectin levels and heart failure is somewhat controversial. For instance, a clinical study showed high adiponectin levels are positively correlated with mortality in heart failure patients[41]; however, the mechanistic regulation of this finding is currently poorly defined. In conclusion, further investigation is required to better understand the role of adiponectin regulation in cardiovascular disease.

1.2.2.2. Adiponectin and diabetes

Adiponectin has also been a recent therapeutic target for diabetes treatment due to its anti-diabetic properties[42]. Previous research suggests the development of diabetes in

adiponectin depleted conditions. Results show that lack of adiponectin leads to reduced glucose and fatty acid uptake, as well as increased gluconeogenesis[21,43]. A clinical study in Japan also confirmed higher circulating adiponectin levels are correlated with a decreased risk of type 2 diabetes in adults[44]. Moreover, the negative relationship between adiponectin and insulin resistance has been well characterized in literature[45,46,47]. Overall, these findings suggest a strong relationship between decreased adiponectin and diabetes risk. Recent literature has suggested the potential regulation of adiponectin mediated insulin resistance via inflammasome activation. Specifically, up-regulation of tumour necrosis factor α (TNF-α) and interleukin-6 (IL-6) have been shown to attenuate insulin sensitivity[48,49]. However, further investigation is needed to fully elucidate the molecular mechanisms of adiponectin regulation in diabetes.

1.2.3. Adiponectin signalling and action

Adiponectin action occurs via two receptors: adiponectin receptor 1 (AdipoR1/AdR1) and adiponectin receptor 2 (AdipoR2/AdR2)[20]. AdipoR1 is predominantly found in skeletal muscle, while AdipoR2 is abundant in the liver. In addition to AdipoR1 and AdipoR2, T-cadherin (T-cad) is a non-transmembrane adiponectin receptor. T-cad specifically binds to HMW and MMW adiponectin in circulation, and T-cad knockout (KO) mice have been shown to cause increased adiponectin concentrations in circulation[50,51]. Although T-cadherin is important for adiponectin binding in serum, it is thought that it plays no critical role in adiponectin signalling due to its lack of a transmembrane domain[51].

AdipoR1 and AdipoR2 are transmembrane proteins, each with 7 transmembrane domains (**Figure 1.1**). Moreover, AdipoR1 and AdipoR2 have an external C-terminus and an internal N- terminus[52]. AdipoR1 and AdipoR2 are known to bind to certain adaptor proteins such as leucine zipper motif 1 (APPL1)[53]. APPL1 has a phosphotyrosine binding domain that binds to the N-terminus of AdipoR1, which stimulates phosphorylation of AMPK (adenosine monophosphate-activated protein kinase) and P38 MAPK (mitogen-activated protein kinases)[54].

AMPK is a serine/threonine protein kinase that is comprised of 3 subunits: α, β and γ. The catalytic α subunit is activated at threonine (Thr) 172, while β and γ are regulatory subunits. Specifically, an increase in adenosine mono-phosphate (AMP) causes γ subunit binding, leading to AMPK activation via Thr172 phosphorylation. This effect is reversed by elevated adenosine tri-phosphate (ATP) levels[55]. AMPK regulation is also mediated by two upstream kinases: liver kinase B1 (LKB1) and Ca2+/calmodulin-dependent protein kinase kinase (CaMKK); both of which are serine and threonine kinases that increase AMPK activity. Specially, adiponectin promotes LKB1 translocation from the nucleus to the cytosol, which is also assisted by APPL1 via BAR (membrane binding) domain interaction[56]. In terms of CaMKK, adiponectin stimulates endoplasmic reticulum (ER) mediated calcium release via phospholipase C activation, causing AMPK activation which is LKB1 independent[56]. P38 is also a serine/threonine kinase that is regulated by adiponectin in an APPL1 dependant manner. APPL1 acts as a scaffolding protein for P38 activation via Transforming growth factor β activated kinase (TAK1)-mitogen-activated protein kinase kinase 3 (MKK3)[57].

APPL2, an APPL1 isoform, also binds to AdipoR1 and AdipoR2. Unlike APPL1, APPL2 negatively regulates AdipoR1 and AdipoR2 dependant signalling. Additionally, APPL2 binds with APPL1 to form a complex via BAR domain interactions. This interaction between APPL1 and APPL2 causes APPL1 to compete for adiponectin receptor binding. Furthermore, adiponectin disrupts APPL2 receptor binding, in order to allow for an APPL1 dependant signalling cascade[58].

AdipoR1 and AdipoR2 display preferences for certain downstream signalling molecules. AdipoR1 prefers to stimulate AMPK while AdipoR2 is more is involved in PPARα (peroxisome proliferator-activated receptors) activation[53]. PPARs are nuclear receptor proteins that are involved in changing gene expression following a signalling cascade. Specifically, PPARα and PPARγ are known to regulate transcription factors that monitor glucose and lipid metabolism[59].

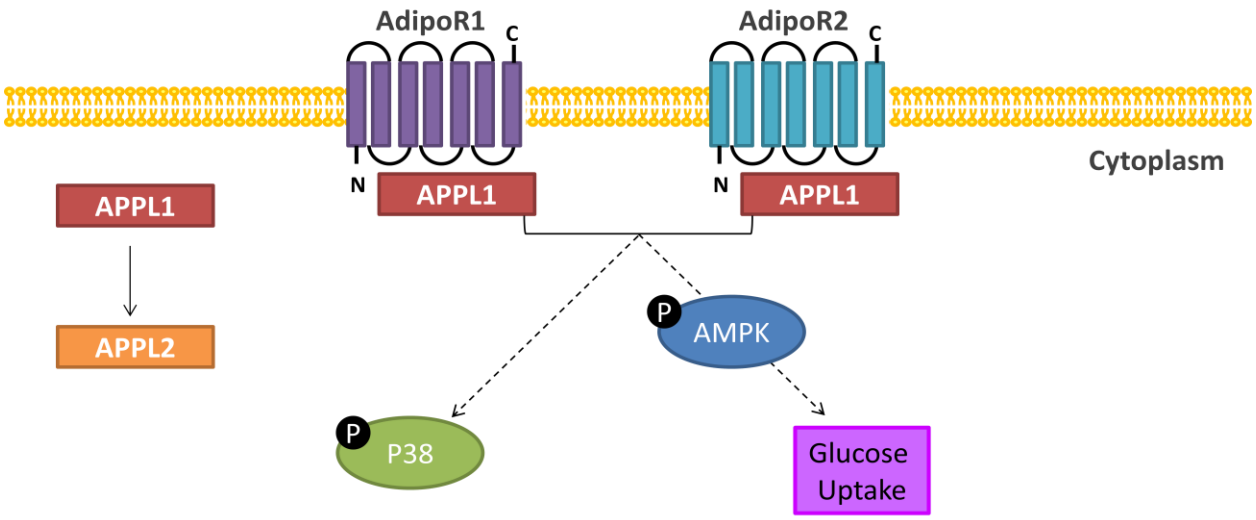

Figure 1.1: A summary of adiponectin signalling. Adiponectin has two transmembrane receptors: AdipoR1 and AdipoR2. Receptor activation upon adiponectin to receptor binding leads to the binding of APPL1 adaptor protein, which is competitively regulated by APPL2. APPL1 to receptor binding initiates activation of adiponectin mediated P38 and AMPK stimulation via phosphorylation, and subsequently glucose uptake.

1.2.3.1. Adiponectin stimulated metabolism

Adiponectin is involved in modulating a number of metabolic processes such as glucose uptake and fatty acid oxidation[16]. Fatty acid metabolism is regulated through phosphorylation of acetyl-coenzyme A (CoA) carboxylate (ACC), while glucose uptake is regulated by glucose transporters types 1-4 (GLUT1-4). GLUT1 is mainly prevalent on the surface of the neonatal heart. GLUT2 is predominately abundant in the kidney, pancreas, liver and small intestine. GLUT3 is highly expressed in the brain, but has also been shown to be expressed in skeletal muscle and the heart in low levels. GLUT4 is highly expressed in tissues that are insulin sensitive such as adipose tissue and the adult heart, but it is mainly expressed in skeletal muscle[60].

Adiponectin has been shown to stimulate both metabolic fatty acid uptake and glucose uptake in the heart. Adiponectin stimulates glucose uptake via GLUT4 translocation to the

plasma membrane[53]. GLUT4 translocation can occur via the activation of AMPK, P38, and Ras-related protein 5 (Rab5); all of which are activated through APPL1 dependant adiponectin receptor activation[61]. Additionally, adiponectin is known to enhance insulin stimulated glucose uptake via Akt (protein kinase B) phosphorylation[62]. Focusing on fatty acid oxidation, adiponectin is known to stimulate lipoprotein lipase (LPL) translocation to the plasma membrane which causes the break-down of low density lipoproteins in circulation[63]. In turn, cardiac metabolic regulation is essential and crucial as the accumulation of sugar or fatty acid chains in the heart can lead to cardiac dysfunction[60].

Adiponectin is also known to regulate glucose and fatty acid metabolism in skeletal muscle. AMPK activation is known to regulate adiponectin induced metabolic pathways[64]. Additionally, other research has demonstrated P38 is also involved in glucose uptake regulation. Activation of P38 and AMPK by adiponectin then results in GLUT4 translocation to the plasma membrane, causing receptor internalization via endocytosis[61]. In terms of fatty acid metabolism, the activation the AMPK pathway upon adiponectin stimulation is known to stimulate ACC phosphorylation. This causes a downstream inhibitory effect of ACC, which results in a reduction in malonyl-CoA, therefore increasing fatty acid-oxidation. Moreover, a study in C2C12 skeletal muscle cells revealed that adiponectin induces fatty acid oxidation via AMPK, P38 and PPARα, which also cause LPL membrane translocation[59].

1.2.3.1 Adiponectin receptor regulation by FOXO

Adiponectin receptor expression is regulated by the action of specific transcription factors, including Forehead box protein (FOXO). The FOXO transcription factors are involved in a number of cellular processes such as cell cycle control, cell differentiation, stress response and apoptosis[65]. The FOXO family consists of four subgroups: FOXO1, FOXO3, FOXO4 and FOXO6. Each subgroup is known for its tissue-specific expression. FOXO4 is expressed in

muscle and kidney, while FOXO6 is expressed in the liver and primarily the brain. FOXO1 and FOXO3 are abundantly expressed in all tissues[66].

FOXO regulation is dependent on post translational modifications including phosphorylation, acetylation, methylation and ubiquitination. In terms of phosphorylation, the phosphoinositide 3 kinase (PI3K) pathway is known to inhibit FOXO regulation via serum glucocorticoid inducible kinase (SGK) and Akt. For instance, phosphorylation of FOXO1 by SGK or Akt at residues Thr24, Ser256 and Ser319 result in a change in cellular localization from the nucleus to the cytoplasm, whereby FOXO1 becomes transcriptionally inactive[67]. For example, gene expression of AdipoR1 and AdipoR2 is controlled by nuclear FOXO1[68]. Moreover, FOXO can be activated by acetylation via macrophage stimulating protein 1 (MST1), c-Jun N-terminal kinases (JNK) and Cyclin-dependent kinase 1 (CDK1). This results in a change FOXO localization from the cytoplasm to the nucleus where it becomes transcriptionally active[65]. Conversely, acetylation of FOXO has been shown to inhibit its DNA binding capacity[69]. The acetylated state of FOXO is regulated by histone deacyteltransferases (HDACs) and histone acyteltransferases (HATs). HDACs such as Silent Information Regulator 2 (SIRT1/2) and HATs such as CREB Binding Protein (CBP/p300), regulate FOXO by promoting or deactivating transcription, respectively[70,69]. In terms of ubiquitination, FOXO can be either mono- or polyubiquitinated[71,72]. Monoubiquitination of FOXO leads to activation of its transcriptional activity in the nucleus, while polyubiquitination results in FOXO localization to the cytoplasm, followed by its degradation. Deubiquitination can also reactivate FOXO under certain conditions[71]. Lastly, there are certain kinases that can regulate transcriptional activity of FOXO. For instance, AMPK dictates the transcriptional profile of FOXO by recruiting other proteins to regulate FOXO transcription[73].

1.2.3.2. AdipoRon, an adiponectin agonist

Adiponectin has been considered a therapeutic target for metabolic syndrome associated disease due to the observation that adiponectin levels are reduced in obese individuals. However, adiponectin as a therapeutic agent is not readily available due to its expensive production[74]. Moreover, adiponectin cannot be orally administered due to proteolysis of the hormone, affecting its ability to reach the bloodstream[75]. Currently, there are two adiponectin agonists, ADP 355 and AdipoRon (AdRon) which are under investigation. A recent cancer study investigated the effects of ADP 355, a peptide-based adiponectin receptor agonist, via intraperitoneal (IP) administration. It was discovered that ADP 355 has the ability to repress breast cancer tumour growth via adiponectin receptor stimulation[35]. In addition to ADP 355, AdRon is also another adiponectin agonist that acts via AMPK signalling pathways, and will be the focus of this introduction.

AdRon, discovered by Okada-Iwabu et al[76], is the first orally active adiponectin receptor stimulator[77]. AdRon binds to both AdipoR1 and AdipoR2, which then stimulates adiponectin action signalling pathways via AMPK and PPARα, respectively. AdRon was also shown to improve cardiac function after reperfusion injury by preventing cardiomyocyte apoptosis after MI[77]. Orally administered AdRon was shown to reduce fasting plasma glucose and insulin levels in HF diet mice. This effect was diminished in AdipoR1 and AdipoR2 double KO mice. AdRon has also been shown to reduce plasma glucose levels, triglyceride content, oxidative stress and inflammation in diabetic phenotype (*db/db)* mice, while also increasing lifespan[76]. Overall, AdRon is a promising therapeutic approach to treat cardiovascular disease and type 2 diabetes. However, further investigations are required to better understand the mechanism of AdRon action in metabolic syndrome associated disease.

1.3 Adiponectin resistance

It is known that adiponectin levels are inversely proportional to body fat percentage in adults[78]. As a result, decreased adiponectin levels also reduce adiponectin action in these individuals. However, it remains unclear if lack of adiponectin action is due to a subnormal biological response to normal, or lower than normal, amounts of adiponectin. This phenomenon is known as adiponectin resistance. Adiponectin resistance is currently a rising topic in the fields of molecular biology; however, the physiological significance and mechanisms remain poorly defined[79].

Adiponectin resistance has been linked to heart failure and diabetes[80,81,82]. For example, an investigation in H9c2 cardiomyocytes examined the role of lipotoxicity induced ER stress and autophagy. A decrease in adiponectin sensitivity was observed via reduced AMPK signalling as well as reduced APPL1 mRNA and protein expression. These findings suggest that adiponectin resistance occurs in a model of lipotoxicity induced heart failure[83]. Multiple studies have also indicated adiponectin resistance in chronic heart failure[79,84.] Metabolic failure has been previously linked to heart failure pathophysiology, by a reduction in AdipoR1, AMPK and PPARα expression[84]. Moreover, adiponectin resistance is seen in heart failure patients with altered glucose and lipid metabolism. Importantly, a reduction in AdipoR1 has provided great insight for adiponectin resistance regulation mechanisms[79]. Moreover, a study conducted in insulin resistant obese mice (ob/ob), showed a reduction in AdipoR1 protein expression in skeletal muscle [68]. Another study examined the effects of gAd on a HF diet mouse model. It was demonstrated that gAd did not induce fatty acid oxidation in HF diet mice, suggesting gAd resistance[85]. Overall, these findings suggest that further investigation is needed in order to better understand the mechanism of adiponectin resistance regulation in cardiovascular diseases and diabetes.

1.4 Iron and iron transport

Iron is an essential mineral necessary for multiple bodily functions. Specifically, iron is a main component of hemoglobin; a protein composed of four subunits, each containing an iron bound atom to form a "Heme" group. Moreover, iron is naturally present in many foods, and is found in two forms: heme and non-heme. Sources of non-heme iron include plant sources and fortified foods, while heme and non-heme iron are present in animal products such as red meats and poultry[86]. Iron supplements can also provide daily iron doses, and is often found in either ferrous (Fe^{2+}) or ferric forms (Fe^{3+}), both of which are absorbed equally well[87]. The type of iron depends on the site in the body during its absorption. Non-heme dietary iron enters the gut via duodenal enterocytes[88,89]. Before entering the cell, ferric iron is reduced into ferrous iron by reducatase duodenal cytochrome *b* (Dcyt*b*), and enters through a divalent metal-ion transporter (DMT1). Heme iron enters the cell by endocytosis. It is thought that heme transport across the enterocyte plasma membrane is assisted by haem carrier protein 1 (HCP1), which is then released by haem oxygenase (HO1)[89]. Iron in the cytoplasm is then stored in a protein-iron complex called ferritin, as free iron is toxic to cells. Iron can also be released from ferritin upon its lysosomal degradation[90]. Free iron then exits the cell using iron exporter ferroportin, a multipass transmembrane protein[91]. Additionally, ferroportin levels are regulated by iron-regulatory hormone, hepcidin. Hepcidin and ferroportin levels are inversely proportional. Low hepcidin and increased ferroportin levels cause increased iron efflux, leading to an iron overload state. Lastly, upon iron release into circulation through ferroportin, iron is bound in the bloodstream by the transport glycoprotein named transferrin[92].

1.4.2. Iron overload

Iron uptake is a process that is tightly regulated in the body, as there are no physiological processes that prioritize iron excretion[89]. The dysregulation of iron can lead to an iron overload state, which can cause iron overload disorders. Clinically known as

haemochromatosis, iron overload disorders result from three different circumstances: genetic mutations, through multiple blood transfusions and by dietary iron supplement overload. Most commonly, hereditary hemochromatosis is due to mutations in the hepcidin gene, formally known as hepcidin antimicrobial peptide (HAMP)[93]. Mutations that are also known to cause hereditary hemochromatosis are found in other iron regulatory proteins such as HFE (also known as the hemochromatosis protein), transferrin receptor 2 (TFR2) or hemojuvelin (HFE2, or HJV)[94,95,96]. These mutations impair or reduce iron detection by hepatocytes, which in turn reduces hepcidin transcription[93]. Consequently, these decreased hepcidin levels lead to reduced ferroportin regulation, resulting in iron overload in multiple tissues. Hemochromatosis can also be caused by transfusion-induced iron overload in anemic patients. Anemia, is a condition marked by a deficiency in red blood cell production, which is accompanied by a reduction in circulating and cellular iron levels. Severe anemia is treated via blood transfusions, whereby donated blood is transfused into the patient via intravenous (IV). Although blood transfusions are a temporary treatment for anemic patients, multiple blood transfusions can lead to iron overload. Transfused red blood cells undergo a process called erythrophagocytosis, whereby red blood cells are ingested by macrophages or other immune cells[97]. This excess iron manages to surpass transferrin, ultimately leading to excess free iron in the targets tissues. As a result, cumulative iron overload leads to toxicity, causing organ dysfunction and damage[97,98]. Lastly, iron overload can also be caused by the consumption of excess iron supplements. A clinical study in 2006 concluded that only patients with documented iron deficiencies should be taking iron suppliments[99]. Moreover, it is important that physicians should carefully supervise iron supplement therapy. Regardless of the cause, iron overload has been shown to cause organ damage and other harmful effects. Specifically, haemochromatosis causes symptoms such as skin darkening, fatigue, weakness, joint pain and stomach pain. However, on a larger spectrum, iron overload has also been shown to cause reproductive problems, liver disease, cancer, cirrhosis, heart disease, and diabetes.

1.4.2.1. Iron overload and heart disease

Iron overload has been linked to cardiomyopathy[100], due to the ability of iron to increase cardiac oxidative stress and fibrosis[101]. However, clinical methodologies to diagnose iron overload induced heart disease are still unknown. In addition, iron overload induced heart disease has been shown to be is potentially lethal and thus, further study is required to improve clinical diagnosis. For instance, newer insight on iron-specific imaging techniques are being developed for iron overload induced cardiac disease to detect cardiomyopathy at earlier stages[100]. Additionally, the role of iron chelators and genetic therapies are in progress, but still require further mechanistic investigation. Overall, iron overload associated cardiomyopathy still requires further exploration in metabolic syndrome associated cardiac disease.

1.4.2.2. Iron overload and diabetes

The link between iron overload and diabetes has been recently well identified[102]. Iron is known to play a role in regulating glucose metabolism[103], as well as insulin resistance regulation[104]. Specifically, in hemochromatosis patients, iron is known to accumulate in the pancreas, where it may have a negative effect on beta cell function via increasing oxidative stress and apoptosis. This in turn affects insulin secreting mechanisms and glucose metabolism. This was demonstrated by a group who investigated hereditary hemochromatosis mouse models. It was found that iron overload mice displayed a loss in the capacity to secrete insulin[105]. An additional study demonstrated that iron overload has been shown to accumulate in adipoctyes. This investigation showed that increased iron was also associated with increased ferritin levels, which has been previously shown to be positively correlated with diabetes risk via insulin resistance[106]. Moreover, mice fed with a high iron diet were shown to have a decreased level of serum adiponectin compared to mice fed with normal chow. To conclude these findings, the overall mechanistic regulation of iron overload induced disease requires further study. Furthermore, the underlying molecular mechanisms of iron overload induced disease via

adipokine regulation, such as adiponectin, currently remains misunderstood and also requires further investigation[102].

1.5 Hypothesis and aims

Adiponectin is known for its anti-diabetic, anti-inflammatory, anti-fibrotic and cardioprotective properties. Therefore, patients with metabolic associated diseases display a lower profile of the beneficial effects mediated by adiponectin. However, it is unclear whether a lack of adiponectin action in patients with metabolic syndrome associated disease is due to a *resistance* in already reduced adiponectin levels in circulation. Thus, the aim of my thesis is to prove the presence of adiponectin resistance, as well as define the underlying molecular mechanisms. Specifically, I am interested in iron overload induced adiponectin resistance in both heart disease and diabetes, as this a phenomenon that is not well characterized in the literature.

Therefore, my first hypothesis is that adiponectin resistance will be induced under iron overload conditions. This phenomenon will be studied by examining iron overloads effects on the gene expression of downstream adiponectin signalling molecules, as well as through changes in adiponectin sensitivity under iron overload conditions. Previous studies have defined adiponectin resistance via reduced expression levels of adiponectin receptors (AdipoR1 and AdipoR2) and their corresponding adaptor protein (APPL1) [68,79], which results in a lack of adiponectin action.

The mechanism of iron overload induced adiponectin resistance is further hypothesized to be regulated by FOXO1 - an AdipoR1 and AdipoR2 transcription factor. I am proposing that iron overload conditions stimulate FOXO1 cytoplasmic localization to the cytoplasm, affecting its ability to transcribe AdipoR1 and AdipoR2. This could explain the lack of adiponectin action in iron overload conditions. The role of FOXO1 in iron overload induced adiponectin resistance will

be examined by tracking FOXO1 localization under iron overload conditions through anti-FOXO1 immunofluorescence. Moreover, the use of a FOXO1 inhibitor will be used to understand the functional significance of FOXO1 under iron overload conditions. Specifically, upon co-treatment of iron overload with a FOXO1 inhibitor in cell culture, the reversal of reduced adiponectin expression could confirm FOXO1`s role in iron overload induced adiponectin resistance regulation.

The following research aims will be investigated via three different models to examine heart disease and diabetic conditions: *in vitro* L6 skeletal muscle cells, *ex vivo* primary rat neonatal cardiomyocytes and an *in vivo* iron overload mouse model. Thus, I propose the following investigations of iron overload induced adiponectin resistance:

<u>Study1:</u> The investigation of iron overload induced adiponectin resistance in the heart, featuring *ex vivo* neonatal cardiomyocytes and an *in vivo* iron overload mouse model.

<u>Study 2:</u> The investigation of iron overload induced adiponectin resistance in skeletal muscle, featuring *in vitro* L6 skeletal muscle cells an *in vivo* iron overload mouse model.

Chapter 2: The investigation of iron overload induced adiponectin resistance in the heart, featuring *ex vivo* neonatal cardiomyocytes and an *in vivo* iron overload mouse model

2.1 Preface

The relationship between metabolic syndrome and heart disease is one that has been recently investigated in the literature. Iron overload has been linked to both metabolic syndrome and heart disease; however the involvement of adipokines, such as adiponectin, in the molecular regulation of iron overload associated heart disease is not well characterized. Furthermore, whether iron overload induces adiponectin resistance is not yet established. In addition, iron overload induced regulation by FOXO1 transcription factor has not been well characterized. *Ex vivo* primary neonatal cardiomyocytes treated with iron and an *in vivo* iron overload mouse model were used to examine the molecular regulation of iron overload induced adiponectin resistance. Decreased AdRon stimulated pAMPK, pP38 and glucose uptake were observed in iron overload conditions, and reduced AdipoR1 and APPL1 expression levels provide a potential mechanistic foundation for adiponectin resistance. Moreover, alleviatory affects of iron overload induced adiponectin resistance were relieved by inhibiting FOXO1, suggesting its mechanistic involvement in adiponectin resistance regulation. Conversely, adiponectin resistance was not evident in the heart of iron overload mice, suggesting the complex balance of adiponectin signalling under stress. Moreover, using echocardiography, impaired cardiac function was observed in iron overload compared to control mice. In summary, FOXO1-regulated iron overload induced adiponectin resistance was shown in neonatal cardiomyocytes. Together, these results suggest altered adiponectin regulation in iron overload conditions, supporting the potential mechanisms for iron overload induced cardiac disease and potential drug targeting.

2.2 Introduction

A cluster of health conditions associated with metabolic syndrome is known to be positively correlated with the prevalence of cardiovascular disease[2] - the leading cause of death worldwide[5]. Cardiovascular disease is characterized by both structural and functional abnormalities that impair cardiac function, which results from conditions such as hypertension and ischemia[7]. The molecular regulation of metabolic syndrome induced heart disease has been strongly linked to adipokine-mediated signalling. Specifically, the link between adiponectin and heart failure has been extensively investigated in previous research[107,83,85]. Adiponectin plays beneficial roles against metabolic related diseases by being cardioprotective against heart failure[17, 108,109,110]. However, adiponectin has also been inversely related to late stage heart disease[78]. Therefore, it remains unclear if lack of adiponectin action in heart failure is due to a subnormal biological response to normal, or lower than normal, amounts of adiponectin. This phenomenon known as adiponectin resistance is a rising topic in the field. However, the physiological significance and mechanisms of this particular adiponectin regulation remains unclear[79].

Emerging studies suggest a correlative, yet poorly characterized relationship between cardiovascular disease and iron overload[100]. The link between iron overload induced adiponectin resistance in the heart is also a phenomenon that remains poorly defined. Therefore, this chapter aims to examine iron overload induced adiponectin resistance. This topic will be studied by examining changes in adiponectin sensitivity as well as through changes in adiponectin signalling protein expression. Upon the presence of iron overload induced adiponectin resistance, it is further hypothesized that FOXO1 - a transcription factor regulating AdipoR1 and AdipoR2 [68] - will control iron overload induced adiponectin resistance in the heart. These hypotheses will be examined in *ex vivo* primary rat neonatal cardiomyocytes and in the heart of an *in vivo* mouse model.

2.3 Materials and Methods

2.3.1 Neonatal Cardiomyocyte Isolation and Culturing

The left ventricles of 1-3 day Wistar rat (*Rattus Norvegicus)* pups were isolated by decapitation, followed by a small ventricle incision through the sternum. Hearts were rinsed with CFBHH (Calcium and Bicarconate Free Hanks with Hepes) buffer (NaCl [137mM], [KCl 5.36mM], $MgSO_4$ [0.81mM], Dextrose [5.55], KH_2PO_4 [0.44], Na_2HPO_4 [0.34], HEPES pH 7.4 [20.06]) and torn apart into small pieces with fine tweezers. Samples were transferred to a flat bottom 50ml conical tube with 10ml of trypsin (1:250) (Gibco #27250-018) dissolved in CFBHH buffer and a small stir bar. Heart pieces were stirred in the cell culture hood on a magnetic plate for 10 min. The supernatant was collected and neutralized with DMEM (Gibco DMEM F12 with L-Glutamine and 2.438 g/L sodium bicarbonate #11320) supplemented with 10% Fetal Bovine Serum (FBS) (Wisent Inc #080-150), 1% Penicillin-Streptomycin (Gibco #15070063) solution and 50mg/L Cellgro Gentamycin sulfate (Life Technologies#30-005-CR). 10ml of trypsin was added to the remaining sample, and these series of steps were repeated until all tissue was digested into a homogenous solution. Homogenized tissue was spun down at 2000RPM for 20min, supernatant was removed, and pellet was respuspened in 10%FBS DMEM. Cells were plated in $10cm^2$ culture dishes (Falcon #6220065) for 1 hour in order to separate fibroblasts from cardiomyocytes. After incubation in a CO_2 incubator at 37ºC, supernatant containing cardiomyocytes was filtered through a 70µm nylon strainer (BD Falcon Cell Strainer 70µm Nylon #352350). Filtrate was supplemented with additional 10% FBS DMEM, and plated on primaria coated culture dishes (Falcon multiwell primaria 6 well #35-3846, 24 well #35-3847, 96 well#35-3848). 24 hours after isolation, cells were washed with Phosphate Buffer Saline (PBS) (Wisent 1X PBS, #311-010-CL). Treatment media (0%, 0.5% or 2% FBS DMEM) was added to begin experiments.

2.3.2. Characterizing intracellular iron:

2.3.2.1. MTT Assay

Neonatal cardiomyocytes were plated onto a primaria coated 96 well plate, and treated at 0µm, 100µm and 250µm of $FeCl_3$ (Sigma #44944) dissolved in dH_2O. Iron overload treatment was incubated for 24 hours (24h) in 0.5% FBS DMEM media. 5mg/ml of Methylthiazolyldiphenyl-tetrazolium (MTT,3-(4,5-Dimethyl-2-thiazolyl)-2,5-diphenyl-2H-tetrazolium bromide) (Sigma #M5655-1G) dissolved in PBS was added to each well 5 hours before the end of 24h treatment. Treatment media was removed with a needle syringe. Maximum working well volume (200µl per well in a 96 well plate) of dimethyl sulfoxide (DMSO) (Biopshop #DMS 555.500) was added to each well and incubated in a CO_2 incubator at 37ºC for 5 minutes. Absorbance was measured at 550nm.

2.3.2.2 IRE-CFP

Iron Response Element - Cyan Fluorescent Protein (IRE-CFP) plasmid was kindly provided by Dr. James R. Connor at Penn State Hershey Medical Centre. Transfection of IRE-CFP into neonatal cardiomyocytes was completed according to manufacturer's protocol (Lipofectamine 3000® [Invitrogen #L3000015]), directly onto glass cover slips (Fisher Scientific #12-546) in a 12 well plate (Falcon via VWR # 353043). After 2 days of incubation in a CO_2 incubator at 37ºC, cells were starved in 0.5% FBS DMEM and treated with 250µm of $FeCl_3$ for 24h. Cells were washed 3X with PBS++ (supplemented with 1% Ca^{2+} and 1% Mg^{2+}), and fixed with 4% paraformaldehyde (PFA) (Sigma-Aldrich #HT5011-1CS) for 20 minutes. Cells were washed 1X with PBS++ and incubated in 1% glycine (Bioshop #GLN001.5) dissolved in PBS++ for 10 minutes, washed 3X with PBS++ and mounted onto glass slides with mounting medium (mixture of Prolong Anti Fade [Invitrogen #P36930] to Mounting Medium for Fluorescence with DAPI [Vectasheild/Vector Labs #H-1200] in a 3 to 1 ratio). Slides were observed with an LSM

700 confocal microscope with DAPI and FITC channels. Pixel intensity per cell was quantified using ImageJ software. IMARIS software was used to create representative 3D images.

2.3.2.3 PGSK

Neonatal cardiomyocytes were plated onto 12 well plates with glass coverslips. Cells were treated with 250µM of $FeCl_3$ for 1 and 24 hours with 0.5% FBS DMEM. 30 minutes prior to end of incubation, cells were incubated with 3µm of Phen Green SK, Diacete (PGSK) (Invitrogen #P14313) dissolved in DMSO, and incubated in a CO_2 incubator at 37ºC for 30 min. Cells were washed 3X with PBS++, and fixed with 4% PFA for 20 minutes. Cells were washed 1X with PBS++ and incubated in 1% glycine for 10 minutes. Cells were washed 3X with PBS++ and mounted onto glass slide with 1 drop mounting medium. Slides were observed with an LSM 700 confocal microscope with DAPI and FITC channels. Pixel intensity per cell was quantified using ImageJ software. IMARIS software was used to create representative 3D images.

2.3.3 Western Blot Analysis

Neonatal cardiomyocytes were seeded in 6 well primaria coated plates. Cells were co-starved with 0.5% FBS DMEM and treated with 250µm of $FeCl_3$ for 24h. 30min prior to iron overload conditions, cells were treated with 1µm of FOXO1 inhibitor AS1842856 (AS) (Emdmillipoe #506081) which was dissolved in DMSO. After treatment, wells were washed 3X with PBS and lysed with 200µl lysis buffer per well. Stock lysis buffer components consisted of 50mM Tris, 0.1% SDS, 30% glycerol. Stock lysis buffer was supplemented with a protease inhibitor cocktail (Calbiochem via VWR #524629) [consisting of Pancreas-extract, Thermolsyin [Metalloprotease], Chymotrypsin, Trypsin, Papain]. 10% of ß-mercaptoethanol, and bromothymol blue was added to stock lysis Buffer with the protease inhibitor cocktail. Lysates were scraped from wells, collected and boiled for 10 minutes at 95ºC, following cooling on ice and storage at -20ºC.

Samples were resolved and separated by Sodium dodecyl sulfate polyacrylamide gel electrophoresis (SDS-PAGE). Gels were run for 2 hours at 100V. Gels were immunoblotted onto methanol activated polyvinylidene fluoride (PVDF) membranes (BioRad #162-0177) at for 1h at 110V. Membranes were blocked with 3% bovine serum albumin (BSA) (Bioshop #ALB001.1) for 1 hour on a rocker at room temperature, and incubated with primary antibody (AdipoR1, AdipoR2, APPL1, APPL2 and FOXO1), 1:1000 dilution in 3% BSA overnight at 4ºC on a rocker. The next day, membranes were washed 3 times with wash buffer containing 1:1000 dilutions of TWEEN 20 (Bioshop #56-40-6) and Nonidet P40 (Bioshop #NON505.500) detergents for 10 minute intervals at room temperature on a rocker. Subsequently, membranes were incubated in secondary horseradish peroxidase (HRP)-conjugated antibody (anti-rabbit or anti-mouse) (1:5000) (Cell Signalling #7074 and #7076, respectively) for 1 hour at room temperature, and then washed 3X. Membranes were incubated in Enhanced chemiluminescence (ECL) reagent (Bio-Rad # 1705061) for 1 minute, placed in a film cassette and exposed with film (GE Health Care via VWR #28906837).

AdipoR1, and AdipoR2 primary antibodies were kindly gifted from AstraZeneca (Sweden). APPL1 antibody was purchased from Antibody Immunoassay Services (AIS, Hong Kong). APPL2 antibody (#H00055 198-B01P) was obtained from Abnova. FOXO1 (#9454S) and β-actin (#4967L) antibodies were obtained from Cell Signalling.

Membranes were re-blotted 1X Re-Blot buffer (Emd Millipore #2504 on a rocker for 20 minutes at room temperature. Membranes were washed 1X for 5 minutes, and re-blocked in 3% BSA for 30 minutes. Membranes were incubated in primary antibody (β-actin) overnight at 4ºC. Developing protocol mentioned previously was followed from this point onward.

Band density was quantified using ImageJ Software, and normalized to appropriate β-actin loading control.

2.3.4 Immunofluorescence

Neonatal cardiomyocytes cells were seeded onto 12 well plates with glass coverslips. Cells were co-starved with 0.5% or 2% DMEM and treated with the following solutions where appropriate: with 250µm of $FeCl_3$ for 24h, 1µm of AS1842856 30 min prior to iron overload conditions, and 20µm of AdRon (AdipoGen® Life Sciences #AG-CR1-0156-M050) for 30min. Cells were washed 3X with PBS++, and fixed with 4% PFA for 20 minutes. Cells were washed 1X with PBS++ and incubated in 1% glycine. Cells were washed 3X with PBS++ and permeabilized with 0.1% TritonX100 for 3mins. Cells were washed with PBS++, and blocked with 3% BSA in PBS++ for 1 hour. Slides were incubated in primary antibody (1:500 in BSA, PBS++) overnight at 4ºC. Slides were washed 3X with PBS++, and incubated in secondary antibody (1:1000 in 3% BSA, PBS++) for 1 hour at room temperature. Cells were washed 4X with PBS++ and mounted onto glass slide with 1 drop of mounting medium. Slides were observed with an LSM700 confocal microscope with DAPI and FITC channels. Pixel intensity per cell was quantified using ImageJ software. IMARIS software was used to create representative 3D images.

Primary antibody pAMPK (Thr 127) (#2531L) and pFOXO1 (Thr24) (#9464L) was obtained from Cell signalling. pP38 MAPK (pThr180/pTyr182) (#44-684G) was obtained from Invitrogen. Secondary anti-rabbit Alexa Fluor 488 conjugate anti-body (#A-11008) was obtained from ThermoFisher Scientific (via VWR).

2.3.5 Glucose uptake

Neonatal cardiomyocytes cells were seeded onto a 24 well plate, and starved with 0% FBS DMEM. Cells were treated with 250µm of $FeCl_3$ for 24h and 20µm of AdRon for 1h prior to the end of iron overload treatments. As a positive control for glucose uptake, cells were treated with 100nm of insulin (Humulin #00586714) for 10 minutes. After treatment, cells were washed

2X with hepes buffer saline (HBS) (140nm NaCl, 20mM Hepes-Na pH=7, 5mM Kcl, 2.5mM $MgSO_4$, 1.0mM $CaCl_2$). For specific glucose uptake, 200µl of transport solution (10uM 2-Deoxy-Glucose, 0.5uCi/ml H^3 2Deoxy-Glucose in HBS [PerkinElmer #800-762-4000]) was added to each well, and incubated for 5 minutes. 10µM of Cytochalasin B (Sigma #C6762) was used for non-specific uptake. Transport solution was aspirated, and wells were washed 3X with ice-cold, 0.9% saline solution (Bioshop #SOD002.5). 200µl of KOH (Bioshop #PHY202.500) was used to lyse cells. 1:20 dilution of lysate:scintillation fluid (National Diagnostics #02010193) was made for a total volume of 3ml. Samples with scintillation fluid were placed into scintillation vials for radioactive counting. Samples were corrected for protein using a bradford assay (Bio-Rad #500-0006) which was measured at 595nm.

2.3.6 *In vivo* Iron Overload Mouse Model

Six 8 week C57 male mice (*Mus musculus*) were intraperitoneally (IP) injected with 10mg/g of ferrous form iron dextran (Santa Cruz #sc-215191) diluted in 0.9% saline for 4 weeks, 5 days per week. Six control mice were injected with 10% dextrose (J.T. Baker#1916-01). The following samples were collected post-sacrifice: heart, soleus, gastrocnemius, tibialis anterior, liver, pancreas, spleen, adipose, brain and serum, and frozen using liquid nitrogen. Samples were stored in -80ºC.

Heart tissues were lysed with RIPA buffer (30mM Hepes pH 7.4, 2.5mM EGTA, 3mM EDTA, 70mM KCl, 20mM β-glycerolphosphate, 20mM NaF, 1Mm Na_3VO_4, 200µM PMSF, 1µM Pepstatin A, 10µM Et64, 1µM Leupeptin, 0.1% NP40, 0.1mM Okadaic acid) and homogenized. Lysates were centrifuged at 10,000RPM for 10mins at 4ºC. Protein concentration of lysates was measured and corrected using a colometric protein assay kit (ThermoFisher #23225). 50µg of protein was loaded into each well. Western blot protocol was followed as previously described.

AdipoR1, and AdipoR2 primary antibodies were kindly gifted from AstraZeneca (Sweden). APPL1 antibody was purchased from Antibody Immunoassay Services (AIS, Hong Kong). APPL2 antibody (#H00055 198-B01P) was obtained from Abnova. FOXO1 (#9454S) and β-actin (#4967L) antibodies were obtained from Cell Signalling.

2.3.6.1. Prussian blue staining

Fresh heart tissues were preserved in tissue freezing medium (Electron Miscroscopy Sciences# 72592) and cut into 10µm slices via cryosectioning. Cryosections were sent to London Health Sciences Centre at University Hospital, London, ON, for Prussian blue staining.

2.3.6.2. Echocardiography

Echocardiography was performed using the Vevo2100 system (Visual Sonics) equipped with an MS550D transducer. Mice were lightly anesthetized using 2.0% isofluorane mixed with 100% O_2 during the time of imaging. M-mode images of the parasternal short-axis view at papillary level were used to calculate the cardiac systolic functions of ejection fraction, fractional shortening and cardiac output. Speckle-tracking cardiac strain analysis was performed using VevoStrain software and movie files acquired were from the B-mode and M-mode view. All parameters were averaged over at least 3 cardiac cycles for analysis.

3.3.7. Statistical Analysis

Statistical analysis between two groups was done using an unpaired two-tailed t-test. P values less than 0.05 were accepted as significant.

2.4 Results

2.4.1. Characterizing intracellular iron overload and cell viability in NeoCM

To characterize an iron overload model in neonatal cardiomyocytes (NeoCM), cells were treated with 250µM of ferric iron for 0, 1 and 24h. At 30min before prior to the end of treatment time, 3µm of Phen Green™ SK (PGSK) - a fluorescent indicator - was added to cells. Upon the presence of heavy metals, PGSK becomes quenched, resulting in a decrease in green fluorescence. This was shown by a gradual decrease in PGSK fluorescence at 1h of iron treatment time compared to 0h control. Moreover, a significant decrease of PGSK fluorescence was observed at 24h compared to 0h of iron treatment (**Figure 2.1 A-C**). Iron overload induced iron response element (IRE) activation was also investigated in NeoCM to characterize intracellular iron regulation. Cells were transfected with a plasmid which encodes a ferratin promoter containing an IRE hairpin stem loop. Upon activation of IRE via iron overload conditions, cyan fluorescent protein (CFP) is transcribed and acts as a detectable readout of IRE activity. Following 24h treatment of iron, a 3.5 fold increase in CFP was observed in iron overload conditions compared to control (**Figure 2.1 D-F)**. Together, these results indicate iron can directly enter NeoCM, and activate intracellular iron regulatory processes.

Cell viability was confirmed using an MTT assay. This assay measures cell metabolic activity by measuring NADPH (Nicotinamide adenine dinucleotide phosphate)-dependent cellular oxidoreductiase enzymes which are known to reduce MTT dye. Following this reaction, the resulting product becomes detectable at 595nm. NeoCM were treated with 0, 100, and 250µM of iron overload for 24h, following the addition of 5mg/ml of MTT 5h prior to end of incubation. Results show no change in cell viability with 100µM and 250µM iron overload compared to control conditions (**Figure 2.1**).

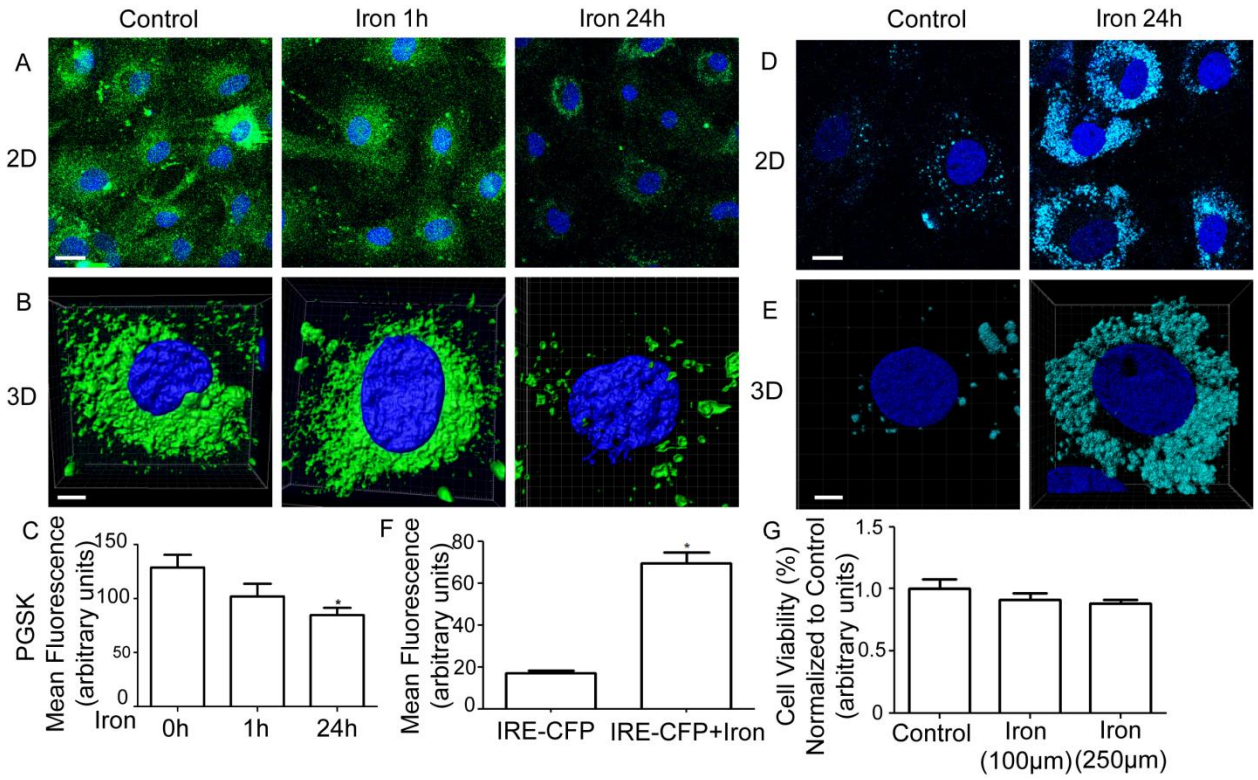

Figure 2.1: Characterizing intracellular iron overload *ex vivo*.
(A-C) Iron overload conditions quenched PGSK probe over time, resulting in less green fluorescence. NeoCM were treated with 250µM of $FeCl_3$ for 0, 1 and 24h. 30min prior to end of incubation, 3µM of PGSK probe was added to cells. Green fluorescence was observed via FTIC channels by confocal microscopy (n=3). A) 2D representative image taken using ZEN software (Scale bar: 1µm). B) 3D representative images created using IMARIS software (Scale bar: 5µm). C) 3-5 fields of view were taken per condition. All cells in field of view were traced and quantified using ImageJ software. Mean intensity values per cell were averaged and plotted for analysis. Statistical analysis was compared to 0h. (* = $P < 0.05$). Error bars display standard error of the mean.
(D-F) Increased iron response element activity was observed under iron overload conditions. NeoCM were transfected with IRE-CFP plasmid, and treated with 250µM of $FeCl_3$ for 24h (n=3). Transcribed cyan fluorescent protein was observed via FTIC channels by confocal microscopy. D) 2D representative image taken using ZEN software (Scale bar: 1µm). E) 3D representative images created using IMARIS software (Scale bar: 5µm). F) 3-5 fields of view were taken per conditions. All cells in field of view were traced and quantified using ImageJ software. Mean intensity values per cell were averaged and plotted for analysis. Statistical analysis was compared to IRE-CFP. (* = $P < 0.05$). Error bars display standard error of the mean.
(G) No significant change in cell viability was observed under iron overload conditions of varying concentrations. NeoCM were treated with 0, 100 and 250µM of $FeCl_3$ 24h. 5h prior to end of incubation, 5mg/ml of MTT was added to cells. Absorbance was measured at 595nm,

and absorbance values were normalized to average of controls (n=3). Statistical analysis was compared to control. Error bars display standard error of the mean.

2.4.2 Iron overload induced adiponectin resistance via adiponectin sensitivity in NeoCM

Following the characterization of intracellular iron overload in NeoCM, adiponectin sensitivity was examined to investigate iron overload induced adiponectin resistance. This was examined by AdRon induced adiponectin signalling via pAMPK and pP38 MAPK signalling molecules. Neonatal cardiomyocytes were treated with iron overload for 24h, followed by AdRon treatment for 30min prior to end of iron overload treatment time. Immunofluorescence featuring pAMPK and pP38 MAPK antibodies was used to investigate changes in adiponectin signalling under these conditions. A significant increase in pAMPK was observed in AdRon conditions compared to basal levels. However, when AdRon was added to iron overload conditions, a significant decrease in pAMPK stimulation was observed compared to AdRon in normal conditions (**Figure 2.2 A-C**). The same trend was also confirmed with pP38 (**Figure 2.2 D-F**). AdRon stimulated glucose uptake - another method of adiponectin action - was used to investigate any adiponectin resistance occurring under iron overload conditions. NeoCM cells treated with iron overload conditions, and later stimulated with AdRon for 30min prior to end of iron overload treatment. This resulted in an increase in glucose uptake was observed in AdRon conditions, while iron overload conditions showed no effect compared to basal levels. Moreover, when AdRon was added to iron overload conditions, a significant decrease in glucose uptake was observed compared to AdRon in normal conditions (**Figure 2.2 G**). Overall, these results show iron overload induced adiponectin resistance via pAMPK and pP38 stimulation, as well as via glucose uptake in NeoCM.

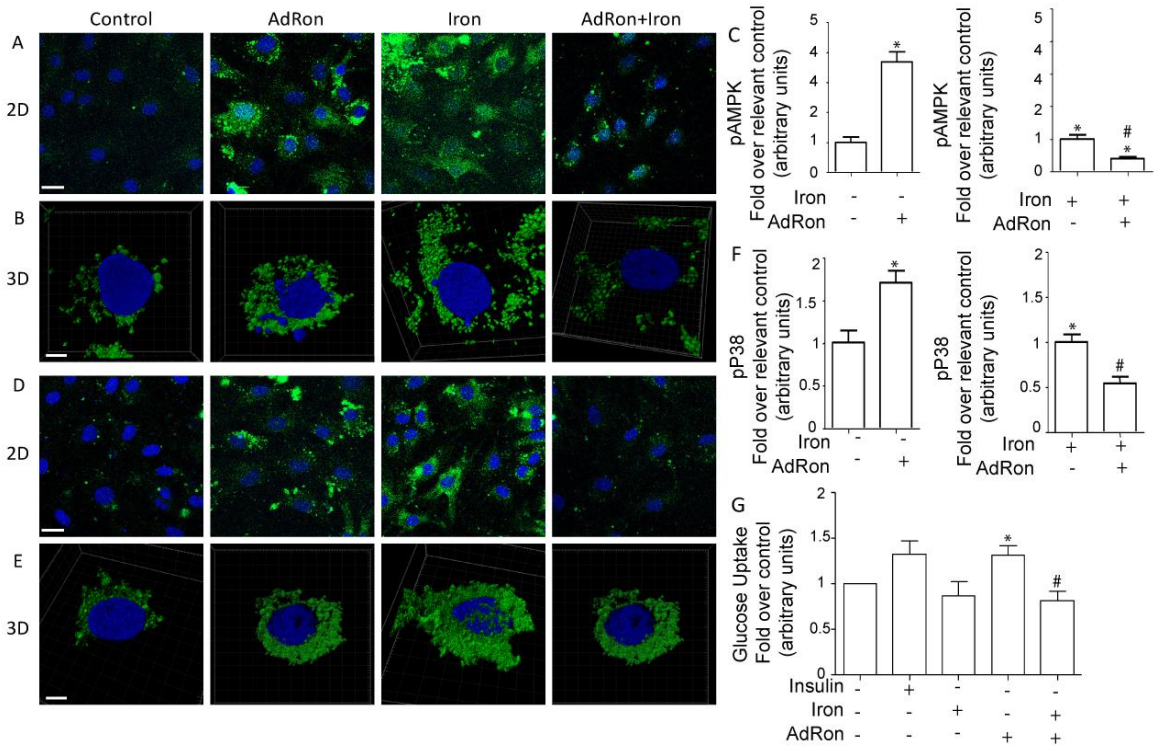

Figure 2.2: Adiponectin resistance was observed via AdRon induced adiponectin signaling (pAMPK and pP38 MAPK) and AdRon stimulated metabolism via glucose uptake.

(A-C) Iron overload decreased adiponectin sensitivity by AdRon induced pAMPK stimulation. NeoCM were treated with 250µM of $FeCl_3$ for 24h, and 20µM AdRon for 30min prior to end of treatment time. Cells were incubated in pAMPK (Thr172) primary antibody, and subsequently incubated in Alexa 488 secondary antibody. Green fluorescence was observed via FTIC channels by confocal microscopy (n=3). A) 2D representative image taken using ZEN software (Scale bar: 1µm). B) 3D representative images created using IMARIS software (Scale bar: 5µm). C) 3-5 fields of view were taken per condition. All cells in field of view were traced and quantified using ImageJ software. Mean intensity values per cell were averaged, and normalized to appropriate control (Raw mean intensity values - Control: 8.288203, AdRon: 30.33062, Iron: 51.51557, Iron+AdRon: 19.31903). Statistical analysis was compared to control. (* = $P < 0.05$) and AdRon conditions (# = $P < 0.05$). Error bars display standard error of the mean.

(D-F) Iron overload decreased adiponectin sensitivity by AdRon induced pP38 MAPK stimulation. NeoCM were treated with 250µM of $FeCl_3$ for 24h, and 20µM AdRon for 30min prior to end of treatment time. Cells were incubated in pP38 MAPK (Thr180/Tyr182) primary antibody, and subsequently incubated in Alexa 488 secondary antibody. Green fluorescence was observed via FTIC channels by confocal microscopy (n=3). D) 2D representative image taken using ZEN software (Scale bar: 1µm). E) 3D representative images created using IMARIS software (Scale bar: 5µm). F) 3-5 fields of view were taken per condition. All cells in field of view were traced and quantified using ImageJ software. Mean intensity values per cell were averaged, and normalized to appropriate control (Raw mean intensity values – Control: 32.29259, AdRon: 55.0053, Iron: 71.82387, Iron+AdRon: 38.91023). Statistical analysis was compared to control. (* = $P < 0.05$) and AdRon conditions (# = $P < 0.05$). Error bars display

standard error of the mean.
(G) Iron overload decreased adiponectin signalling by AdRon induced glucose uptake. NeoCM were treated with 250µm of $FeCl_3$ for 24h, and 20µM of AdRon 1h prior to end of treatment time. As a positive control, NeoCM were stimulated with 100nM of insulin for 10 minutes. Cells were treated with radioactive H^3 2 deoxy-D-(3H) – glucose for 5min. Cells were lysed, collected for scintillation counting, and corrected for protein concentration. (n=4).Statistical analysis was compared to control (* = P <0.05) and compared to AdRon (# = P <0.05). Error bars display standard error of the mean.

2.4.3 Iron overload regulation by FOXO1 in NeoCM

Next, it was proposed that iron overload regulation is controlled via FOXO due to analysis of previous literature. FOXO1 regulation itself is dependent on post-translational modifications which in turn result in a change in cellular localization. Iron overload regulation by FOXO1 was investigated by immunofluorescence featuring total FOXO1 and pFOXO1 (Thr24). NeoCM cells were treated with iron overload for 24h, fixed and stained with either total FOXO1 and pFOXO1 (Thr24). Results showed a significant increase in total FOXO1 expression by a 3.5 fold (**Figure 2.3 A-C**). Moreover, a 30 fold increase in pFOXO1 (Thr24) was observed compared to basal levels (**Figure 2.3 D-F**). Overall, these results show that iron overload causes a significant increase in cytoplasmic localization via an increase in pFOXO1. Moreover, iron overload also caused a significant increase in overall protein expression shown by an increase in total FOXO1.

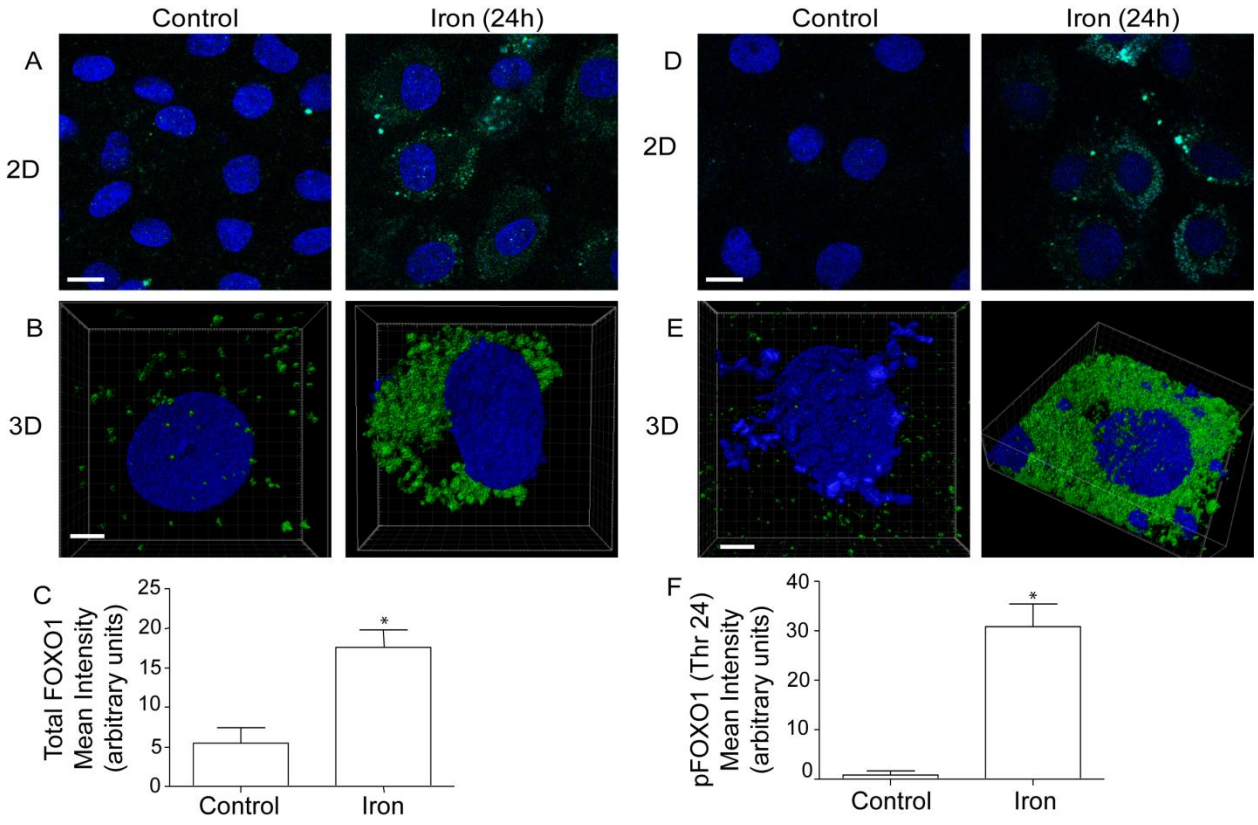

Figure 2.3: Iron overload regulation by FOXO1.
(A-C) Iron overload increased FOXO1 expression. NeoCM were treated with 250µM of $FeCl_3$ for 24h. Cells were incubated in total FOXO primary antibody, and subsequently incubated in Alexa 488 secondary antibody. Green fluorescence was observed via FTIC channels by confocal microscopy (n=3). A) 2D representative image taken using ZEN software (Scale bar: 1µm). B) 3D representative images created using IMARIS software (Scale bar: 5µm). C) 3-5 fields of view were taken per condition. All cells in field of view were traced and quantified using ImageJ software. Mean intensity values per cell were averaged, and normalized to control. Statistical analysis was compared to control. (* = $P < 0.05$). Error bars display standard error of the mean.
(D-F) Iron overload increased pFOXO1 (Thr24) regulation. NeoCM were treated with 250µM of $FeCl_3$ for 24h. Cells were incubated in pFOXO1 (Thr24) primary antibody, and subsequently incubated in Alexa 488 secondary antibody. Green fluorescence was observed via FTIC channels by confocal microscopy (n=3). D) 2D representative image taken using ZEN software (Scale bar: 1µm). E) 3D representative images created using IMARIS software (Scale bar: 5µm). F) 3-5 fields of view were taken per condition. All cells in field of view were traced and quantified using ImageJ software. Mean intensity values per cell were averaged, and normalized to control. Statistical analysis was compared to control. (* = $P < 0.05$). Error bars display standard error of the mean.

2.4.4 Iron overload induced adiponectin resistance regulation by FOXO1 in NeoCM

After confirming FOXO1's a role in iron overload regulation, the potential regulation of iron overload induced adiponectin resistance by FOXO was examined. This was investigated using the FOXO inhibitor, AS1842856, which prevents FOXO-DNA binding, and ultimately preventing transcription. Anti-pAMPK (Thr172) immunofluorescence analysis was used to investigate the effects of iron overload induced adiponectin resistance regulation by FOXO inhibition. NeoCM were treated with AS1842856 30min prior to iron overload for 24h, following a 30min AdRon treatment prior to end of iron overload. As shown previously, AdRon increased pAMPK stimulation significantly compared to control, however this affect was reduced upon iron overload conditions. Further, AS1842856 treatment had no significant effect on pAMPK levels. However, when combined with iron and AdRon, AS1842856 treatment alleviated iron overloads' effects on AdRon, resulting in a significant increase of pAMPK back to AdRon only conditions. This was also shown by a significant increase in pAMPK in iron, AdRon and AS1842856 conditions compared to iron and AdRon conditions only (**Figure 2.4 A-C**). Overall, this effect confirms FOXO1's role in iron overload induced adiponectin resistance regulation.

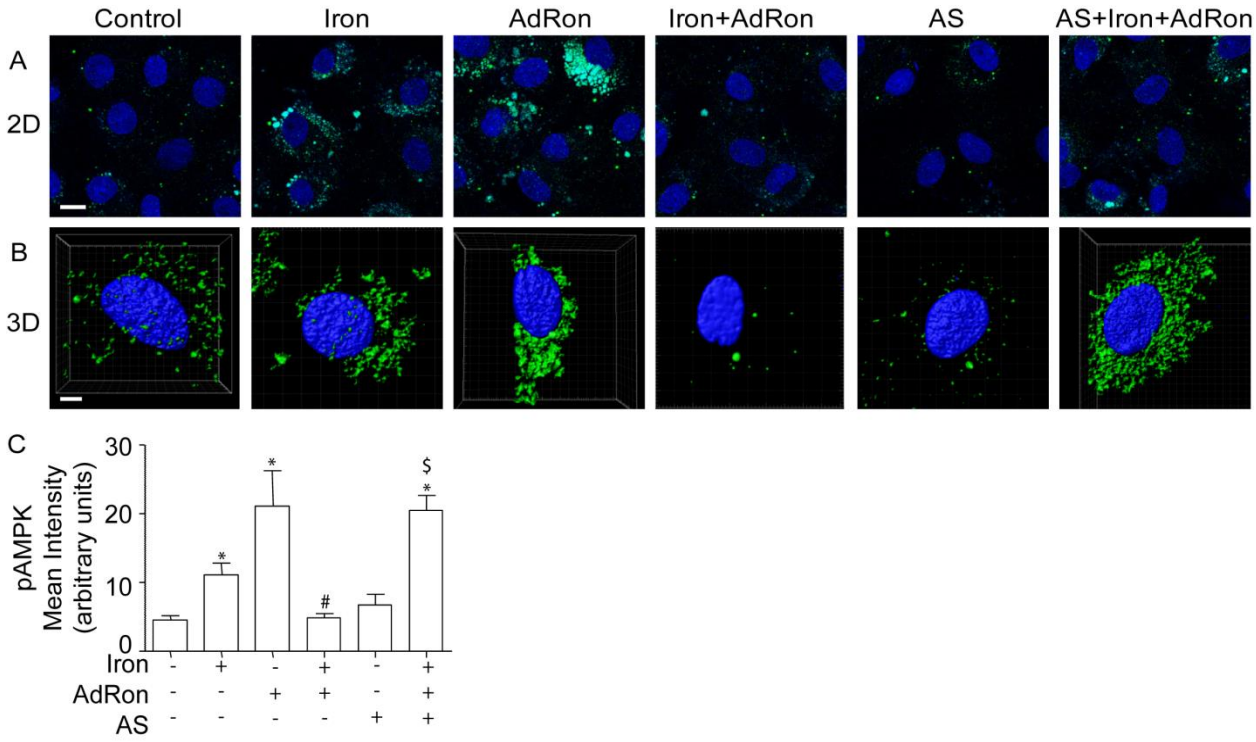

Figure 2.4: Iron overload induced adiponectin resistance regulation by FOXO1. NeoCM were treated with 250µM of $FeCl_3$ for 24h, and 20µM of AdRon for 30min prior to end of treatment time. 30min prior to iron incubation, cells were treated with 1µM of FOXO inhibitor, AS1842856. Cells were incubated in pAMPK (Thr172) primary antibody, and subsequently incubated in Alexa 488 secondary antibody. Green fluorescence was observed via FTIC channels by confocal microscopy (n=3). A) 2D representative image taken using ZEN software (Scale bar: 1µm). B) 3D representative images created using IMARIS software (Scale bar: 5µm). C) 3-5 fields of view were taken per condition. All cells in field of view were traced and quantified using ImageJ software. Mean intensity values per cell were averaged, and normalized to control. Statistical analysis was compared to control (* = $P < 0.05$), AdRon (# = $P < 0.05$) or Iron+AdRon ($ = $P < 0.05$). Error bars display standard error of the mean.

2.4.5 Iron overload induced adiponectin resistance via adiponectin signalling in NeoCM

Next, iron overload induced adiponectin resistance was investigated by examining adiponectin receptor levels as well as other downstream targets of adiponectin signalling. FOXO1 inhibitor, AS1842856, was used to examine any changes in gene expression of adiponectin signalling molecules, and to observe its effects on iron overload induced adiponectin resistance regulation. NeoCM were treated with AS1842856 30min prior to 24h iron overload conditions. Western blot analysis was used to examine the expression of the following proteins: AdipoR1, APPL1, AdipoR2 and APPL2. Under iron overload conditions, a significant decrease in AdipoR1 and APPL1 was observed. Additionally, APPL2 also showed a decrease in expression by approximately 50% compared to control levels. However, AdipoR2 gene expression did not change under iron overload conditions. Furthermore, no changes in gene expression in AdipoR1, APPL1, AdipoR2 and APPL2 were evident using FOXO1 inhibitor, AS1842856 (**Figure 2.5 A-E**). Therefore, no further alleviatory effect with iron and AS1842856 conditions were observed. Overall, this data confirms iron overload induced adiponectin resistance occurs via reduced adiponectin signalling molecule expression levels. Conversely, FOXO1 may not play a regulatory role in iron overload induced adiponectin resistance regulation on the level of adiponectin signalling protein expression.

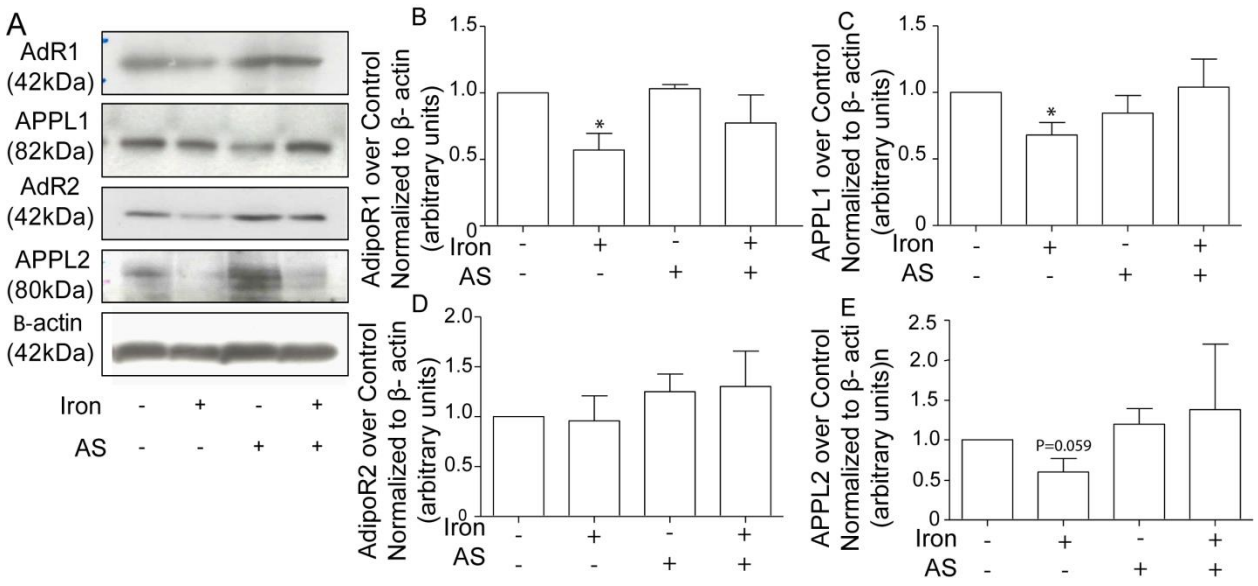

Figure 2.5: Iron overload induced adiponectin resistance regulation by FOXO via adiponectin signalling. NeoCM were treated with 250µM of $FeCl_3$ for 24h, and 1µM AS1842856 30min prior to iron overload incubation. Cells were lysed, proteins of interest were analyzed by Western blotting. Proteins of interest were tagged with the following primary antibodies: AdipoR1, APPL1, AdipoR2, APPL2 and β-actin, which were subsequently tagged with HRP-conjugated secondary antibodies (n=4/7). A) Representative western blots of AdipoR1, APPL1, AdipoR2, APPL2 and β-actin. (B-E) Quantitative representation of AdipoR1, APPL1, AdipoR2 and APPL2. Western blot band intensity was quantified using ImageJ software, normalized to β-actin, and further normalized to control. Statistical analysis was compared to control conditions (* = $P < 0.05$). Error bars display standard error of the mean.

2.4.6. *In vivo* iron overload induced adiponectin resistance in the heart

Cardiac iron overload induced adiponectin resistance was further examined via an *in vivo* iron overload mouse model. Male C57 mice of 8 weeks were IP injected with 10mg/g of ferrous iron for 4 weeks, 5 days per week. To characterize the presence iron overload in this mouse model, Prussian blue staining of heart tissue cryosections was conducted. An increase in Prussian blue staining was observed in iron overload mice compared to control mice, confirming the ability of iron to reach the target tissues (**Figure 2.6 A-B**).

Next, western blot analysis was used to examine the protein expression of AdipoR1, APPL1, AdipoR2, APPL2 and FOXO1 (**Figure 2.7 A-F**). No changes were evident in AdipoR1 and APPL1 expression. However, a significant increase by approximately two fold was seen in AdipoR2. Conversely, a very significant reduction in APPL2 by approximately 90% was seen in iron overload mice compared to control. No significant changes in FOXO expression were evident in iron overload mice compared to control. In conclusion, this model suggests altered adiponectin regulation via a significant reduction in APPL2 expression.

2.4.6.1. Echocardiography

Further characterization and analysis by echocardiography was used to investigate any cardiac dysfunction in iron overload conditions. Overall body weight was significantly reduced in iron overload (**Figure 2.7 A**). Additionally, a significant decrease in heart rate (**Figure 2.7 B**) and cardiac output (**Figure 2.7 D**) was also observed. No significant changes were seen in posterior wall thickness (**Figure 2.7 B**), ejection fraction, fractional shortening, left ventricular (LV) mass and stroke volume (**Figure 2.7 E-H**). Furthermore, no changes in strain peak (PK)/strain rate were observed (**Figure 2.7 I-J**), however a significant increase was observed in maximal opposing wall delay strain/maximal opposing wall delay (**Figure K-L**). In conclusion, results indicate cardiac dysfunction in iron overload mice compared to control.

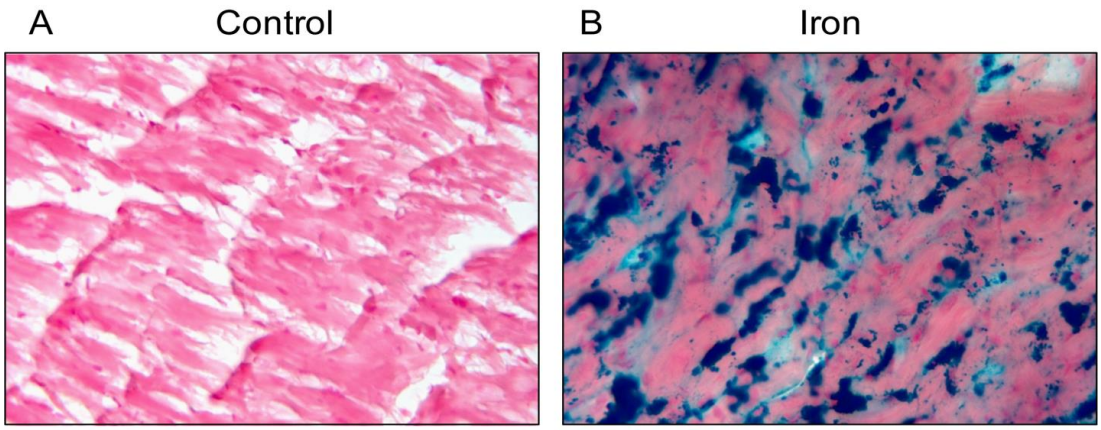

Figure 2.6: Characterizing iron overload in vivo. Iron overload mice display increased amount of Prussian blue staining compared to control. 8 week C57 male mice were IP injected with 10mg/g of ferrous iron. Heart tissue cryosections were stained with prussian blue and analyzed by histopathology. (n=3). A) Representative image of control mice. B) Representative image of iron overload mice. Original magnification X100 for all micrographs.

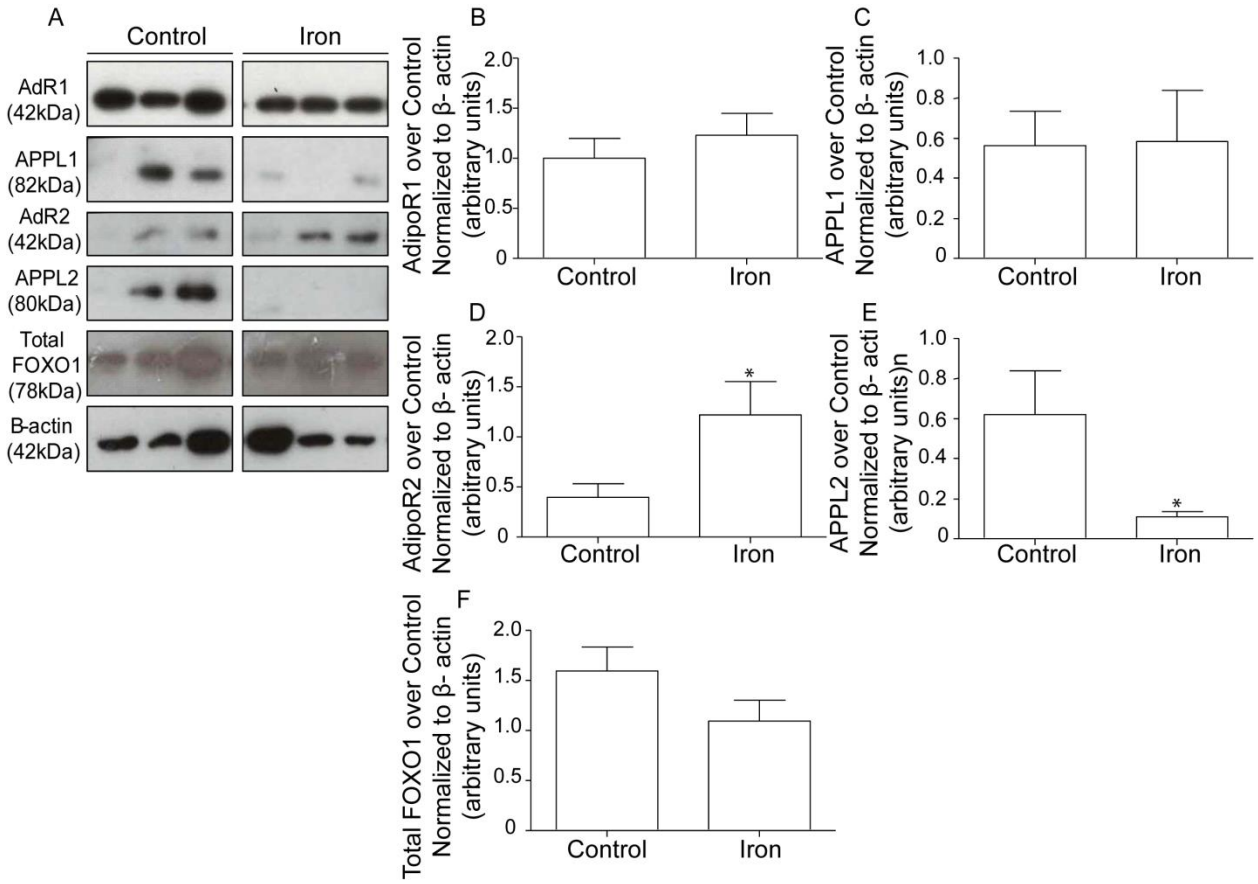

Figure 2.7: Iron overload altered adiponectin signalling *in vivo* via changes in expression of adiponectin signalling proteins. 8 week C57 male mice were IP injected with 10mg/g of ferrous iron. Heart tissues were lysed, proteins of interest were analyzed by Western blotting. Proteins of interest were tagged with the following primary antibodies: AdipoR1, APPL1, AdipoR2, APPL2, total FOXO1 and β-actin, which were subsequently tagged with HRP-conjugated secondary antibodies (n=6). A) Representative western blots of AdipoR1, APPL1, AdipoR2, APPL2, total FOXO1 and β-actin. (B-F) Quantitative representation of AdipoR1, APPL1, AdipoR2, APPL2 and total FOXO1. Western blot band intensity was quantified using ImageJ software, normalized to β-actin, and further normalized to control. Statistical analysis was compared to control conditions (* = $P < 0.05$). Error bars display standard error of the mean. Note: For uncut Western blots, see Appendix A: A3.

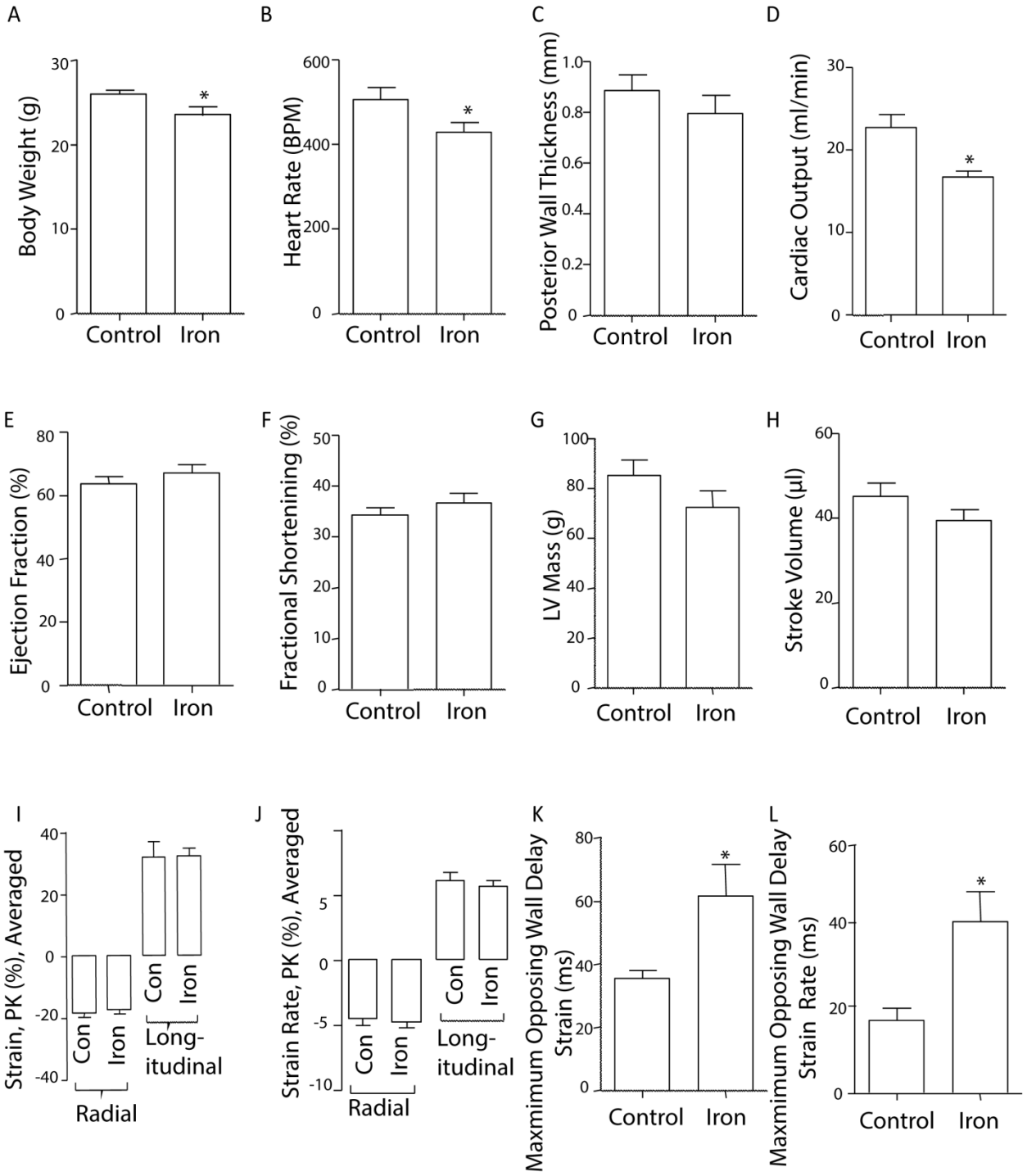

Figure 2.8: Iron overload induced mice display cardiac dysfunction via echocardiography. Figures display representative graph of A) body weight, B) heart rate, C) posterior wall thickness, D) cardiac output, E) ejection fraction, F) fractional shortening, G) LV mass, H) stroke volume, I) strain PK, J) strain rate K) maximal opposing wall delay strain, and L) maximal opposing wall delay strain rate. M-mode images of the parasternal short-axis view at papillary level were used to calculate the cardiac systolic functions of ejection fraction,

fractional shortening and cardiac output. Speckle-tracking cardiac strain analysis was performed using VevoStrain software (n=4). All parameters were averaged over at least 3 cardiac cycles for analysis. Statistical analysis was compared to control conditions (* = $P < 0.05$). Error bars display standard error of the mean.

2.5. Discussion

2.5.1. Iron accumulates in NeoCM and activates IREs

The validation of iron overload in NeoCM was essential prior to examining the possibility of iron overload induced adiponectin resistance. PGSK, a green-fluorescent indicator, was used to characterize intracellular iron in a time-dependent manner. When iron binds to PGSK, green-fluorescence becomes quenched[111]. Results indicate that iron overload quenches, which was observed by a gradual time dependent decrease in green fluorescence from 0h to 24h (**Figure 2.1 A-C**). An IRE-CFP reporter construct was also used to confirm functional effectiveness of iron delivered to cells. Iron overload conditions activated IRE regulatory elements, suggesting an increase in ferritin regulation and thus confirming iron overload conditions in NeoCM [112](**Figure 2.1 D-F**). Moreover, the cell viability of iron overload induced NeoCM was examined with an MTT assay. This assay is based on the conversion of MTT into formazan crystals by NAD(P)H-dependent cellular oxidoreductase enzymes in living cells, which is a direct measure of mitochondrial activity, and is commonly used as a readout of cell viability[113]. As no significant change in cell viability was observed using 100µM and 250µM of $FeCl_3$ during 24h, a concentration of 250µM was used to induce iron overload in future experiments (**Figure 2.1 G**); a concentration previously used in cell culture iron overload studies[114]. To conclude, iron overload conditions in NeoCM did not induce cell death. Moreover, PGSK and IRE-CFP assays confirm the ability of iron to enter the cell, as well as initiate changes in iron regulatory response elements, respectively.

2.5.2 Iron overload induced adiponectin resistance via adiponectin sensitivity and action in NeoCM

AMPK and P38 MAPK are down-stream targets of AdipoR1 and AdipoR2, and are both known to be stimulated by adiponectin[53] and AdRon[77]. In NeoCM, stimulation of pAMPK and pP38 via AdRon was used as a direct readout of adiponectin sensitivity. Using immunofluorescence based pAMPK and pP38 detection, the investigation of iron overload induced adiponectin resistance was examined by observing changes in levels of green fluorescence (**Figure 2.2 A-C and 2.2 D-F**). pAMPK and pP38 levels significantly increased with AdRon as expected. This confirms AdRon's ability to stimulate adiponectin signalling in this experimental model[77]. However, combined with iron overload, AdRon stimulated pAMPK and pP38 levels were significantly reduced. This lack in adiponectin signalling due to iron overload conditions is the first evidence of iron overload induced adiponectin resistance in NeoCM. This is supported by a previous study whereby adiponectin resistance in chronic heart failure has been characterized by a decrease in pAMPK levels[84]. Somewhat unexpectedly, pAMPK and pP38 levels also increased in iron overload only conditions. pAMPK mediates majority of all aspects of cellular regulation, therefore cross-talk between various signalling pathways are likely initiated by pAMPK[115]. For instance, iron has been previously shown to activate pAMPK in HF diet mice, suggesting iron plays a role in the regulation of pAMPK glucose metabolism[116]. Additionally, iron has also been shown to regulate pP38 activation via various inflammatory pathways[117]. To conclude, iron overload induced adiponectin resistance.

Glucose uptake, another direct readout of adiponectin action, was also used to examine iron overload induced adiponectin resistance in NeoCM. Adiponectin and AdRon have been previously shown to stimulate glucose uptake on multiple occasions[16,77]. Previous studies have also used glucose uptake as a method to investigate the mechanisms of adiponectin resistance[84]. As expected, AdRon significantly increased glucose uptake in NeoCM compared

to control conditions (**Figure 2.2 G**). Moreover, no change in glucose uptake was observed in iron overload, as compared to control conditions. However, iron overload and AdRon conditions together reduced glucose uptake compared to AdRon only conditions. This data further supports that iron overload conditions suppress AdRon action via glucose uptake[84], suggesting iron overload induced adiponectin resistance.

2.5.3 FOXO1 regulates iron overload in NeoCM

Iron overload induced adiponectin resistance in the heart is a phenomenon that is poorly characterized and thus its mechanisms are also poorly understood. I hypothesized that FOXO1 is involved in iron overload induced adiponectin resistance regulation. Thus, it was necessary to first characterize FOXO1's role in iron overload conditions. This was done by examining FOXO1 expression and pFOXO1 stimulation under iron overload via immunofluorescence. An increase in total FOXO1 expression, and also pFOXO1 stimulation was evident under iron overload (**Figure 2.3 A-C** and **2.3 D-F**). This is significant as iron has been previously shown to modulate the post-translational profiles of FOXO1 by specifically regulating its phosphorylation via reactive oxygen species (ROS) production[118,119,120].

2.5.4. FOXO1 regulates iron overload induced adiponectin resistance in NeoCM

After characterizing iron's ability to regulate FOXO1, the role of FOXO1 mediated iron overload induced adiponectin resistance was investigated by examining adiponectin sensitivity via adiponectin signalling. FOXO1 mediated regulation of iron overload induced adiponectin resistance was examined using a FOXO1 inhibitor, AS1842856, which works by directly binding to active FOXO1[121]. First, anti-pAMPK immunofluorescence was used to investigate the role of FOXO1 in iron overload induced adiponectin resistance (**Figure 2.4 A-C**). As previously shown, iron overload induced adiponectin resistance occurs by reduced pAMPK stimulation in iron and AdRon conditions compared to AdRon only conditions. AS1842856 had no affect on pAMPK

stimulation compared to control. However, when added to iron and AdRon conditions, pAMPK levels were similar to AdRon only conditions. This suggests that FOXO1 plays a role in regulating iron overload induced adiponectin resistance, and when FOXO1 is inhibited, AdRon stimulated adiponectin signalling is alleviated from iron overload's affects. This data is supported by iron overload induced adiponectin resistance regulation in adipoctyes[122]. Previous literature has suggested the regulation of iron overload induced adiponectin resistance via FOXO1 transcription factor regulation[122].

Moreover, FOXO1 inhibitor AS1842856 was used to investigate FOXO1 mediated iron overload induced adiponectin resistance via regulation of critical adiponectin signalling molecules (**Figure 2.5 A-E**). Under iron overload conditions, a significant decrease in AdipoR1 and APPL1 was observed. APPL2 also showed insignificant decrease in expression compared to control levels. Moreover, no significant changes in AdipoR2 gene expression were observed. These findings support the iron overload induced adiponectin resistance hypothesis via adiponectin signalling molecule gene expression. This is supported by previous literature whereby adiponectin resistance is observed by a decreased in AdipoR1[84], as well as APPL1 - an AdipoR1 and AdipoR2 stimulator[54]. Furthermore, no changes in gene expression of AdipoR1, APPL1, AdipoR2 and APPL2 were evident using FOXO1 inhibitor, AS1842856 (**Figure 2.5 A-E**). Therefore, there was no further alleviatory effect provided by AS1842856, which was previously seen with pAMPK (**Figure 2.4 A-C**). FOXO1 may not play a regulatory role in iron overload induced adiponectin resistance regulation on the level of adiponectin signalling protein expression as expected, and it may be regulated by an alternate mechanism other than FOXO1. Overall, no definitive conclusions can be made regarding the regulation of iron overload induced adiponectin resistance on the level of adiponectin signalling protein expression, and further investigations are required to elucidate the exact mechanisms.

However, these results support my hypothesis, whereby FOXO1 regulates iron overload induced adiponectin resistance via adiponectin sensitivity.

2.5.5. Iron overload altered myocardial adiponectin signalling in mouse model

After characterizing iron overload induced adiponectin resistance in NeoCM, an *in vivo* iron overload mouse model was investigated to further examine the presence of adiponectin resistance in the heart. Iron overload induced adiponectin regulation has not been well-studied in IP injected iron overload mouse models.

First, Prussian blue staining was used to characterize cardiac iron accumulation in iron overload mice. Prussian blue staining utilizes a histochemical reaction involving hydrochloric acid and potassium ferrocyanide. Following the release of $FeCl_3$ with hydrochloric acid, the combination with ferrocyanide results is a blue colour, also known as Prussian blue[123]. Ultimately, Prussian blue staining displayed cardiac iron accumulation in iron overload mice compared to control mice, confirming an iron overload model (**Figure 2.6 A-B**).

Next, Western blot analysis of AdipoR1, APPL1, AdipoR2 and APPL2 was conducted in order to examine iron overload induced changes in gene expression. A reduction in AdipoR1 and APPL1 was not evident in iron mice compared to control mice as expected (**Figure 2.7 A-C**). Moreover, an increase observed in AdipoR2 and a significant loss in APPL2. As APPL2 competitively binds to APPL1 to compete for AdipoR1 and AdipoR2 binding, a loss in APPL2 may suggest an up-regulation in adiponectin receptor action via APPL1 activation[58]. Previous literature supports the potential of iron overload increased adiponectin signalling via an increase in adiponectin monomer in dietary iron overload mice[122]. Conversely, another study examining iron fed mice showed reduced adiponectin compared to control mice, while also showing that mice with hereditary hemochromatosis displayed increased levels of adiponectin[122]. Therefore, further investigation is required to understand iron overloads role in adiponectin signalling

regulation in *in vivo* models. Moreover, adiponectin signalling regulation was also observed via Western blot analysis by observing FOXO1 expression levels. No changes in FOXO1 expression were evident in iron overload mice compared to control, thus no strong conclusions on adiponectin signalling can be made and require further investigation.

Further analysis of heart tissue adiponectin levels in IP injected iron overload mice should be assessed in order to confirm these findings. This model does not confirm adiponectin resistance hypothesis as seen in NeoCM, however it does suggest that adiponectin regulation is altered by iron overload conditions. This level of altered adiponectin action by iron overload is a phenomenon that involves further investigation. Thus, I am proposing iron overload induced adiponectin regulation is dependent on the level and timing of iron overload. Although iron overload has been characterized in both *ex vivo* and *in vitro* models, the level of iron overload is something that is greatly misunderstood. As mentioned previously, earlier studies have confirmed the presence both iron overload induced adiponectin resistance, as well as iron overload induced adiponectin signalling up-regulation. Therefore, this balance of adiponectin action may greatly depend on the severity of iron overload. For instance, it is well characterized that adiponectin is cardioprotective against heart disease[108,109,110], however several cases have suggested otherwise[8,9,124]. Therefore, it is further hypothesized that adiponectin resistance could occur under mild instances of iron overload while an up-regulation of adiponectin signalling is required to alleviate the affects of chronic iron overload. To conclude, understand the regulation of iron overload on a spectrum, rather than an "on and off" state, is essential to comprehend iron overload's effects on cardiac metabolism.

2.5.5.1. Iron overload causes altered cardiac functioning

Further characterization and analysis of iron overload induced altered cardiac function was examined by echocardiography. First, we observed that a significant decrease in overall

body weight was evident in iron overload mice. Previous literature has indicated a link between hemochromatosis patients and weight loss. Moreover, iron overload mice have also previously shown to have reduced body weight in iron fed mice, but in mice not with hereditary hemochromatosis[122]. Moving onto cardiac function, iron overload mice showed a significant decrease in heart rate and cardiac output, which could be explained as a compensatory mechanism for the reduced trend in LV mass. These results are consistent with clinical cases, whereby young thalassemia patients were also found to have a decreased heart rate, which they proposed as a potential contributor to cardiac disease[125]. No significant changes were seen in posterior wall thickness, ejection fraction, fractional shortening, and stroke volume. These results are similar to a study whereby mice were IP injected weekly with iron-dextran for 13 weeks. They found no changes in systolic function, left ventricular wall thickness or diastolic dimension were observed in iron mice via echocardiography[126]. Moreover, another group examined genetic β-thalassemia mice, whereby they found cardiac function was conserved between β-thalassemia and control mice, indicated by a constant stroke volume[127]. No changes in strain PK/strain rate, also described as myocardial deformation, were indentified in this iron overload mouse model. However, a previous study found reduced myocardial deformation in patients with β-thalassemia major, indicating altered cardiac functioning in iron overload patients[128]. Furthermore, the impact of iron overload on myocardial deformation rate is a concept which requires future analysis. A significant increase in maximal opposing wall delay strain/maximal opposing wall delay in iron overload mice reveal early cardiac dysfunction. A study examining echocardiography in patients with thalassemia observed wall motion abnormalities in patients with iron overload as well[129]. In conclusion, results indicate altered cardiac functioning in iron overload mice shown by reduced heart rate, cardiac output, a maximal opposing wall delay - all of which are indicators of myocardial iron overload, a contributor to cardiomyopathy and heart failure[130].

Chapter 3: The investigation of iron overload induced adiponectin resistance in skeletal muscle, featuring *in vitro* L6 skeletal muscle cells and an *in vivo* iron overload mouse model

3.1 Preface

The relationship between metabolic syndrome and diabetes has been extensively investigated. Iron overload-induced diabetes has also been well characterized; however the mechanistic regulation of iron overload induced diabetes - and the role of adiponectin regulation in iron overload disease - is currently unknown. Moreover, the investigation of iron overload induced adiponectin resistance mediated by FOXO1 transcription factor regulation has not been established in skeletal muscle. Firstly, *in vivo* L6 myoblasts treated with iron were used to examine iron overload induced adiponectin resistance in skeletal muscle. Adiponectin resistance was characterized by reduced AdipoR1, APPL1 and adiponectin expression, as well as reduced fAd stimulated AMPK phosphorylation, and AdRon stimulated glucose uptake. The regulation of iron overload induced adiponectin resistance by FOXO1 was confirmed via pFOXO1 cytoplasmic localization under iron overload conditions, in addition to the alleviation of iron overload inhibited AdRon glucose uptake via the inhibition of FOXO1. Secondly, an *in vivo* animal model showed adiponectin signalling was up-regulated in iron overload mice skeletal muscle, as well as altered glucose metabolism. In conclusion, these results suggest a dysregulation of adiponectin action in iron overload conditions, which provides more mechanistic and functional insight for iron overload induced diabetes regulation.

3.2 Introduction

The prevalence of diabetes in metabolic syndrome has shown a strong correlation in previous research[12,13,15-,32,131,132]. Diabetes arises from the inability to produce or respond to insulin, causing abnormal carbohydrate metabolism and elevated blood sugar levels[11]. This regulation of glucose in diabetes has been previously linked to regulation by adiponectin[133,78,131]. Adiponectin is a therapeutic target for diabetes treatment, due to its anti-diabetic properties[42]. Reduced adiponectin plasma concentrations are observed in the development of diabetes,[32] and decreased adiponectin levels are associated with the onset of insulin resistance[42,44]. In addition, several studies proposed a phenomenon known as adiponectin resistance[59, 134]. This can be defined as subnormal biological response to normal adiponectin concentrations. Adiponectin resistance occurs under stress conditions; however, the physiological significance and mechanistic regulation of this novel phenomenon in skeletal muscle currently remain unclear.

The link between iron overload and diabetes has been recently well characterized[102]. Iron is known to play a role in regulating glucose metabolism[103], as well as insulin resistance regulation[104]. However, the mechanistic regulation regarding the underlying molecular mechanisms via adiponectin currently remains misunderstood[102]. Moreover, the phenomenon of iron overload induced adiponectin resistance in skeletal muscle has not been well researched. Thus, this chapter aims to investigate the presence iron overload induced adiponectin resistance in skeletal muscle, and further the understanding of this mechanism though its potential regulation by the transcription factor FOXO1. Changes in adiponectin signalling gene expression and adiponectin sensitivity will be studied. Overall, these hypotheses will be examined using *in vivo* L6 myoblasts and the skeletal muscle of an iron overload with *in vivo* mouse model.

3.3 Materials and Methods

3.3.1 L6 Skeletal Muscle Culturing

L6 (*Rattus Norvegicus*) skeletal muscle myoblasts were maintained in 10% FBS AMEM (Wisent Inc. #310-010-CL) and 1% Antibiotic-Antimycotic (Gibco Life technologies #15240-602). Cells were grown in 75cm² flasks (Falcon via VWR #353136), and were split when confluency reached 70%. When confluent conditions were reached, 3ml of trypsin (Wisent Inc. #325-043) was added to 75cm² flasks which were placed in a 37ºC incubator for 2 minutes. Flasks were gently tapped, and floating cells were collected and neutralized with 3ml of 10% FBS AMEM in a 15ml conical tube. Cells were spun down for 5 minutes at 2000 RPM and respuspened in 10ml of 10% FBS AMEM. 10% of total suspension was used for further culturing and plating.

3.3.2. Characterizing intracellular iron:

3.3.2.1. IRE-CFP

IRE-CFP Assay was completed as previously described with the following modifications. After transfection, cells were incubated in a CO_2 incubator at 37ºC for 2 days. Then, cells were co-starved in 0.5% FBS AMEM and treated with 250µm of $FeCl_3$ for 24h, following fixation and visualization with an LSM 700 confocal microscope with DAPI and FITC channels. Pixel intensity was quantified using ImageJ software. IMARIS software was used to create representative 3D images.

3.3.3 Western Blot Analysis

L6 myoblasts were seeded in 6 well plates (Falcon #353046). Cells were starved with 0.5% FBS AMEM, and treated with 1µm of AS1842856 for 30min. Cells were then treated with 250µm of $FeCl_3$ for 24h. 30min prior to the end of iron overload conditions, myoblasts were treated with 20µm of AdRon for 30min. Cell lysate and western blot protocol mentioned previously was followed this point onward.

Membranes were blotted for the following proteins: AdipoR1, AdipoR2 and APPL1. AdipoR1, and AdipoR2 primary antibodies were kindly gifted from AstraZeneca (Sweden). APPL1 antibody was purchased from Antibody Immunoassay Services (AIS, Hong Kong). β-actin (#4967L) antibody was obtained from Cell Signalling.

3.3.4 Immunofluorescence

L6 myoblasts were seeded onto 12 well plates with glass coverslips. Cells were starved with 0.5% AMEM and treated with the following solutions where appropriate: with 250µm of $FeCl_3$ for 0, 0.5, 1, 2, 4 or 24h, 100nm of insulin for 15min, 20µm of AdRon for 30min or 5µg/ml of fAd for 30min. Cells were fixed, visualized and quantified using ImageJ software plugin JACop to obtain Person Correlation Coefficient values of nuclear overlap for both FOXO1 and pFOXO1.

Primary antibodies FOXO1 (#9454S) and pFOXO1 (Thr24) (#9464L) were obtained from Cell signalling. Secondary anti-rabbit Alexa Fluor 488 conjugate anti-body (#A-11008) was obtained from ThermoFisher Scientific (via VWR).

3.3.5 Glucose uptake

Glucose uptake was performed using GLUT4-myc L6 myoblasts. Cells were seeded onto a 24 well plate (Falcon #353047), and starved with 0.5% FBS DMEM. Cells were treated with 250µm of $FeCl_3$ for 24h and 20µm of AdRon for 1h. As a positive control for glucose uptake, cells were treated with 100nm of insulin for 10 minutes. Glucose uptake protocol as previously described was followed from this point onward.

3.3.6 *In vivo* Iron Overload Mouse Model

Six 8 week C57 male mice were intraperitoneally (IP) injected with 10mg/g of ferrous form iron dextran for 4 weeks, 5 days per week. Soleus tissue was collected, homogenized and immunoblotted as previously described. The prepared samples were blotted for the following

proteins: AdipoR1, AdipoR2, APPL2, APPL2, FOXO1 and β-actin. AdipoR1, and AdipoR2 primary antibodies were kindly gifted from AstraZeneca (Sweden). APPL1 antibody was purchased from Antibody Immunoassay Services (AIS, Hong Kong). APPL2 antibody (#H00055 198-B01P) was obtained from Abnova. GAPDH (#2118L) antibody was obtained from Cell Signalling.

2.3.6.1. Prussian blue staining

Fresh soleus tissue was preserved in tissue freezing medium (Electron Miscroscopy Sciences #72592) and cut into 10µm slices via cryosectioning. Cryosections were sent to London Health Sciences Centre at University Hospital, London, ON, for Prussian blue staining.

3.3.6.1. ITT

For insulin tolerance testing, mice were starved for 6h and IP injected with 1unit/kg of body weight after 3 weeks of iron injections. Plasma glucose levels were measured at 0, 20, 40, 60 and 80 minutes using a glucose meter (Accu-check #0088).

3.3.6.2. GTT

For glucose tolerance testing, mice were starved for 16h and IP injected with 2g/kg of body weight after 4 weeks of iron injections. Plasma glucose levels were measured at 0, 15, 30, 60 and 120 minutes using a glucose meter.

3.3.6.3. Urine glucose

To test for glucose content in the urine, mice were starved for 0h and 6h. Urine glucose levels were measured using a glucose meter.

3.3.7. Statistical Analysis

Statistical analysis between two groups was done using an unpaired two-tailed t-test. P values less than 0.05 were accepted as significant.

3.4 Results

3.4.1. Characterizing intracellular iron in L6 myoblasts

Intracellular iron overload was characterized in L6 myoblasts via IRE activity as previously described. Upon 24h hour treatment of iron, a significant 5.5 fold increase in CFP expression was observed in iron overload conditions compared to non-treated cells (**Figure 3.1 A-C**). Overall, these results confirm iron overload via the activation of intracellular iron regulatory processes.

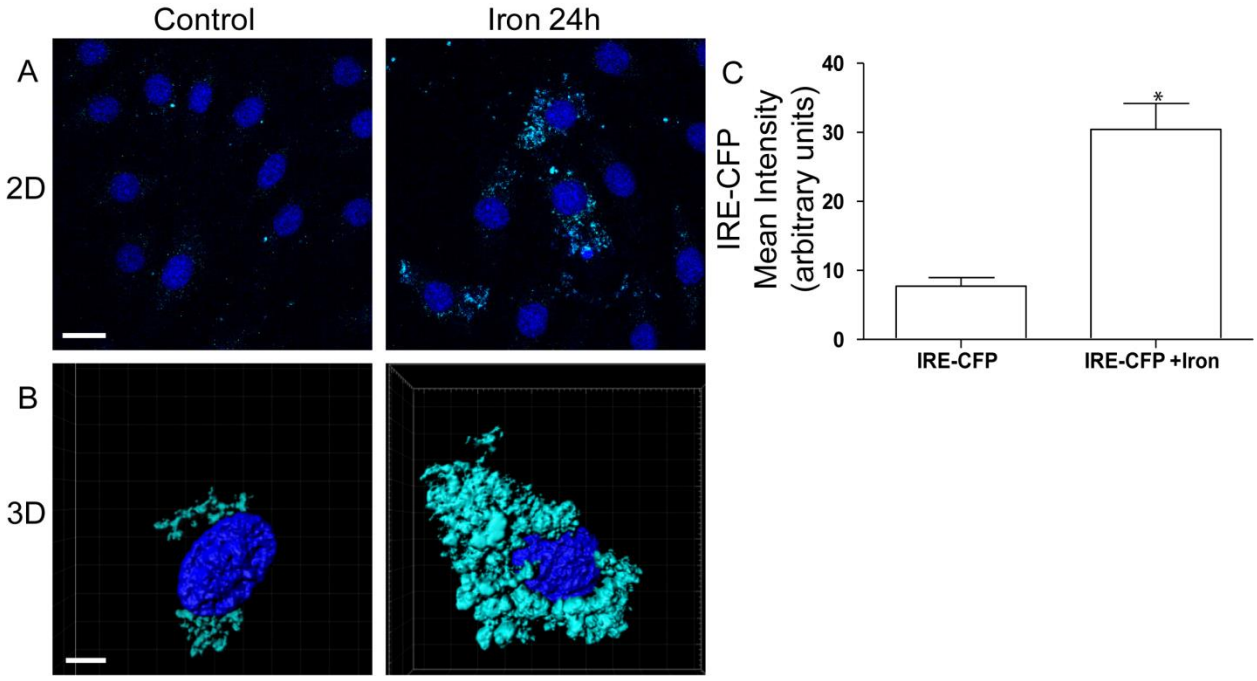

Figure 3.1: Characterizing intracellular iron overload *in vitro*. Increased iron response element activity was observed under iron overload conditions. L6 myoblasts were transfected with IRE-CFP plasmid, and treated with 250µm of $FeCl_3$ 24h (n=3). Transcribed cyan fluorescent protein was observed via FITC channels by confocal microscopy. A) 2D representative image taken using ZEN software (Scale bar: 2µm). B) 3D representative images created using IMARIS software (Scale bar: 10µm). C) 3-5 fields of view were taken per condition. All cells in field of view were traced and quantified using ImageJ software. Mean intensity values per cell were averaged and plotted for analysis. Statistical analysis was compared to IRE-CFP. (* = $P < 0.05$). Error bars display standard error of the mean.

4.2. Iron overload induced adiponectin resistance in L6 myoblasts

After characterizing intracellular iron overload, the potential for iron overload induced adiponectin resistance was further investigated. After 24h iron overload treatment, western blot analysis was used to examine the expression and regulation of the following proteins: AdipoR1, APPL1, AdipoR2, APPL2, pAMPK and adiponectin. A decrease in AdipoR1 and APPL1 expression were observed in iron overload conditions (**Figure 3.2 A and B**), however, no changes in AdipoR2 and APPL2 expression were observed (**Figure 3.2 C and D**). Moreover, iron overload conditions also reduced adiponectin monomer expression (**Figure 3.2** F). L6 myoblasts were treated with fAd 30min prior to the end of iron treatment. Adiponectin sensitivity under iron overload conditions were analysed via pAMPK. With adiponectin only treatment, pAMPK levels increased compared to control. However, a decrease in pAMPK stimulation was evident in iron overload conditions when co-treated with adiponectin (**Figure 3.2 E**). Together, these results confirmed iron overload induced adiponectin resistance via reduced expression of adiponectin signalling markers, as well as through a reduction adiponectin sensitivity via pAMPK.

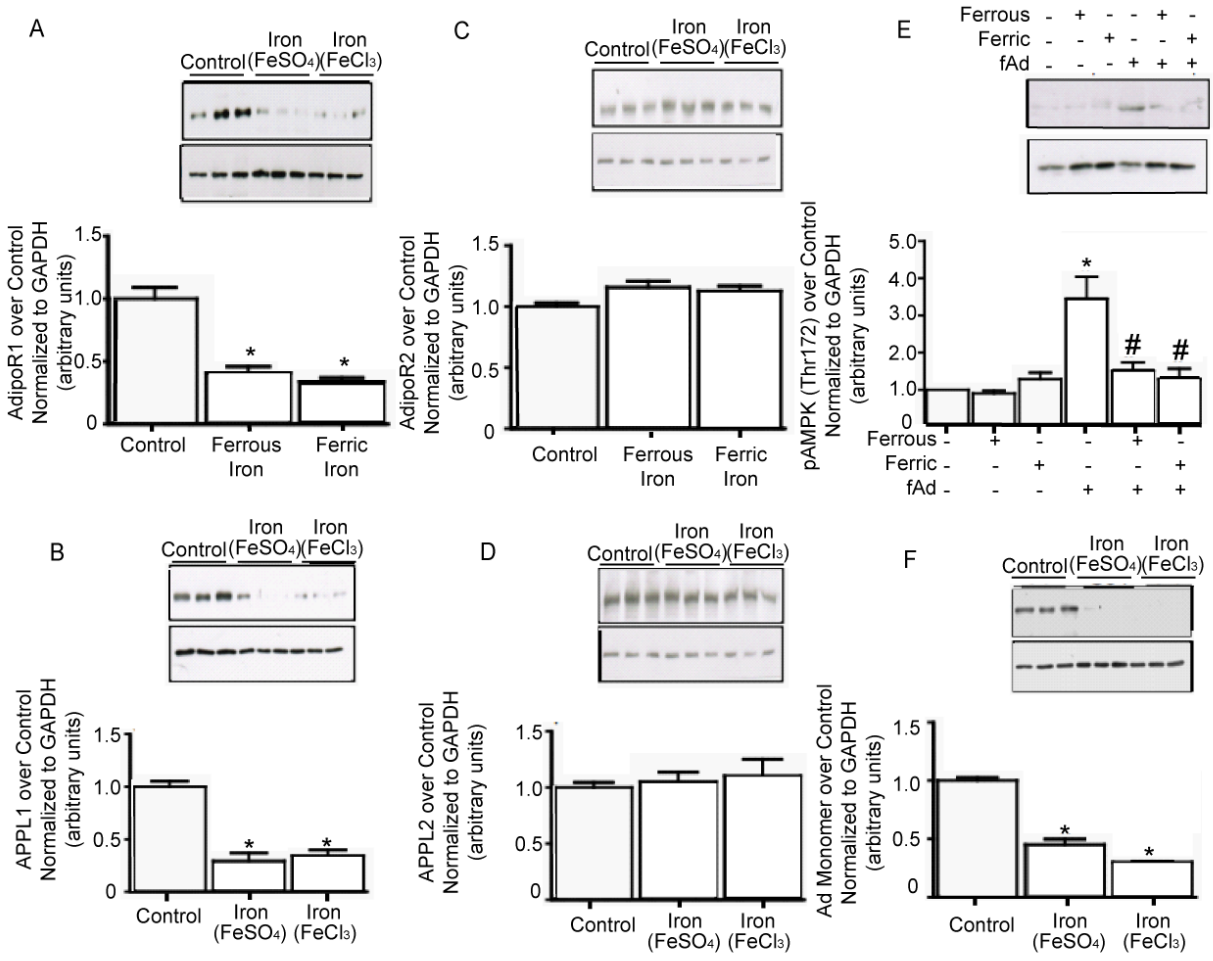

Figure 3.2: Iron overload induced adiponectin resistance via adiponectin signalling. L6 myoblasts were treated with 250µM of $FeCl_3$ $FeSO_4$ for 24h, and with 5µg/ml of fAd for 30min (Part E only). Cells were lysed, and proteins of interest were analyzed by Western blotting. Proteins of interest were tagged with the following primary antibodies: AdipoR1, APPL1, AdipoR2, APPL2, pAMPK, adiponectin and GAPDH, which were subsequently tagged with HRP-conjugated secondary antibodies (n=4). (A-F) Representative western blots of AdipoR1, AdipoR2, APPL1, APPL2, pAMPK, adiponectin and GAPDH. Quantitative representation of AdipoR1, AdipoR2, APPL1, APPL2, pAMPK and adiponectin. Western blot band intensity was quantified using ImageJ software, normalized to β-actin, and further normalized to control. Statistical analysis was compared to control conditions (* = $P < 0.05$). Error bars display standard error of the mean.

3.4.3. Iron overload regulation by FOXO1 in L6 myoblasts

After the confirmation of iron overload induced adiponectin resistance in L6 myoblasts, the regulation of iron overload by FOXO1 was further investigated. L6 skeletal muscle cells were treated with iron overload conditions for 0.5, 1, 2, 4 and 24h. Immunofluorescence was used to investigate changes in cellular localization of total FOXO1 and pFOXO1 (Thr24) under iron overload conditions. Pearson's overlap correlation coefficient (PCC) was used to monitor total FOXO1 and pFOXO1 colocalization with the nucleus. An increase in PCC suggests an increase in nuclear overlap, while a decrease in PCC suggests cytoplasmic localization. A decreased PCC of total FOXO1 was observed at 1h compared to control, however recovers back to basal levels at 2h. At 4h, FOXO1 levels continue to decrease below 1h levels, following a significant decrease in PCC at 24h (**Figure 3.3 A, B and E**). In terms of pFOXO1, PCC gradually increased from 0h to 4h. However, a significant decrease in PCC of pFOXO1 was evident at 24h time point (**Figure 3.3 C, D and F**). To conclude, this data shows that total FOXO1 and pFOXO1 is involved in the regulation of iron overload in L6 myoblasts

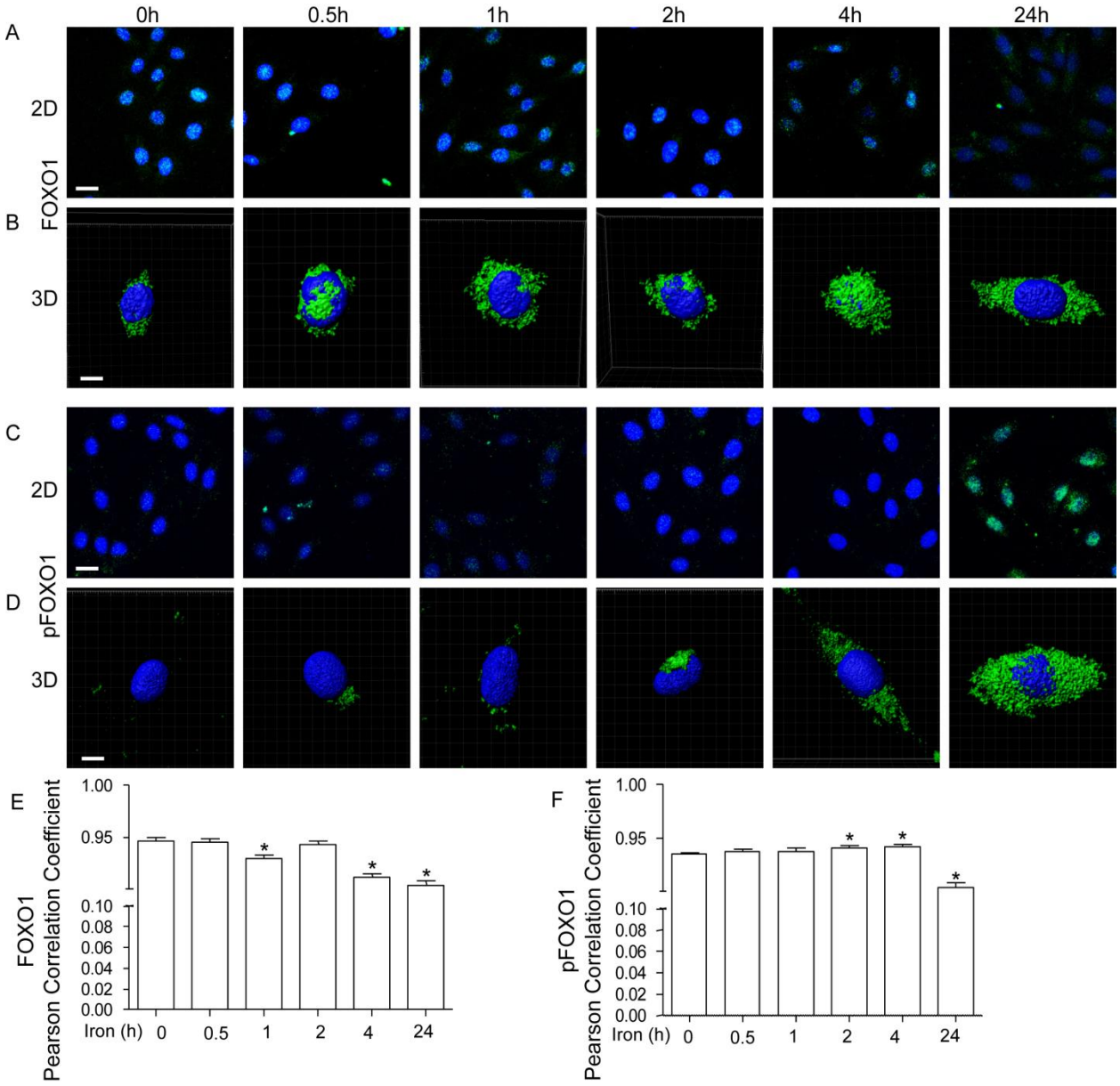

Figure 3.3: Iron overload conditions induced total FOXO1 and pFOXO1 cytoplasmic localization.

(A-B and E) Iron overload conditions induced total FOXO1 cytoplasmic localization. L6 myoblasts were treated with 250µM of $FeCl_3$ for 0, 0.5, 1, 2, 4 and 24h. Cells were fixed and incubated in total FOXO1 primary antibody, and subsequently incubated in Alexa 488 secondary antibody. Green fluorescence was observed via FITC channels by confocal microscopy (n=3). A) 2D representative images of FOXO1 taken using ZEN software (Scale bar: 2µm). B) 3D representative images of FOXO1 created using IMARIS software (Scale bar: 10µm). (E) 3-5 fields of view were taken per condition. All cells in field of view were quantified using ImageJ software. ImageJ plugin JACop was used to obtain Person Correlation Coefficient values of nuclear overlap of FOXO1. Mean correlation values were averaged, and normalized to control. Statistical analysis was compared to 0h (* = $P < 0.05$). Error bars display standard error

of the mean.

(C-D and F) Iron overload conditions induced pFOXO1 (Thr24) cytoplasmic localization. L6 myoblasts were treated with 250µM of $FeCl_3$ for 0, 0.5, 1, 2, 4 and 24h. Cells were fixed and incubated in pFOXO1 primary antibody, and subsequently incubated in Alexa 488 secondary antibody. Green fluorescence was observed via FITC channels by confocal microscopy (n=3). A) 2D representative images of pFOXO1 taken using ZEN software (Scale bar: 2µm). B) 3D representative images of pFOXO1 created using IMARIS software (Scale bar: 10µm). (F) 3-5 fields of view were taken per condition. All cells in field of view were quantified using ImageJ software. ImageJ plugin JACop was used to obtain Person Correlation Coefficient values of nuclear overlap of FOXO1. Mean correlation values were averaged, and normalized to control. Statistical analysis was compared to 0h (* = $P < 0.05$). Error bars display standard error of the mean.

3.4.4. Iron overload induced adiponectin resistance regulated by FOXO1

Following the confirmation of FOXO1's role in iron overload, iron overload induced adiponectin resistance regulation by FOXO1 was further investigated. Firstly, L6 myoblasts were treated with iron overload conditions, later stimulated with fAd 30min prior to end of iron overload treatments. Immunofluorescence featuring total FOXO1 and pFOXO1 (Thr24) was used to investigate changes in cellular localization iron overload induced stimulated with fAd. Insulin and AdRon treatments increased total FOXO1 and pFOXO1 nuclear colocalization via an increase in PCC. Co-treatment with iron overload and fAd conditions caused both total FOXO1 and pFOXO1 localization to the cytoplasm as indicated by a decreased in PCC (**Figure 3.4 A-F**). Therefore, this suggests iron overload induced adiponectin resistance via changes in localization of total FOXO1 and pFOXO1.

In addition, iron overload induced adiponectin resistance regulation by FOXO was examined via glucose uptake. L6 myoblasts over-expressing GLUT4 receptors were treated with FOXO inhibitor, AS1842856, 30min prior to 24h iron overload conditions iron overload conditions for 24h, following 30min of AdRon treatment prior to end of iron overload treatments. A decrease in glucose uptake was observed in iron overload conditions with AdRon compared to AdRon only conditions. Moreover, treating L6 myoblasts with AS1842856, iron and AdRon alleviated glucose uptake levels back to AdRon only conditions (**Figure 3.4 G**). Furthermore, AS1842856 alone significantly increased glucose uptake as well. To conclude, this data also shows iron overload induced adiponectin resistance via AdRon stimulated glucose uptake, and further the regulation by FOXO via AS1842856.

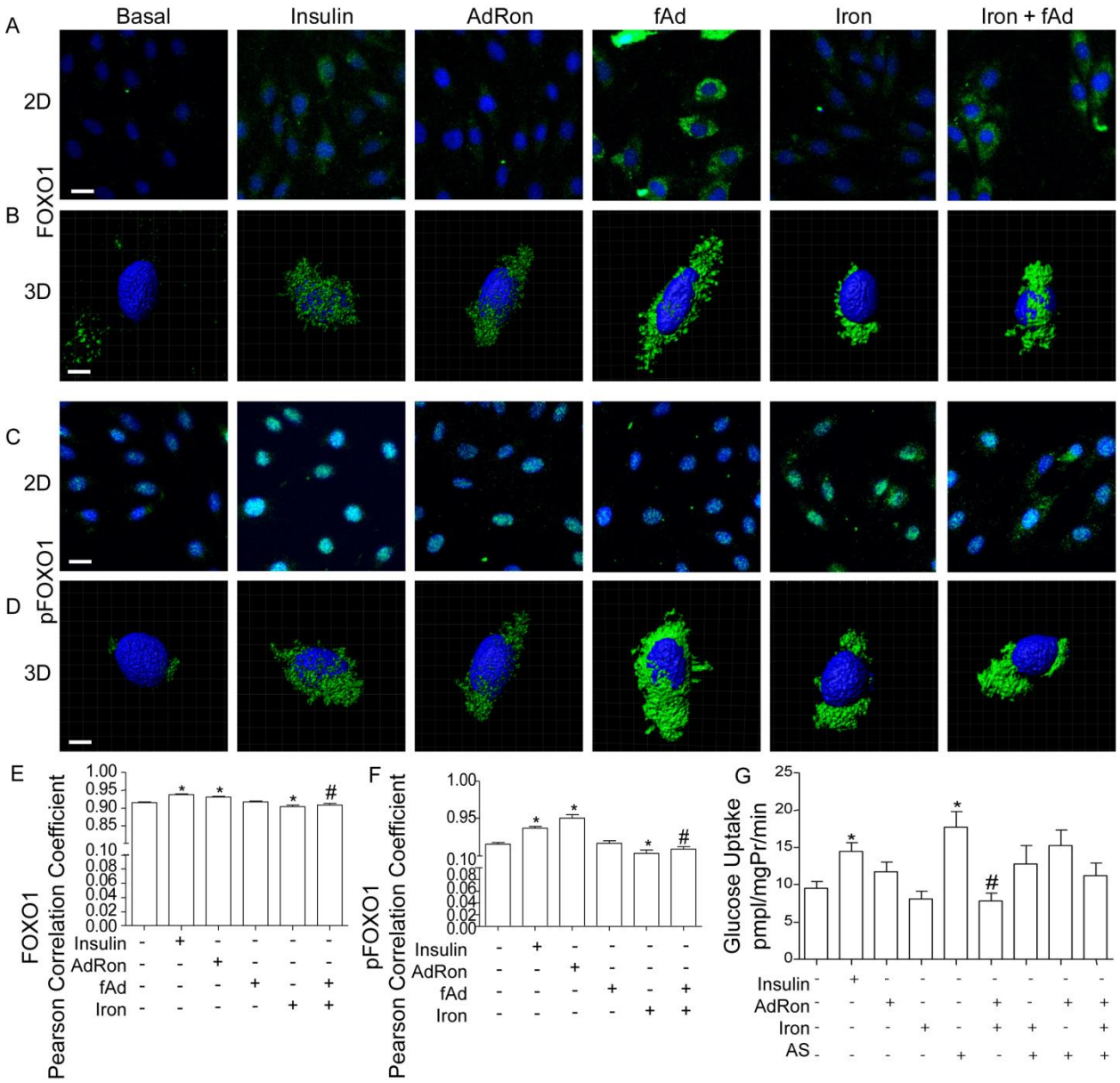

Figure 3.4: Iron overload induced adiponectin resistance via fAd stimulated pFOXO1 and AdRon stimulated glucose uptake.

(A-B and E) Iron overload causes reduced fAd induced cytoplasmic localization of total FOXO1 and pFOXO1. L6 myoblasts were treated with 250µM of $FeCl_3$ for 24h, and 5µg/ml of fAd for 30min prior to the end of iron overload incubation. Insulin (100nm for 10min) and AdRon (20µM for 30min) was used as a positive control cytoplasmic localization of total FOXO1. Cells were fixed and incubated in total FOXO1 primary antibody, and subsequently incubated in Alexa 488 secondary antibody. Green fluorescence was observed via FTIC channels by confocal microscopy (n=2). A) 2D representative images of FOXO1 taken using ZEN software (Scale bar: 2µm). B) 3D representative images of FOXO1 created using IMARIS software (Scale bar: 10µm). E) 3-5 fields of view were taken per condition. All cells in field of view were quantified using ImageJ software. ImageJ plugin JACop was used to obtain Person Correlation Coefficient values of nuclear overlap of FOXO1. Mean correlation values per cell were averaged, and

normalized to control. Statistical analysis was compared to basal (* = P < 0.05) or fAd (# = P < 0.05). Error bars display standard error of the mean.

(C-D and F) Iron overload causes reduced fAd induced cytoplasmic localization of pFOXO1 (Thr24). L6 myoblasts were treated with 250µM of $FeCl_3$ for 24h, and 5µg/ml of fAd for 30min prior to the end of iron overload incubation. Insulin (100nm for 10min) and AdRon (20µM for 30min) was used as a positive control cytoplasmic localization of pFOXO1 (Thr24). Cells were fixed and incubated in pFOXO1 (Thr24) primary antibody, and subsequently incubated in Alexa 488 secondary antibody. Green fluorescence was observed via FTIC channels by confocal microscopy (n=2). C) 2D representative images of pFOXO1 taken using ZEN software (Scale bar: 2µm). D) 3D representative images of pFOXO1 created using IMARIS software (Scale bar: 10µm). F) 3-5 fields of view were taken per condition. All cells in field of view were quantified using ImageJ software. ImageJ plugin JACop was used to obtain Person Correlation Coefficient values of nuclear overlap pFOXO1. Mean correlation values per cell were averaged, and normalized to control. Statistical analysis was compared to basal (* = P < 0.05) or fAd (# = P < 0.05). Error bars display standard error of the mean.

(G) Iron overload induced adiponectin resistance via glucose uptake is regulation by FOXO1. L6 GLUT4-myc myoblasts were treated with 250µm of $FeCl_3$ for 24h, and 20µM of AdRon 30min prior to end of treatment time. 30min prior to iron incubation, cells were treated with 1µM of FOXO inhibitor, AS1842856. As a positive control, cells were stimulated with 100nM of insulin for 10 minutes. Cells were treated with radioactive H^3 2 deoxy-D-(3H) – glucose for 5min. Cells were lysed, collected for scintillation counting, and corrected for protein concentration. (n=4). Statistical analysis was compared to control (* = P <0.05) and compared to AdRon (# = P <0.05). Error bars display standard error of the mean.

3.4.5. Iron overload induced adiponectin resistance regulation by FOXO1 via adiponectin signalling

Iron overload induced adiponectin resistance regulation by FOXO was further investigated. L6 skeletal muscle cells were treated with a FOXO1 inhibitor AS1842856 for 30min prior to 24h iron overload conditions. Western blot analysis was used to investigate the expression of the following proteins: AdipoR1, APPL1 and AdipoR2. AdipoR1 expression decreased by 50% under iron overload conditions. Moreover, AS1842856 increased AdipoR1 expression, following a further increase in iron overload and AS1842856 conditions (**Figure 3.5 B**). APPL1 and AdipoR2 expression did not change in iron overload conditions; however, an increase was also evident under AS1842856 conditions (**Figure 2.5 C and D**). (Note: no bands were present for APPL2 and require further optimization). In terms of iron and AS1842856 conditions, no obvious trend was observed in APPL1 and AdipoR2 expression compared to AS1842856 only conditions. To conclude, this data shows that iron overload induced adiponectin resistance regulation by FOXO via expression is unclear.

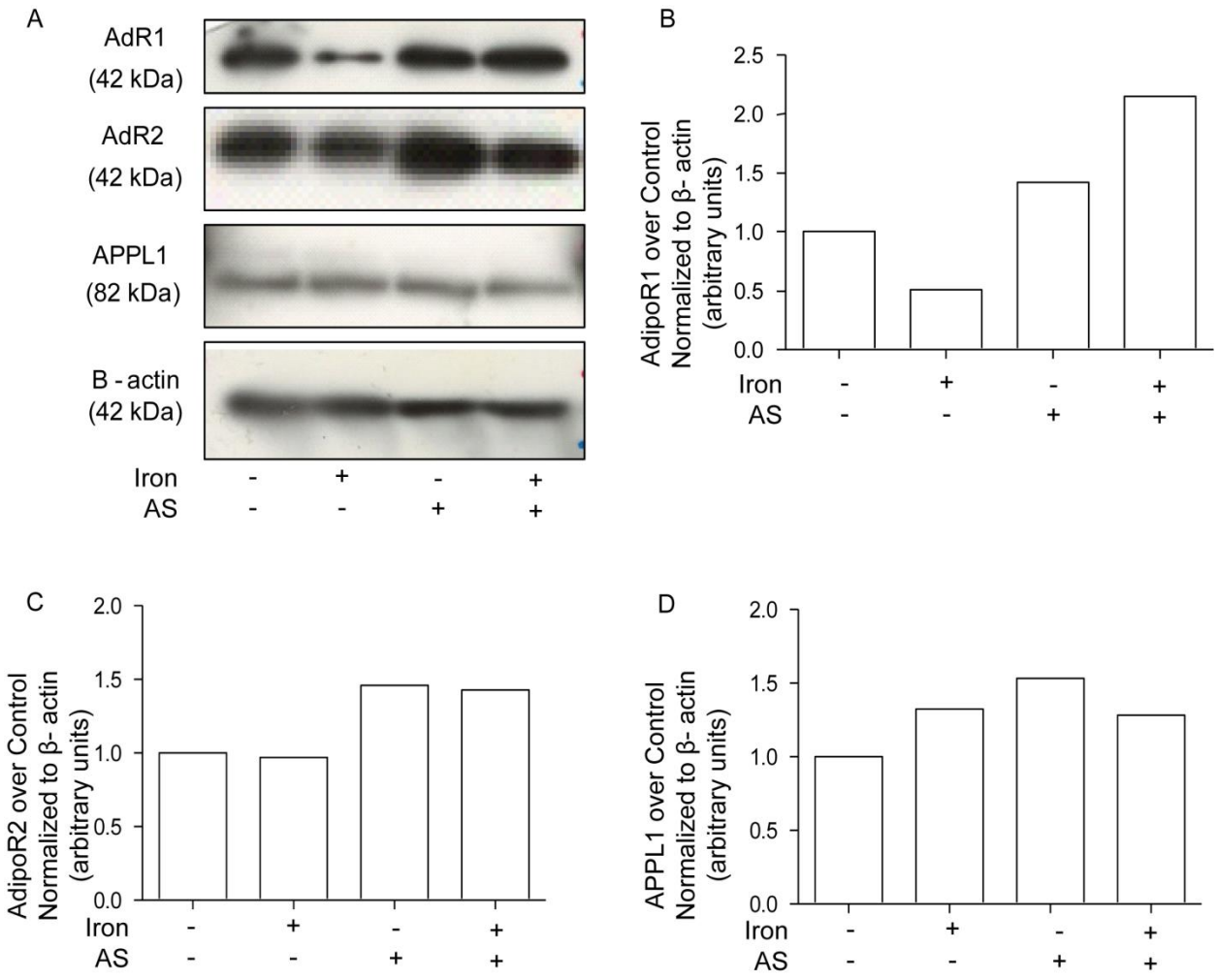

Figure 3.5: Iron overload induced adiponectin resistance regulation by FOXO via adiponectin signalling. L6 myoblasts were treated with 250μM of $FeCl_3$ for 24h, and 1μM of AS1842856 30min prior to iron overload incubation. Cells were lysed, proteins of interest were analyzed by Western blotting. Proteins of interest were tagged with the following primary antibodies: AdipoR1, APPL1 and AdipoR2 and β-actin, which were subsequently tagged with HRP-conjugated secondary antibodies (n=1). A) Representative western blots of AdipoR1, APPL1, AdipoR2 and β-actin. B-D) Quantitative representation of AdipoR1, APPL1 and AdipoR2. Western blot band intensity was quantified using ImageJ software, normalized to β-actin, and further normalized to control.

3.4.6. *In vivo* iron overload induced adiponectin resistance in skeletal muscle

Iron overload induced adiponectin resistance was further examined in the skeletal muscle of previously described iron overload mice. Male C57 mice of 8 weeks were IP injected with 10mg/g of ferrous iron for 4 weeks. Prussian blue staining of soleus tissue cryosections was conducted. An increase in Prussian blue staining was observed in iron overload mice compared to control mice, confirming irons ability to reach the target tissues (**Figure 3.7 A-B**). Western blot analysis of AdipoR1, APPL1, AdipoR2, and APPL2 was used to examine changes in gene expression of adiponectin signalling molecules (**Figure 3.7 A-D**). Results indicate no changes were evident in AdipoR1 and AdipoR2 expression. However, a significant increase by approximately two fold was seen in APPL1. Similar to the heart, a significant loss in APPL2 expression by approximately 90% was seen in iron overload mice compared to control. In conclusion, this model shows the presence of iron overload induced adiponectin resistance via a significant reduction in APPL2 expression.

3.4.6.1. Glucose metabolism 4 week iron overload mice

Next, glucose metabolism was investigated to characterize metabolic profiles in iron overload mice. Iron overload mice were starved for 6h and injected with insulin at various time points in order to investigate insulin tolerance via analysis of plasma glucose levels. In control mice, plasma glucose levels dropped by 50% during 0 to 20 minute time points, followed by steady plasma glucose levels up to 80min. However, plasma glucose levels iron overload mice gradually decreased by 50% at 0 to 40min, followed by a steady level of glucose up to 80min (**Figure 3.8 A**). Moreover, iron overload had significantly less plasma glucose levels compared to control mice as indicated by area under curve (AUC) (**Figure 3.8 B**). Next, iron overload mice were starved for 16h and injected with glucose at various time points for glucose tolerance testing. Control mice displayed a spike in glucose levels at 15min time-point by a 4 fold,

followed by a rapid decrease in plasma glucose levels at 1h. Iron overload mice doubled their plasma glucose levels at 15min, followed by a steady decline in glucose levels at 1h. Moreover, both control and overload mice plasma glucose levels plateau from 1h to 2h time points (**Figure 3.8 C**). Furthermore, iron overload mice show overall lower plasma glucose levels compared to control mice (**Figure 3.8 D**). Lastly, urine glucose levels were compared in control and iron overload mice after either 0h or 6h of starvation. At 0h, control mice show no level of urine glucose levels, however, iron overload mice have approximately 1.5mmol/L of glucose levels in urine (**Figure 3.8 E**). Conversely, iron overload mice show a decrease by 50% in urine glucose levels at 6h of starvation compared to control mice. These data suggests an altered metabolic profile in iron overload load via changes in plasma and urine glucose levels.

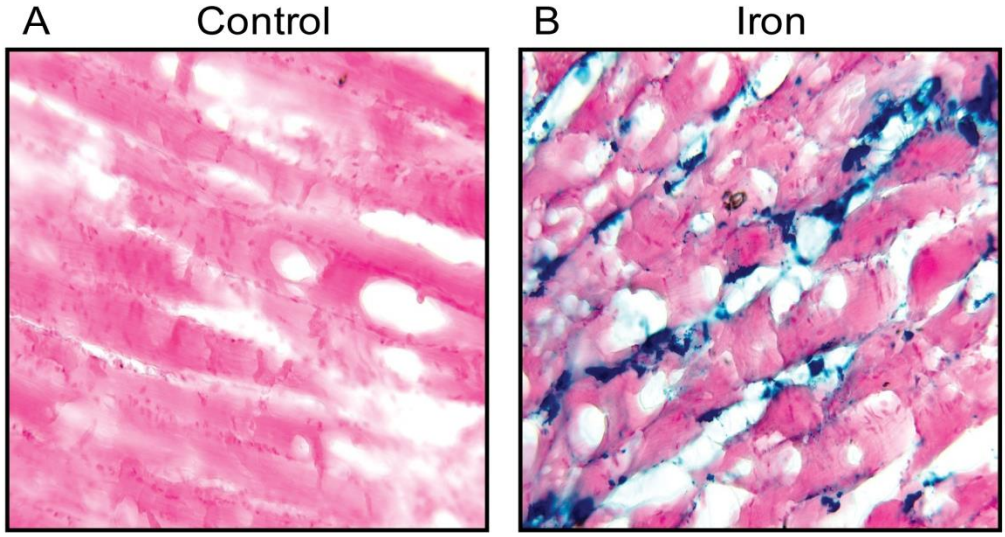

Figure 3.6: Characterizing iron overload *in vivo*. Iron overload mice display increased amount of Prussian blue staining compared to control. 8 week C57 male mice were IP injected with 10mg/g of ferrous iron. Soleous tissue cryosections were stained with Prussian blue and analyzed by histopathology. (n=3). A) Representative image of control mice. B) Representative image of iron overload mice. Original magnification X100 for all micrographs.

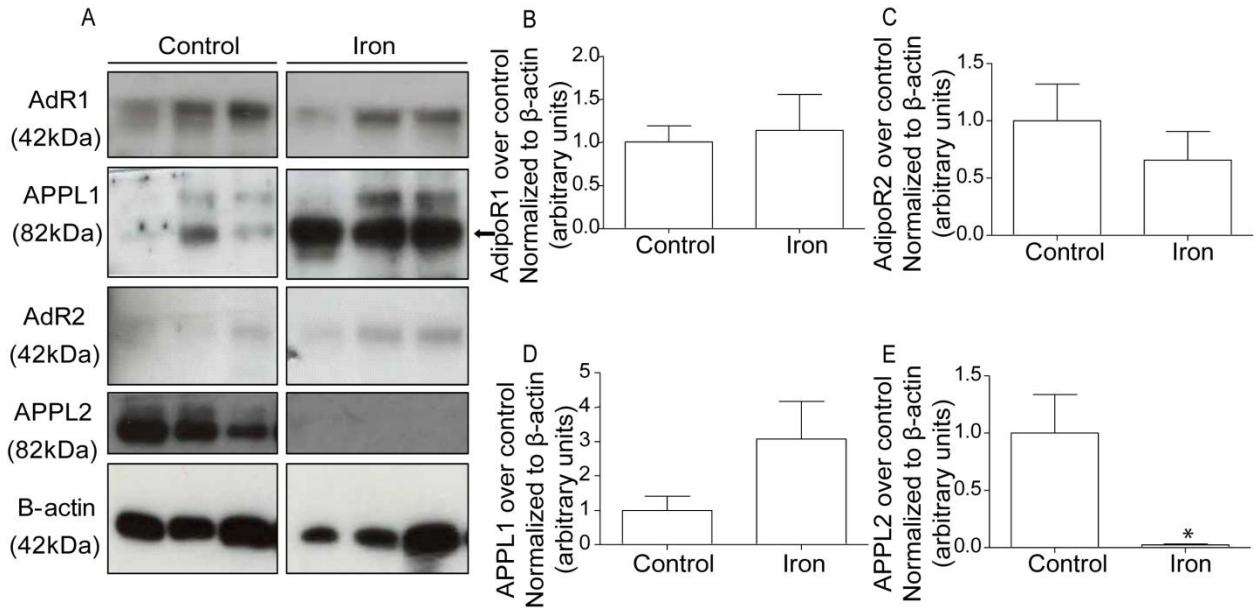

Figure 3.7: Iron overload altered adiponectin signalling *in vivo* via changes in expression of adiponectin signalling proteins. 8 week C57 male mice were IP injected with 10mg/g of ferrous iron. Soleus tissue was lysed, and proteins of interest were analyzed by Western blotting. Proteins of interest were tagged with the following primary antibodies: AdipoR1, APPL1, AdipoR2, APPL2 and β-actin, which were subsequently tagged with HRP-conjugated secondary antibodies (n=6). A) Representative western blots of AdipoR1, APPL1, AdipoR2, APPL2 and β-actin. B-E) Quantitative representation of AdipoR1, APPL1, AdipoR2 and APPL2. Western blot band intensity was quantified using ImageJ software, normalized to β-actin, and further normalized to control. Statistical analysis was compared to control conditions (* = $P < 0.05$). Error bars display standard error of the mean. Note: For uncut Western blots, see Appendix A: Figure A3.

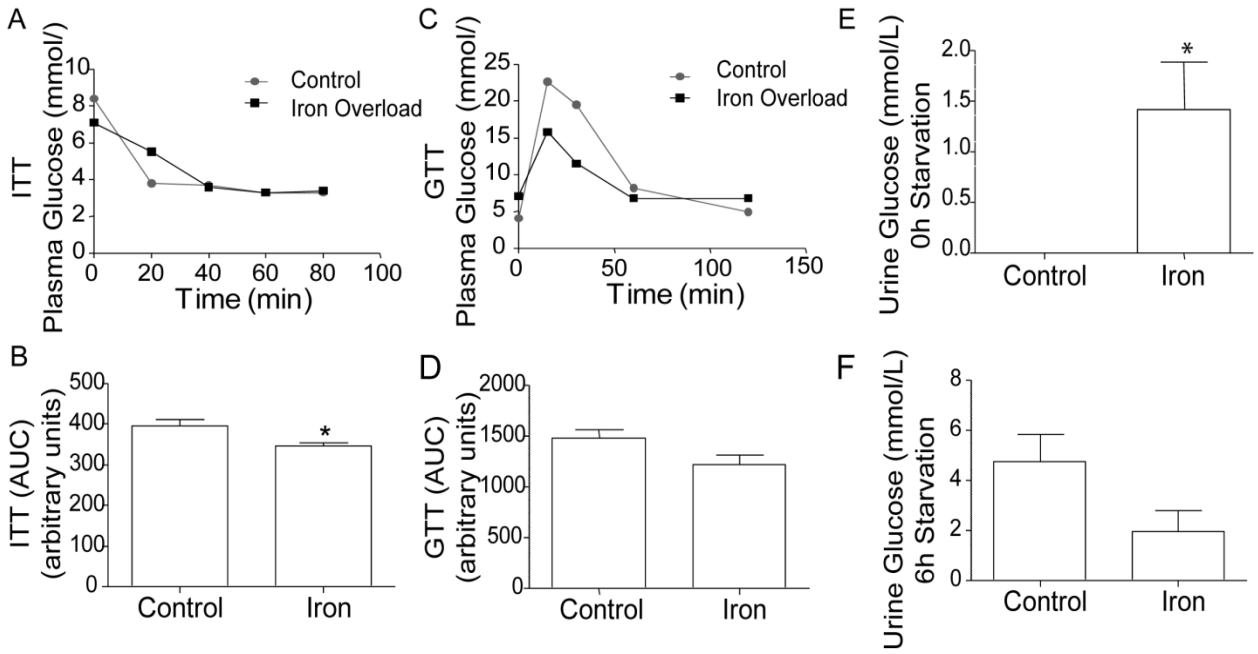

Figure 3.8: Iron overloads effect on glucose blood and urine levels in an *in vivo* iron overload mouse model. 8 week C57 male mice were IP injected with 10mg/g of ferrous iron. A) Insulin tolerance test (ITT). Mice were starved for 6h and injected with 1unit/kg of body weight after 3 weeks of iron injections. Plasma glucose levels were measured at 0, 20, 40, 60 and 80 minutes using a glucose meter. B) Displays area under the curve of ITT. C) Glucose tolerance test (GTT). Mice were starved for 16h and IP injected with 2g/kg of body weight after 4 weeks of iron injections. Plasma glucose levels were measured at 0, 15, 30, 60 and 120 minutes using a glucose meter. D) Displays area under the curve of GTT. (E-F) Urine glucose test. Mice were starved for 0h and 6h, respectively. Urine glucose levels were measured using a glucose meter. Statistical analysis was compared to control conditions (* = $P < 0.05$). Error bars display standard error of the mean.

3.5 Discussion

3.5.1 Iron overload activated IREs in L6 myoblasts

An IRE-CFP reporter assay was used to confirm IRE activation upon iron overload treatment in L6 myoblasts. As mentioned previously, this construct contains a sequence that encodes the ferritin promoter region upstream of CFP[112]. As with NeoCM, 24h iron overload conditions increased CFP levels cyan suggesting an increase in ferritin expression (**Figure 3.1 A-C**). This confirms iron-stimulated gene expression of iron regulatory proteins upon iron overload treatment. Moreover, our lab has also showed time-dependant PGSK quenching, and confirmed no changes in cell viability using MTT in L6 myoblasts (Jang et al, unpublished data).

3.5.2. Iron overload induced adiponectin resistance in L6 myoblasts: changes in adiponectin signalling and adiponectin expression

The potential for adiponectin resistance in L6 myoblasts was suggested by a significant decrease in AdipoR1 after iron overload, which has also been suggested recently in the literature[79]. Additionally, APPL1 levels were decreased under iron overload conditions; however no significant changes in AdipoR2 and APPL2 were evident (**Figure 3.2 A-F**). These results are also consistent with NeoCM adiponectin signalling (**Figure 2.5 A-E**). In terms of adiponectin sensitivity, a decrease pAMPK was evident in iron overload conditions when co-treated with adiponectin, suggesting adiponectin resistance can also occur downstream of adiponectin receptor level expression[84]. This finding is also consistent to NeoCM anti-pAMPK immunofluorescence (**Figure 2.2 A-C**). Iron overload conditions also decreased adiponectin monomer expression, a phenomenon that has also been characterized previously in adipocytes[106]. Overall, this data confirms iron overload induced adiponectin resistance in L6 myoblasts.

3.5.3. Iron overload induced adiponectin resistance is regulated by FOXO1 in L6 myoblasts

As previously discussed in NeoCM, FOXO1 - a transcription factor regulator of AdipoR1 and AdipoR2 expression - has been recently suggested as a mechanistic mediator of iron overload induced adiponectin resistance[106]. By inhibiting FOXO1 DNA binding with AS1842856, I have demonstrated that FOXO1 plays a role in iron overload induced adiponectin resistance regulation; this has been demonstrated by changes in AdipoR1 and pAMPK. In NeoCM, the decrease of expression with iron overload is recovered after inhibition of FOXO1, suggesting that when FOXO1 is inhibited, adiponectin resistance is no longer under its mechanistic regulation (**Figure 2.4 A-C**).

A different approach was used in L6 myoblasts by observing cellular localization of FOXO1. Changes in FOXO1 localization were observed in a time dependant matter via an iron overload time course in L6 myoblasts. At 24h of iron overload conditions, PCC values of total FOXO1 and pFOXO1 (Thr24) levels decrease significantly compared to control. This suggests that iron overload regulates FOXO1 translocation to the cytoplasm. Moreover, upon cytoplasmic translocation, FOXO1 can no longer act in the nucleus to regulate AdipoR1 and AdipoR2 transcription, suggesting that this may be a potential mechanism to cause a decrease in AdipoR1 expression (**Figure 3.3 A-C**).

This was further investigated by observing FOXO1 expression and regulation via iron overload conditions stimulated with adiponectin. Previously, it was already established that an increase in FOXO1 localization was observed in iron overload conditions. In adiponectin only conditions, adiponectin caused no significant change in FOXO1 expression or localization compared to control conditions (**Figure 3.4 A-C**). However, during iron overload conditions with adiponectin, a decrease in nuclear overlap was observed in comparison to adiponectin only

conditions, further supporting that FOXO1 regulates iron overload induced adiponectin resistance in skeletal muscle.

3.5.4 Iron overload induced adiponectin resistance: analysis of AdRon stimulated glucose uptake in GLUT4-myc L6 myoblasts

Glucose uptake is a read-out of adiponectin action, as adiponectin has been shown to stimulate GLUT4 mediated glucose uptake in previous literature[21]. A decrease in glucose uptake was observed in iron overload and AdRon conditions compared to AdRon only conditions (**Figure 3.3 G**). This further supports that iron overload conditions suppresses AdRon which normally stimulate glucose uptake[77]. Moreover, this is also supported by consistent findings in glucose uptake using NeoCM (**Figure 2.2 G**).

FOXO1 inhibitor was used in combination with iron overload and AdRon treatments in L6 myoblasts in order to investigate the mechanistic regulation of iron overload induced adiponectin resistance (**Figure 3.3 G**). In terms of adiponectin regulation, FOXO1 inhibitor recovers iron overload and AdRon glucose uptake levels, back to AdRon stimulated levels, supporting FOXO1's role in glucose metabolism regulation by AdRon. FOXO1 inhibitor AS1842856 significantly increased glucose uptake as well, which could be explained by FOXO1's role in glucose homeostasis in hemochromatosis [106]. To conclude, this data suggests that FOXO1 plays a role in iron overload induced adiponectin resistance by mediating adiponectin sensitivity.

3.5.6. FOXO1 mediated iron overload induced adiponectin resistance via adiponectin signalling

After establishing iron overload induced adiponectin resistance in L6 myoblasts via adiponectin signalling (**Figure 2.3 A-F**), potential regulation by FOXO was further investigated. FOXO1 inhibitor AS1842856 increased AdipoR1 expression, followed by a further increase in iron overload combined with AS1842856 (**Figure 3.5 B**). Similarly, an increase in APPL1 and

AdipoR2 was also evident using AS1842856 (**Figure 2.5 C and D**). In terms of iron and AS1842856 conditions, no obvious trend was observed in APPL1 and AdipoR2 expression compared to AS1842856 only conditions. In conclusion, FOXO1 may play a regulatory role in iron overload induced adiponectin resistance in L6 myoblasts via regulation of AdipoR1 expression. This can be supported by previous literature, as FOXO1 is known to directly modulate AdipoR1 expression in skeletal muscle[68,79]. Conversely, iron overload induced adiponectin resistance regulation by FOXO via expression is unclear, and more replicates are required to confirm FOXO1 regulation in iron overload induced adiponectin resistance regulation. Furthermore, as previously investigated in NeoCM, FOXO1 may not play a regulatory role in iron overload induced adiponectin resistance regulation on the level of adiponectin signalling protein expression. Other potential mechanisms may be involved in the regulation of iron overload induced adiponectin resistance in skeletal muscle.

3.5.6 Iron overload altered adiponectin signalling in skeletal muscle of *in vivo* iron overload mouse model

After examining iron overload induced adiponectin resistance in L6 skeletal muscle, further investigation in skeletal muscle of *in vivo* iron overload mice was investigated. Similar to investigations in the heart, Prussian blue staining was used to characterize iron overload in soleus muscle, whereby an increase in Prussian blue was observed in iron overload mice (**Figure 3.6 A-B**). Western blot analysis was used to investigate adiponectin signalling regulation in iron overload mice (**Figure 3.7 A-E**). Consistent with heart Western blot analysis, no change was observed in AdipoR1, APPL2 and although AdipoR2 levels show a decreasing trend, the reduction in expression is not significant. Additionally, a loss of APPL2 was observed in soleus muscle, like with heart Western blot analysis. Again, this indicates an increase in adiponectin signalling, rather than a resistance, due to the competitive inhibition of APPL1 by APPL2. This suggests a potential up-regulation in adiponectin receptor action via increased

APPL1 activation[58]. As previously discussed, these conflicting results call for further investigation to comprehend the severity of iron overload as a spectrum, and additionally, its effects on skeletal muscle metabolic regulation.

3.5.6.1. Glucose metabolism is altered in iron overload mouse model

The investigation of glucose metabolism was crucial to understand an iron overload mouse model, due to the association of iron overload with diabetes[102]. Specifically, glucose metabolism of iron overload mice was investigated to characterize any changes in their metabolic profiles. This is because iron is known to be associated with glucose metabolism and insulin resistance regulation [103,104]. First, an insulin tolerance test showed that iron overload mice display insulin resistance, a connection that has been recently well established[135]. This is shown by more stable glucose levels upon insulin injections in iron over load mice (**Figure 3.8 A**). Moreover, iron overload mice display lower total plasma glucose levels compared to control (**Figure 3.8 B**). A study in hepcidin KO mice also observed reduced blood glucose levels in iron overload mice. These findings confirm iron overloads ability to impair glucose homeostasis in mice[136], which can be explained by increased iron deposition in the liver[136]; an observation also made in the liver of our iron overload mice (data not shown) (Dang et al, unpublished data). In terms of glucose tolerance, these iron overload mice seem to display a higher glucose tolerance (**Figure 3.8 C**). Conversely, previous literature has also indicated an up-regulation of glucose with iron overload[135], though the glucose tolerance observed is not significant as indicated by AUC (**Figure 3.8 D**). To conclude, abnormal glucose tolerance and diabetes are also evident in patients with hereditary iron overload and require further elucidation[137]. Lastly, to further examine the discrepancies in glucose metabolism in iron overload mice, urine glucose was measured in starved (6h) and non-starved mice. At 0h starvation, iron overload mice showed elevated urine glucose levels, compared to control mice which show no levels of urine glucose (**Figure 3.8 E)**. Moreover, no significant changes were observed in urine glucose levels at 6h

starvation in iron overload mice compared to control. These findings are similar to clinical trials of hemochromatosis patients, whereby an increase in urine glucose, medically known as glycosuria, is also observed in these patients[138]. Overall, these results indicate iron overload's ability to cause altered glucose metabolism via the presence of insulin resistance and glycosuria, both of which are known characteristics of diabetes.

Chapter 4: General conclusions and future directions

Metabolic syndrome is characterized by a combination of reversible, physiological abnormalities that are associated with severe health conditions such as cardiovascular disease and diabetes[1]. Although cardiovascular disease is known to be the number one cause of death worldwide[5], and the incidence of heart failure is steadily increasing [139]. While a link has been previously made with heart disease and metabolic syndrome[4], the molecular regulation of cardiovascular disease requires further investigation. Diabetes is also positively correlated to metabolic syndrome[12,13]. Diabetes prevalence is also increasing, resulting in a diabetes epidemic in some countries[140]. While recent research has developed further conclusions towards molecular and physiological cardiovascular disease and diabetes regulation, further investigation is needed to better understand metabolic profiling in disease.

Iron overload has shown to be associated with heart failure and diabetes regulation. Iron overload is a clinical condition that can result from the accumulation of intracellular or circulatory iron, which can cause organ dysfunction and damage[97,98]. The correlative relationship between iron overload and heart disease is illustrated by iron overload having recently been linked cardiac oxidative stress and fibrosis[100]. However, the clinical implications of iron overload induced cardiovascular disease still requires further characterization. Moreover, the link between diabetes and iron overload has recently been well established, mainly due to irons role in glucose homeostasis [103,104]. At the molecular level, iron overload is not well characterized in cardiovascular disease and diabetes regulation, and further, the regulation of iron overload via adipokine signalling - such as adiponectin - also currently remains misunderstood and requires further investigation.

By examining the regulation of iron overload induced adiponectin resistance in the heart and skeletal muscle, I have shown that adiponectin regulation is similarly altered by iron overload conditions in both tissues. First, I showed that iron accumulation occurs in both

NeoCM and L6 myoblasts after iron overload treatment, using PGSK and IRE-CFP assays. Next I have proved iron overload adiponectin resistance occurs in both models. This was characterized by a decrease in AdipoR1 and APPL1 protein expression under iron overload conditions in both NeoCM and L6 cells. Moreover, I confirmed lack of adiponectin signalling via AdRon induced pAMPK and pP38 in NeoCM, and fAd stimulated pAMPK in L6 myoblasts. I have showed AdRon induced that glucose uptake is impaired by iron overload in NeoCM and GLUT4-myc L6 myoblasts.

Next, I have confirmed the mechanistic regulation of iron overload induced adiponectin resistance via FOXO1 in both models. In NeoCM and L6 myoblasts, I found that total FOXO1 and pFOXO1 cellular localization changed to the cytoplasm under iron overload conditions. In NeoCM, I showed an alleviation of AdRon stimulated pAMPK signalling under iron overload conditions using a FOXO1 inhibitor. While in L6, I used a different approach by showing a change pFOXO1 localization to the cytoplasm when treated with iron overload and fAd. However, when examining protein expression of AdipoR1/2 and APPL1/2 with FOXO1 inhibitor, both models indicated no significant change in protein expression, suggesting FOXO1 regulation of iron overload adiponectin resistance only occurs on the level of adiponectin sensitivity.

Moreover, I investigated adiponectin signalling in an iron overload mouse model, focusing on heart and soleus muscle. I started by confirming iron overload deposition to the tissues via Prussian blue staining. I then used western blot analysis to examine changes in the following adiponectin signalling proteins: AdipoR1/2 and APPL1/2. Although adiponectin resistance was not observed in both tissues by a marked reduction in AdipoR1 and APPL1 expression, both heart and soleus muscle showed a complete loss of APPL2, suggesting a potential up-regulation in adiponectin signalling. Moreover, I confirmed that iron overload mice display altered cardiac functioning, glucose metabolism, and reduced body mass, which in turn correlate with iron overload induced disease studies.

In future, it is important to characterize a mechanism for the reduction of AdipoR1 and APPL1 in both NeoCM and L6 myoblasts. For instance, JNK and CDK1 have been shown to modulate FOXO1 activity via acetylation, and therefore may have the potential to regulate iron overload induced adiponectin resistance on the level of FOXO1 regulation[65]. More so, SIRT1/2 and CBP/p300 regulate FOXO by either promoting or deactivating transcription, respectively[70,69], and thus may also have the potential to indirectly regulate iron overload induced adiponectin resistance. Furthermore, over-expressing FOXO1 under iron overload conditions could help elucidate it`s role adiponectin receptor level regulation. Previous literature in adipocytes showed increased AdipoR1/2 expression under constituently active FOXO1; however, AdipoR1/2 levels were reduced despite FOXO1 up-regulation, due to inactive FOXO1 regulation under stress conditions[68]. In addition, it is important to further characterize adiponectin resistance in L6 myoblasts via pAMPK regulation. Anti-pAMPK immunofluorescence featuring AdRon, iron overload and AS1842856 will confirm iron overload induced adiponectin resistance and FOXO1 regulation via the investigation of adiponectin sensitivity.

Lastly, characterizing iron overload induced adiponectin resistance in an *in vivo* model is necessary to understand the physiological mechanisms of iron overload induced cardiovascular disease and diabetes. This can be accomplished via the optimization of iron overload as a spectrum by either decreasing or increasing iron overload injections to achieve an adiponectin resistant state. Genetic iron overload models, or orally induced iron overload may also be of interest to help to achieve this effect. Once this is confirmed, an iron overload model stimulated with either fAd or AdRon can be used to investigate adiponectin sensitivity via pAMPK and pP38 levels. Furthermore, a cardiac or muscle specific FOXO1 KO mouse model can help elucidate a mechanistic perspective towards iron overload induced adiponectin resistance after the confirmation of reduced pAMPK and pP38 levels under iron overload alone.

In summary, adiponectin resistance is beginning to be characterized in fields of

molecular biology and physiology in recent research. My studies show that iron overload induced adiponectin resistance occurs in heart and skeletal muscle models via changes in adiponectin signalling. Moreover, I have confirmed the regulation of iron overload induced adiponectin resistance by the FOXO1 transcription factor. Despite these conclusions, further investigation is required to fully elucidate adiponectin regulation in diseased states in order to better understand the balance between adiponectin resistance and adiponectin signalling up-regulation. To conclude, iron overload induced adiponectin resistance and its underlying mechanisms is a phenomenon that should be continue to be elucidated in order to determine precise mechanistic understanding that will be useful to metabolic syndrome related disease drug targeting.

References

1. Epidemiology, F. *et al.* Harmonizing the Metabolic Syndrome International Atherosclerosis Society ; and International Association for the Study of Obesity. (2009). doi:10.1161/CIRCULATIONAHA.109.192644
2. Han, T. S. & Lean, M. E. J. A clinical perspective of obesity , metabolic syndrome and cardiovascular disease. 1–13 (2016). doi:10.1177/2048004016633371
3. Titmuss, A. T. & Srinivasan, S. Metabolic syndrome in children and adolescents: Old concepts in a young population. *J. Paediatr. Child Health* **52,** 928–934 (2016).
4. Perrone-Filardi, P. *et al.* The role of metabolic syndrome in heart failure. *Eur. Heart J.* **36,** 2630–2634 (2015).
5. Haslam, D. W. & James, W. P. T. Obesity. *Lancet* **366,** 1197–1209 (2005).
6. Kenchaiah, et al. Obesity and the risk of heart failure. *Nejm* **339,** 61–68 (1998).
7. Kemp, C. D. & Conte, J. V. The pathophysiology of heart failure. *Cardiovasc. Pathol.* **21,** 365–371 (2012).
8. Kalantar-Zadeh, K., Block, G., Horwich, T. & Fonarow, G. C. Reverse epidemiology of conventional cardiovascular risk factors in patients with chronic heart failure. *J. Am. Coll. Cardiol.* **43,** 1439–1444 (2004).
9. Lavie, C. J., Mehra, M. R. & Milani, R. V. Obesity and heart failure prognosis: Paradox or reverse epidemiology? *Eur. Heart J.* **26,** 5–7 (2005).
10. FG, B. & CH, B. The internal secretion of the pancreas. 251–265 (1922).
11. World Health Organization. Global Report on Diabetes. *Isbn* **978,** 88 (2016).
12. Dekker, J. M. *et al.* Metabolic syndrome and 10-year cardiovascular disease risk in the Hoorn Study. *Circulation* **112,** 666–673 (2005).
13. Galassi, A., Reynolds, K. & He, J. Metabolic Syndrome and Risk of Cardiovascular Disease: A Meta-Analysis. *Am. J. Med.* **119,** 812–819 (2006).
14. Mokdad, A. H. *et al.* Prevalence of Obesity, Diabetes, and Obesity-Related Health Risk Factors, 2001. **289,** 2001–2004 (2015).
15. Felber, J.-P. *et al.* Pathways from obesity to diabetes. *Int. J. Obes.* **26,** S39–S45 (2002).
16. Saxena, A. K. Emerging global epidemic of obesity: The renal perspective. *Ann. Saudi Med.* **26,** 288–295 (2006).
17. Musi, N. & Guardado-Mendoza, R. Adipose Tissue as an Endocrine Organ. *Cell. Endocrinol. Heal. Dis.* **89,** 229–237 (2014).
18. Jo, J. *et al.* Hypertrophy and/or hyperplasia: Dynamics of adipose tissue growth. *PLoS Comput. Biol.* **5,** (2009).
19. Goossens, G. H. The Metabolic Phenotype in Obesity: Fat Mass, Body Fat Distribution, and Adipose Tissue Function. *Obes. Facts* **10,** 207–215 (2017).
20. Conde, J. *et al.* Adipokines: Biofactors from white adipose tissue. A complex hub among inflammation, metabolism, and immunity. *BioFactors* **37,** 413–420 (2011).
21. Palanivel, R. *et al.* Globular and full-length forms of adiponectin mediate specific changes in glucose and fatty acid uptake and metabolism in cardiomyocytes. *Cardiovasc. Res.* **75,** 148–157 (2007).
22. Min, X. *et al.* Crystal structure of a single-chain trimer of human adiponectin globular domain. *FEBS Lett.* **586,** 912–917 (2012).
23. Chandran, M., Phillips, S. A., Ciaraldi, T. & Henry, R. R. Adiponectin: More than just another fat cell hormone? *Diabetes Care* **26,** 2442–2450 (2003).
24. Wang, Y. *et al.* Adiponectin inhibits cell proliferation by interacting with several growth factors in an oligomerization-dependent manner. *J. Biol. Chem.* **280,** 18341–18347 (2005).
25. Berg, A. H., Combs, T. P. & Scherer, P. E. Acrp30/adiponectin: an adipocytokine

regulating glucose and lipid metabolism. *Trends Endocrinol Metab.* **13,** 84–89 (2002).
26. Tsao, T. S., Murrey, H. E., Hug, C., Lee, D. H. & Lodish, H. F. Oligomerization state-dependent activation of NF-KB signaling pathway by adipocyte complement-related protein of 30 kDa (Acrp30). *J. Biol. Chem.* **277,** 29359–29362 (2002).
27. Waki, H. *et al.* Generation of globular fragment of adiponectin by leukocyte elastase secreted by monocytic cell line THP-1. *Endocrinology* **146,** 790–796 (2005).
28. Díez, J. J. & Iglesias, P. The role of the novel adipocyte-derived hormone adiponectin in human disease. *Eur. J. Endocrinol.* **148,** 293–300 (2003).
29. Nedvídková, J., Smitka, K., Kopský, V. & Hainer, V. Adiponectin, an adipocyte-derived protein. *Physiol. Res.* **54,** 133–140 (2005).
30. Erding Hu, Peng Liang, and B. M. S. AdipoQ Is a Novel Adipose-specific Gene Dysregulated in Obesity. *Am. Soc. Biochem. Mol. Biol.* **271,** 10697–10703 (1996).
31. Arita, Y. *et al.* Paradoxical Decrease of an Adipose-Specific Protein, Adiponectin, in Obesity. *Biochem. Biophys. Res. Commun.* **257,** 79–83 (1999).
32. Kadowaki, T. *et al.* Review series Adiponectin and adiponectin receptors in insulin resistance , diabetes , and the metabolic syndrome. *J. Clin. Invest.* **116,** 1784–1792 (2006).
33. Monzillo, L. U. *et al.* Effect of Lifestyle Modification on Adipokine Levels in Obese Subjects with Insulin Resistance. *Obes. Res.* **11,** 1048–1054 (2003).
34. Esposito, K. *et al.* Vascular Inflammatory Markers in Obese Women: A Effect of Weight Loss and Lifestyle Changes on Effect of Weight Loss and Lifestyle Changes on Vascular Inflammatory Markers in Obese Women. *JAMA Public Heal. Obesity; Women's Heal. Women's Heal. Other; Randomized Control. Trial* **28928914,** 1799–1804 (2003).
35. Otvos, L. *et al.* Design and development of a peptide-based adiponectin receptor agonist for cancer treatment. *BMC Biotechnol.* **11,** 90 (2011).
36. Liao, Y. *et al.* Exacerbation of heart failure in adiponectin-deficient mice due to impaired regulation of AMPK and glucose metabolism. *Cardiovasc. Res.* **67,** 705–713 (2005).
37. Rei Shibata1, 4, Noriyuki Ouchi1, 4, Masahiro Ito2, Shinji Kihara3, Ichiro Shiojima1, David R Pimentel2, Masahiro Kumada3, Kaori Sato1, Stephan Schiekofer1, Koji Ohashi3, T. & Funahashi3, Wilson S Colucci2, and K. W. Adiponectin-mediated modulation of hypertrophic signals in the heart. *Obesity* **17,** 1736–1743 (2010).
38. Fujita, K. *et al.* Adiponectin protects against angiotensin II-induced cardiac fibrosis through activation of PPAR-alpha. *Arterioscler. Thromb. Vasc. Biol.* **28,** 863–870 (2008).
39. Kojima, S. *et al.* The variation of plasma concentration of a novel adipocyte derived protein, adiponection, in patients with acute myocardial infarction. *Heart* **89,** 667–668 (2003).
40. Wang, Y. J. *et al.* Cardioprotective effect of adiponectin is partially mediated by its AMPK-independent antinitrative action. *Am. J. Physiol. Metab.* **297,** E384–E391 (2009).
41. Kistorp, C. *et al.* Plasma adiponectin, body mass index, and mortality in patients with chronic heart failure. *Circulation* **112,** 1756–1762 (2005).
42. Kadowaki, T. & Yamauchi, T. Adiponectin and adiponectin receptors. *Endocr. Rev.* **26,** 439–451 (2005).
43. Sheng, T. & Yang, K. Adiponectin and its association with insulin resistance and type 2 diabetes. *J. Genet. Genomics* **35,** 321–326 (2008).
44. Yamamoto, S. *et al.* Circulating adiponectin levels and risk of type 2 diabetes in the Japanese. *Nutr. Diabetes* **4,** e130 (2014).
45. Matsubara, M., Namioka, K. & Katayose, S. Decreased plasma adiponectin concentrations in women with low-grade C-reactive protein elevation. *Eur. J. Endocrinol.* **148,** 657–662 (2003).
46. Yamamoto, Y. *et al.* Correlation of the adipocyte-derived protein adiponectin with insulin resistance index and serum high-density lipoprotein-cholesterol, independent of body

mass index, in the Japanese population. *Clin. Sci. (Lond).* **103,** 137–42 (2002).
47. Cnop, M. *et al.* Relationship of adiponectin to body fat distribution, insulin sensitivity and plasma lipoproteins: evidence for independent roles of age and sex. *Diabetologia* **46,** 459–469 (2003).
48. Physiol, A. J. *et al.* Adipose tissue tumor necrosis factor and interleukin-6 expression in human obesity and insulin resistance Adipose tissue tumor necrosis factor and interleukin-6 expression in human obesity and insulin resistance. **72205,** 745–751 (2013).
49. Senn, J. J., Klover, P. J., Nowak, I. A. & Mooney, R. A. Interleukin-6 induces cellular insulin resistance in hepatocytes. *Diabetes* **51,** 3391–3399 (2002).
50. Jt, D. *et al.* T-cadherin is critical for adiponectin-mediated cardioprotection in mice. **120,** (2010).
51. Hug, C. *et al.* T-cadherin is a receptor for hexameric and high-molecular-weight forms of Acrp30/adiponectin. *Proc. Natl. Acad. Sci. U. S. A.* **101,** 10308–13 (2004).
52. Yamauchi, T. *et al.* Cloning of adiponectin receptors that mediate antLabeliabetic metabolic effects. *Nature* **423,** 762–769 (2003).
53. Buechler, C., Wanninger, J. & Neumeier, M. Adiponectin receptor binding proteins - recent advances in elucidating adiponectin signalling pathways. *FEBS Lett.* **584,** 4280–4286 (2010).
54. Mao, X. *et al.* APPL1 binds to adiponectin receptors and mediates adiponectin signalling and function. *Nat. Cell Biol.* **8,** 516–523 (2006).
55. Hardie, D. G. AMPK: a key regulator of energy balance in the single cell and the whole organism. *Int. J. Obes.* **32,** S7–S12 (2008).
56. Zhou, L. *et al.* Adiponectin activates AMP-activated protein kinase in muscle cells via APPL1/LKB1-dependent and phospholipase C/Ca2+/Ca2+/calmodulin-dependent protein kinase kinase-dependent pathways. *J. Biol. Chem.* **284,** 22426–22435 (2009).
57. Xin, X., Zhou, L., Reyes, C. M., Liu, F. & Dong, L. Q. APPL1 mediates adiponectin-stimulated p38 MAPK activation by scaffolding the TAK1-MKK3-p38 MAPK pathway. *Am. J. Physiol. Endocrinol. Metab.* **300,** E103-10 (2011).
58. Wang, C. *et al.* Yin-Yang regulation of adiponectin signaling by APPL isoforms in muscle cells. *J. Biol. Chem.* **284,** 31608–31615 (2009).
59. Yoon, M. J. *et al.* Adiponectin Increases Fatty Acid Oxidation in Skeletal Muscle Cells by Sequential Activation of AMP-Activated Protein Kinase, p38 Mitogen-Activated Protein Kinase, and Peroxisome Proliferator–Activated Receptor α. *Diabetes* **55,** 2562–2570 (2006).
60. Shao, D. & Tian, R. Glucose Transporters in Cardiac Metabolism and Hypertrophy. *Compr. Physiol.* **6,** 331–351 (2015).
61. Deepa, S. S. & Dong, L. Q. APPL1: role in adiponectin signaling and beyond. *AJP Endocrinol. Metab.* **296,** E22–E36 (2008).
62. Fang, X. *et al.* An APPL1-AMPK signaling axis mediates beneficial metabolic effects of adiponectin in the heart. *Am. J. Physiol. Endocrinol. Metab.* **299,** E721–E729 (2010).
63. Ganguly, R. *et al.* Adiponectin increases LPL activity via RhoA/ROCK-mediated actin remodelling in adult rat cardiomyocytes. *Endocrinology* **152,** 247–254 (2011).
64. Kahn, B. B., Alquier, T., Carling, D. & Hardie, D. G. AMP-activated protein kinase: Ancient energy gauge provides clues to modern understanding of metabolism. *Cell Metab.* **1,** 15–25 (2005).
65. Daitoku, H., Sakamaki, J. ichi & Fukamizu, A. Regulation of FoxO transcription factors by acetylation and protein-protein interactions. *Biochim. Biophys. Acta - Mol. Cell Res.* **1813,** 1954–1960 (2011).
66. Van der Vos, K. & Doffer, P. J. The extending network of FOXO transcriptional target genes. 579–593 (2011).
67. Yan, L. *et al.* PP2A regulates the pro-apoptotic activity of FOXO1. *J. Biol. Chem.* **283,**

7411–7420 (2008).
68. Tsuchida, A. *et al.* Insulin/Foxo1 pathway regulates expression levels of adiponectin receptors and adiponectin sensitivity. *J. Biol. Chem.* **279,** 30817–30822 (2004).
69. Matsuzaki, H. *et al.* Acetylation of Foxo1 alters its DNA-binding ability and sensitivity to phosphorylation. *Proc. Natl. Acad. Sci.* **102,** 11278–11283 (2005).
70. Brunet, A. & Et., A. Stress Dependant Regulation of FOCO Transcription Factors by the SIRT1 Deacetylase. (2004).
71. van der Horst, A. *et al.* FOXO4 transcriptional activity is regulated by monoubiquitination and USP7/HAUSP. *Nat. Cell Biol.* **8,** 1064–1073 (2006).
72. Matsuzaki, H., Daitoku, H., Hatta, M., Tanaka, K. & Fukamizu, A. Insulin-induced phosphorylation of FKHR (Foxo1) targets to proteasomal degradation. *Proc. Natl. Acad. Sci. U. S. A.* **100,** 11285–90 (2003).
73. Greer, E. L. *et al.* The energy sensor AMP-activated protein kinase directly regulates the mammalian FOXO3 transcription factor. *J. Biol. Chem.* **282,** 30107–30119 (2007).
74. Almeda-Valdes, P. *et al.* Total and high molecular weight adiponectin have similar utility for the identification of insulin resistance. *Cardiovasc. Diabetol.* **9,** 26 (2010).
75. Fisman, E. Z. & Tenenbaum, A. Adiponectin: a manifold therapeutic target for metabolic syndrome, diabetes, and coronary disease? *Cardiovasc. Diabetol.* **13,** 103 (2014).
76. Kadowaki, T. & et al. A small-moleculae AdipoR agonist for type 2 diabetes and short life in obesity. 493–513 (2013).
77. Zhang, Y. *et al.* AdipoRon, the first orally active adiponectin receptor activator, attenuates postischemic myocardial apoptosis through both AMPK-mediated and AMPK-independent signalings. *Am. J. Physiol. - Endocrinol. Metab.* **309,** E275–E282 (2015).
78. Fridlyand, L. E. & PhilipsJ. P. Whitehead,1 A. A. Richards,1 I. J. Hickman,1,3 G. A. Macdonald1,2 and J. B. Prinson, L. H. Adiponectin – a key adipokine in the metabolic syndrome. *Diabetes. Obes. Metab.* **8,** 264–280 (2006).
79. Sente, T., Van Berendoncks, A. M., Hoymans, V. Y. & Vrints, C. J. Adiponectin resistance in skeletal muscle: pathophysiological implications in chronic heart failure. *J. Cachexia. Sarcopenia Muscle* 261–274 (2016). doi:10.1002/jcsm.12086
80. Lara-Castro, C. *et al.* Adiponectin multimers and metabolic syndrome traits: relative adiponectin resistance in African Americans. *Obesity (Silver Spring).* **16,** 2616–23 (2008).
81. Springer, J., Anker, S. D. & Doehner, W. Editorial: Adiponectin resistance in heart failure and the emerging pattern of metabolic failure in chronic heart failure. *Circ. Hear. Fail.* **3,** 181–182 (2010).
82. Lin, H. V *et al.* Adiponectine resistance exacerbates Insulin Receptor Transgenic / Knockout Mice. *Diabetes* **56,** (2007).
83. Park, M., Sabetski, A., Kwan Chan, Y., Turdi, S. & Sweeney, G. Palmitate Induces ER Stress and Autophagy in H9c2 Cells: Implications for Apoptosis and Adiponectin Resistance. *J. Cell. Physiol.* **230,** 630–639 (2015).
84. Van Berendoncks, A. M. *et al.* Functional adiponectin resistance at the level of the skeletal muscle in mild to moderate chronic heart failure. *Circ. Hear. Fail.* **3,** 185–194 (2010).
85. Park, M. *et al.* Globular adiponectin, acting via AdipoR1/APPL1, protects H9c2 cells from hypoxia/reoxygenation-induced apoptosis. *PLoS One* **6,** (2011).
86. Wessling-Resnick M. Iron. In: Ross AC, Caballero B, Cousins RJ, Tucker KL, Ziegler RG, E. Modern Nutrition in Health and Disease. 176–188 (1995).
87. Box, U. S. S. P. O. Ullmann's Encyclopedia of Industrial Chemistry. *J. Am. Chem. Soc.* **7863,** 11134–11136 (1997).
88. Drakesmith, H. & Prentice, A. Viral infection and iron metabolism. *Nat. Rev. Microbiol.* **6,** 541–552 (2008).
89. Mackenzie, B. & Garrick, M. D. Iron Imports. II. Iron uptake at the apical membrane in the

intestine. *Am. J. Physiol. Gastrointest. Liver Physiol.* **289,** G981–G986 (2005).
90. Zhang, Y. *et al.* Lysosomal proteolysis is the primary degradation pathway for cytosolic ferritin and cytosolic ferritin degradation is necessary for iron exit. 999 (2010).
91. Tomas Ganz, and E. N. Hepacidin and Iron Homeostasis. *Biochim. Biophys. Acta - Mol. Cell Res.* **1823,** 1434–1443 (2014).
92. Fuqua, B. K., Vulpe, C. D. & Anderson, G. J. Intestinal iron absorption. *J. Trace Elem. Med. Biol.* **26,** 115–119 (2012).
93. Dev, S. & Babitt, J. L. Overview of iron metabolism in health and disease. *Hemodial. Int.* (2017). doi:10.1111/hdi.12542
94. Roetto, A. *et al.* Mutant antimicrobial peptide hepcidin is associated with severe juvenile hemochromatosis. *Nat. Genet.* **33,** 21–22 (2002).
95. Camaschella, C. *et al.* The gene TFR2 is mutated in a new type of haemochromatosis mapping to 7q22. *Nat. Genet.* **25,** 14–15 (2000).
96. Papanikolaou, G. *et al.* Mutations in HFE2 cause iron overload in chromosome 1q–linked juvenile hemochromatosis. *Nat. Genet.* **36,** 77–82 (2004).
97. Shander, A., Cappellini, M. D. & Goodnough, L. T. Iron overload and toxicity: The hidden risk of multiple blood transfusions. *Vox Sang.* **97,** 185–197 (2009).
98. Lu, J. P. & Hayashi, K. Selective iron deposition in pancreatic islet B cells of transfusional iron-overloaded autopsy cases. *Pathol. Int.* **44,** 194–9 (1994).
99. Barton, J., Lee, P., West, C. & Bottomely, S. Iron overload and prolonged ingestion of iron supplimentsL clinical features and mutation analysis of hemochromatosis-asociated genes in four cases. *Am.J.Hematol.* **81,** 760–767 (2006).
100. Gujja, P. & Rosing, D. Iron Overload CardiomyopathyBetter Understanding of an Increasing Disorder. *J. Am. Coll. Cardiol.* **56,** 1001–1012 (2010).
101. Das, S. K. *et al.* Iron-overload injury and cardiomyopathy in acquired and genetic models is attenuated by resveratrol therapy. *Sci. Rep.* **5,** 18132 (2015).
102. Simcox, J. A. & McClain, D. A. Iron and diabetes risk. *Cell Metab.* **17,** 329–341 (2013).
103. Fernández-Real, J. M., McClain, D. & Manco, M. Mechanisms Linking Glucose Homeostasis and Iron Metabolism Toward the Onset and Progression of Type 2 Diabetes. *Diabetes Care* **38,** 2169–76 (2015).
104. Henry, W. L. Perspectives in diabetes. *J. Natl. Med. Assoc.* **54,** 476–478 (1962).
105. Cooksey, R. C. *et al.* Oxidative stress, Beta-cell apoptosis, and decreased insulin secretory capacity in mouse models of hemochromatosis. *Endocrinology* **145,** 5305–5312 (2004).
106. Gabrielsen, J. S. *et al.* adipocyte ion regulates adiponectin and insulin sensitivity Sup. **122,** 9–10 (2012).
107. Han, S. H., Quon, M. J., Kim, J. & Koh, K. K. Adiponectin and Cardiovascular Disease. *J. Am. Coll. Cardiol.* **49,** 531–538 (2007).
108. Ouchi, N., Shikata, R. & Walsh, K. Cardioprotection by Adiponectin. *Trends Cardiovasc Med* **16,** 141–146 (2006).
109. Nanayakkara, G., Kariharan, T., Wang, L., Zhong, J. & Amin, R. The cardio-protective signaling and mechanisms of adiponectin. *Am. J. Cardiovasc. Dis.* **2,** 253–66 (2012).
110. Villarreal-Molina, M. T. & Antuna-Puente, B. Adiponectin: Anti-inflammatory and cardioprotective effects. *Biochimie* **94,** 2143–2149 (2012).
111. Epsztejn, S., Breuer, W. & Cabantchik, Z. I. A Review of Fluorescence Methods for Assessing Labile Iron in Cells and Biological Fluids 1. *Anal. Biochem.* **18,** 1–18 (2002).
112. Henderson, R. J., Patton, S. M. & Connor, J. R. Development of a fluorescent reporter to assess iron regulatory protein activity in living cells. *Biochim. Biophys. Acta - Mol. Cell Res.* **1743,** 162–168 (2005).
113. Gomez, L. a, Alekseev, a E., Aleksandrova, L. a, Brady, P. a & Terzic, A. Use of the MTT assay in adult ventricular cardiomyocytes to assess viability: effects of adenosine and

potassium on cellular survival. *J. Mol. Cell. Cardiol.* **29,** 1255–66 (1997).
114. Glei, M. *et al.* Iron-overload induces oxidative DNA damage in the human colon carcinoma cell line HT29 clone 19A. *Mutat. Res. Toxicol. Environ. Mutagen.* **519,** 151–161 (2002).
115. Hardie, D. G. AMP-activated protein kinase — an energy sensor that regulates all aspects of cell function. 1895–1908 (2011). doi:10.1101/gad.17420111.crease
116. Huang, J. *et al.* Iron regulates glucose homeostasis in liver and muscle via AMP-activated protein kinase in mice. *FASEB J.* **27,** 2845–2854 (2017).
117. Mallein-gerin, R. I. C. *et al.* A Common Pathway in Differentiation and Inflammation : p38 Mediates Expression of the Acute Phase SIP24 Iron Binding Lipocalin in Chondrocytes. *J. Cell. Physiol.* **737,** 728–737 (2006).
118. Klotz, L. *et al.* Redox Biology Redox regulation of FoxO transcription factors. *Redox Biol.* **6,** 51–72 (2015).
119. Walter, P. L. *et al.* Modulation of FoxO signaling in human hepatoma cells by exposure to copper or zinc ions. *Arch. Biochem. Biophys.* **454,** 107–113 (2006).
120. Chai, X. *et al.* ROS-mediated iron overload injures the hematopoiesis of bone marrow by damaging hematopoietic stem/progenitor cells in mice. *Sci. Rep.* **5,** 10181 (2015).
121. Zou, P. *et al.* Targeting FoxO1 with AS1842856 Suppresses Adipogenesis. *Cell Cycle* 3759–3767 (2014).
122. J. Scott Gabrielsen, 1 Yan Gao, 1 Judith A. Simcox, 1 Jingyu Huang, 1 David Thorup, 1 Deborah Jones, 1 Robert C. Cooksey, 1, 2 David Gabrielsen, 1 Ted D. Adams, 3 Steven C. Hunt, 3 Paul N. Hopkins, 3 William T. Cefalu, 4 and Donald A. McClain1. Adipocyte iron regulates adiponectin and insulin sensitivity. 122: 3529-3540 (2012).
123. Agrisuelas, J., García-jareño, J. J., Gimenez-romero, D. & Vicente, F. Insights on the Mechanism of Insoluble-to-Soluble Prussian Blue Transformation. (2009). doi:10.1149/1.3177258
124. Kalantar-Zadeh, K., Block, G., Humphreys, M. H. & Kopple, J. D. Reverse epidemiology of cardiovascular risk factors in maintenance dialysis patients. *Kidney Int.* **63,** 793–808 (2003).
125. Veglio, F. *et al.* Blood Pressure and Heart Rate in Young Thalassemia Major Patients. *AJH* **7061,** 539–547 (1998).
126. Musumeci, M. *et al.* Iron excretion in iron dextran-overloaded mice. *Blood Transfus* **12,** 4–9 (2014).
127. Jackson, L. H. *et al.* Non-invasive MRI biomarkers for the early assessment of iron overload in a humanized mouse model of β -thalassemia. *Nat. Publ. Gr.* 1–10 (2017). doi:10.1038/srep43439
128. Cheung, Y. *et al.* Myocardial Deformation in Patients with Beta-Thalassemia Major : A Speckle Tracking Echocardiographic Study Methods : *Echocardiography* 253–259 (2010). doi:10.1111/j.1540-8175.2009.01005.x
129. Vogel, M. *et al.* Tissue Doppler echocardiography in patients with thalassaemia detects early myocardial dysfunction related to myocardial iron overload. *Eurpean Soc. Cardiol.* 113–119 (2003). doi:10.1016/S0195-668X(02)00381-0
130. Mavrogeni, S. Evaluation of myocardial iron overload using magnetic resonance imaging. 183–187 (2009). doi:10.2450/2008.0063-08
131. Choi, K. M. *et al.* Serum adiponectin concentrations predict the developments of type 2 diabetes and the metabolic syndrome in elderly Koreans. *Clin. Endocrinol. (Oxf).* **61,** 75–80 (2004).
132. Eckel, R. H. Mechanisms of the components of the metabolic syndrome that predispose to diabetes and atherosclerotic CVD. *Proc. Nutr. Soc.* **66,** 82–95 (2007).
133. Felder, T. K. *et al.* Hepatic adiponectin receptors (ADIPOR) 1 and 2 mRNA and their relation to insulin resistance in obese humans. *Int. J. Obes. (Lond).* **34,** 846–851 (2010).

134. Mullen, K. L., Smith, A. C., Junkin, K. A. & Dyck, D. J. Globular adiponectin resistance develops independently of impaired insulin-stimulated glucose transport in soleus muscle from high-fat-fed rats. *Am. J. Physiol. Endocrinol. Metab.* **293,** E83-90 (2007).
135. Dongiovanni, P. *et al.* Dietary iron overload induces visceral adipose tissue insulin resistance. *Am. J. Pathol.* **182,** 2254–63 (2013).
136. Ramey, G., Faye, A., Durel, B., Viollet, B. & Vaulont, S. Iron overload in Hepc1 -/- mice is not impairing glucose homeostasis. *FEBS Lett.* **581,** 1053–1057 (2007).
137. Mcclain, A. D. A. High prevalence of abnormal glucose homeostasis secondary to decreased insulin secretion in individuals with hereditary haemochromatosis. *Diabetologia* 1661–1669 (2006). doi:10.1007/s00125-006-0200-0
138. Buchanan, J. INSULIN RESISTANCE IN HAEMOCHROMATOSIS. *Postgrad. Med. J.* **42,** 551–554 (1966).
139. Dimmeler, S. Cardiovascular disease review series. *EMBO Mol Med* **5,** 697 (2011).
140. Abdulfatai B. Olokoba, Olusegun A. Obateru, L. B. O. Type 2 Diabetes Mellitus: A Review of Current Trends. *Oman Med. J.* **27,** 269–273 (2012).

Appendix A: Supplementary Figures

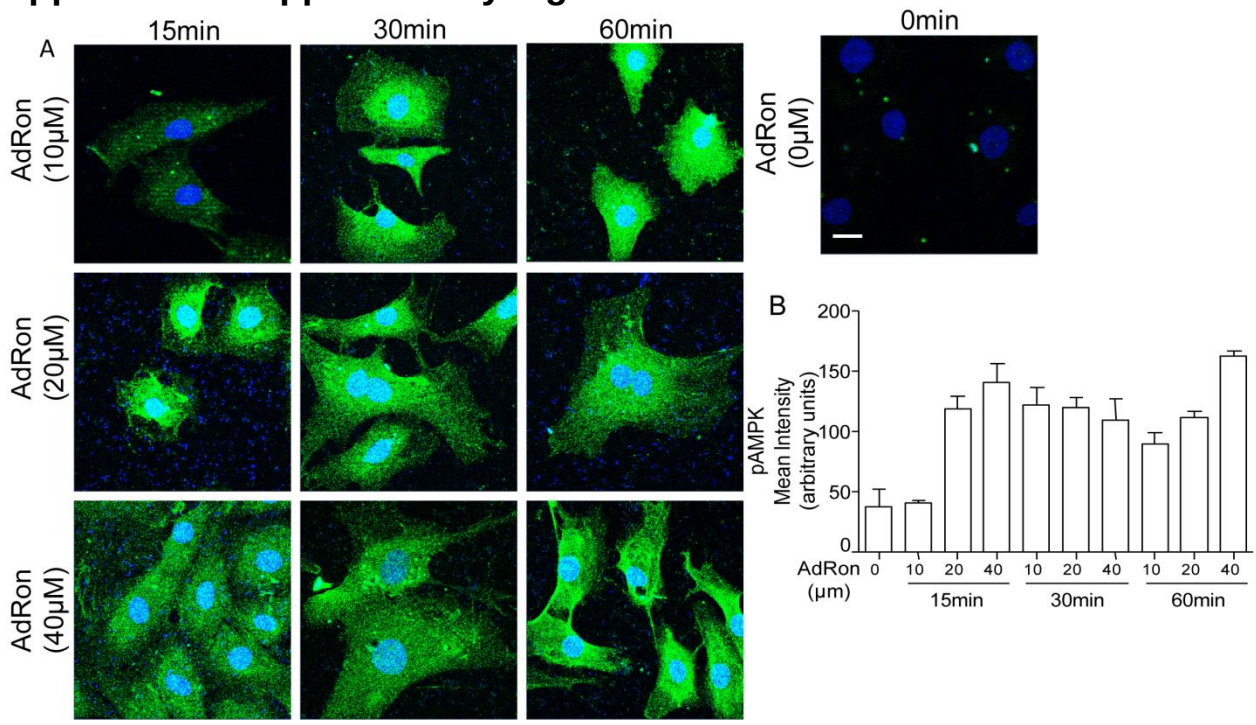

Figure A1: Optimizing AdRon treatment concentration and time via stimulation of pAMPK. NeoCM were treated with 0, 10, 20 and 40μM of AdRon for 0, 15, 30 and 60 min. 20μM for 30min was used as treatment conditions for future studies. Cells were incubated in pAMPK (Thr172) primary antibody, and subsequently incubated in Alexa 488 secondary antibody. Green fluorescence was observed via FTIC channels by confocal microscopy (n=1). A) 2D representative image taken using ZEN software (Scale bar: 1μm). B) 3-5 fields of view were taken per condition. All cells in field of view were traced and quantified using ImageJ software. Mean intensity values per cell were averaged, and normalized to control. Error bars display standard error of the mean.

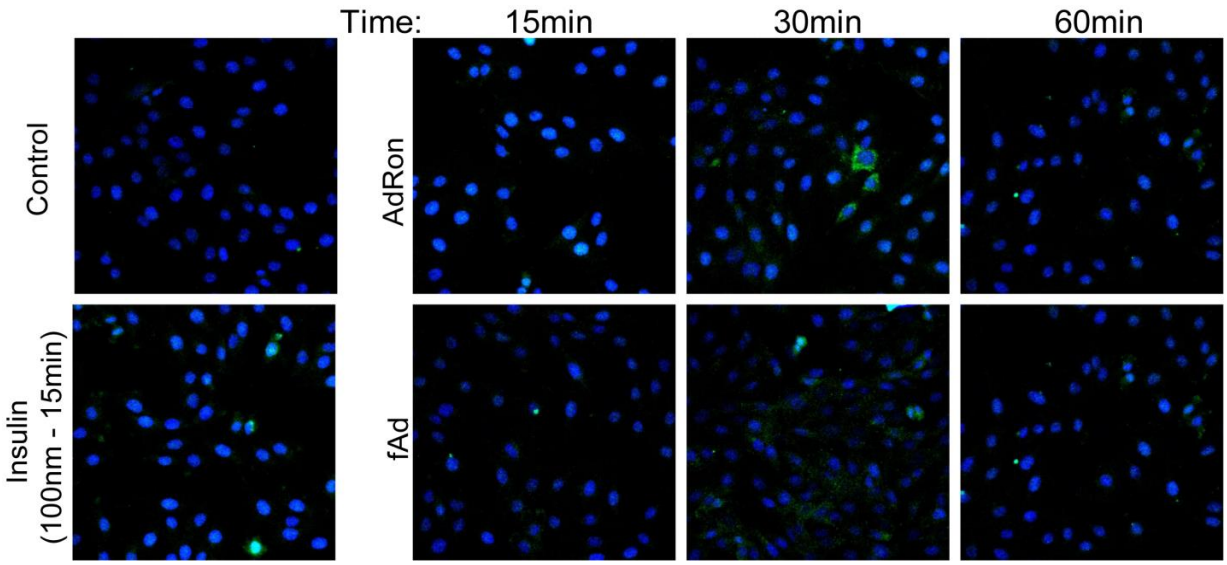

Figure A2: Optimizing AdRon and fAd treatment time via cytoplasmic localization of pFOXO1 . L6 myoblasts were treated with 20µM of AdRon, or 5µg/ml of fAd, for 15, 30 or 60min. As a positive control for cytoplasmic pFOXO1 localization, cells were stimulated with 100nM of insulin for 10 minutes (n=1). 30min time point was used for future experiments due to increase in cytoplasmic green fluorescence. Cells were incubated in pFOXO1 (Thr24) primary antibody, and subsequently incubated in Alexa 488 secondary antibody. Green fluorescence was observed via FTIC channels by confocal microscopy. 2D representative image taken using ZEN software.

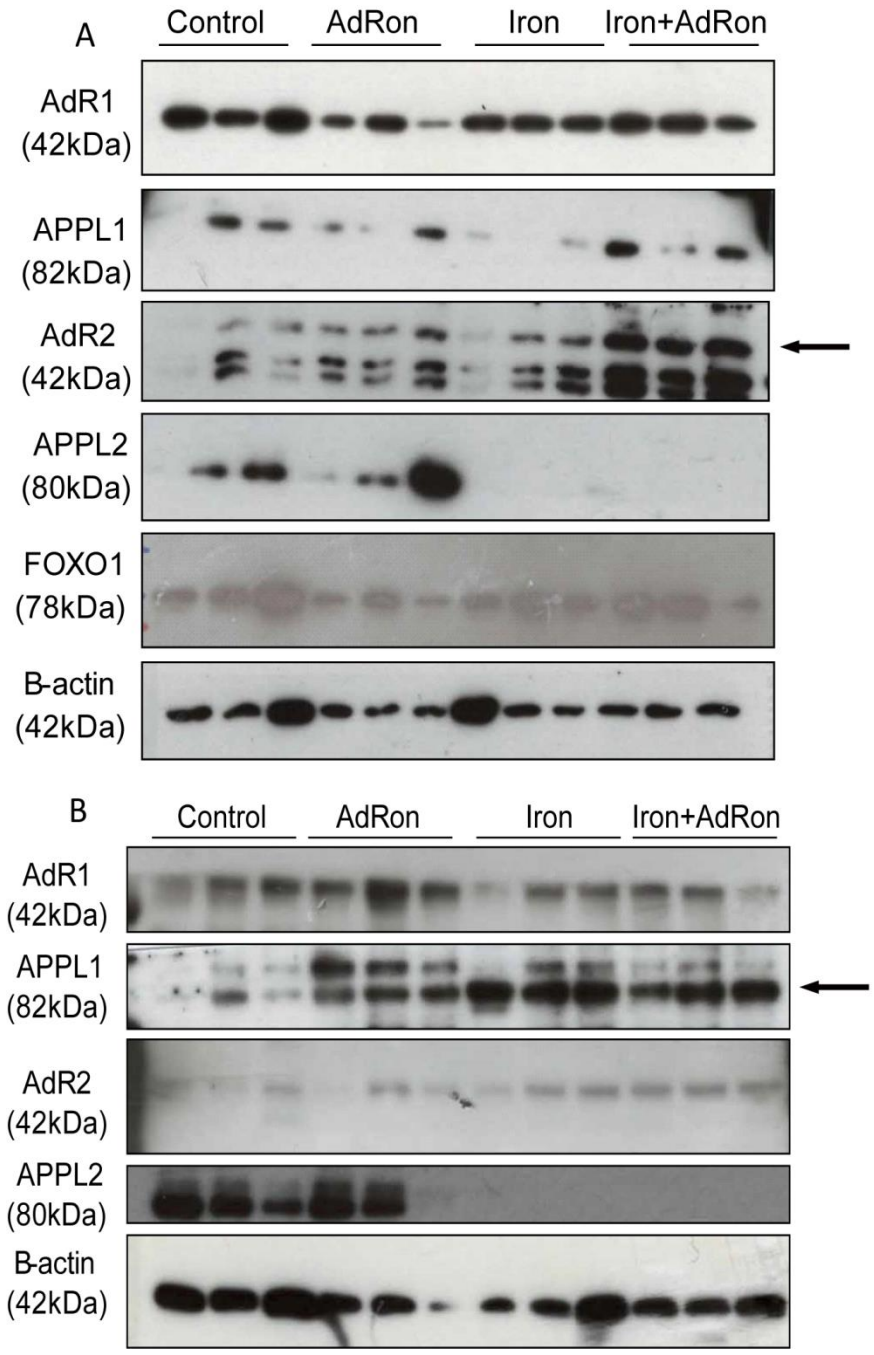

Figure A3: Uncut Western Blots of Figures 2.7 and 3.6, respectively. Twelve 8 week C57 male mice were IP injected with 10mg/g of ferrous iron. 3 control and 3 iron overload mice were injected with 25mg/kg of AdRon for 30 min prior to sacrifice; however, AdRon injected mice were not considered for this study and require further optimization. Heart and soleus tissue were immunoblotted with primary antibody for the following proteins of interest: AdipoR1, APPL1, AdipoR2, APPL2, total FOXO1 and β-actin, which were subsequently tagged with HRP-conjugated secondary antibodies (n=3). A) Representative western blots of AdipoR1, APPL1, AdipoR2, APPL2, FOXO1 and β-actin in the heart. B) Representative western blots of AdipoR1, APPL1, AdipoR2, APPL2 and β-actin in soleus muscle.

Appendix B: List of Contributions

This thesis was written and researched by Michelle Prioriello (MP), whereby MP contributed to majority of experimental contributions. MP worked with Karam Dahyaleh (KD) as a mentor for a Research Practicum, whereby MP trained KD to perform cellular and molecular assays. Contributions by KD are listed as follows:

1. Figure 2.5: Developed APPL1 and β-actin representative blots
2. Figure 3.1: 2 of 3 total n numbers were performed by KD
3. Figure 3.5: Performed by KD

Echocardiography, was performed and quantified by James Jang (JJ), using a separate batch of iron overload mice than those used in this study, which were created by Nancy Dang (ND). List of contributors are as follows.

1. Figure 2.8: Performed by JJ, using iron overload mice by ND

Preliminary evidence for iron overload induced adiponectin resistance was contributed by Palanivel Rengasamy (PR). PR's contributions to the project are as follows:

1. Figure 3.2: Performed by PR

Data quantification of 3D Z-stacks was completed by Eric Danielson (Massachusetts Institute of Technology, USA). Contributions are as follows:

1. Figure 3.3: Quantified by ED
2. Figure 3.4: Quantified by ED

Lastly, ND completed Prussian blue staining in soleus muscle. ND also tested urine glucose after 6h of starvation. List of contributions are as follows:

1. Figure 3.6: Performed by ND
2. Figure 3.8 (F): Performed by ND, using iron overload mice by ND